To the Graduate Council:

I am submitting herewith a dissertation written by Mark D. Potter entitled "MOLECULAR AND PHENOTYPIC ANALYSIS OF A MUTANT LOCUS, DESIGNATED *fitness 1* (*fit1*), SPECIFYING GROWTH RETARDATION, REDUCED VIABILITY, AND ABNORMAL HEMATOPOIESIS IN THE MOUSE." I have examined the final copy of this dissertation for form and content and recommend that it be accepted in partial fulfillment of the requirements for the degree of Doctor of Philosophy, with a major in Biomedical Sciences.

E.M. Rinchik

E.M. Rinchik, Major Professor

We have read this dissertation
and recommend its acceptance:

Fred C. Hartman

Eugenia T. Bodfrey

Linda B Russell

Ralph P. Woychik

Accepted for the Council:

Associate Vice Chancellor

and Dean of the Graduate School

MOLECULAR AND PHENOTYPIC ANALYSIS OF A MUTANT LOCUS, DESIGNATED *fitness 1* (*fit1*), SPECIFYING GROWTH RETARDATION, REDUCED VIABILITY, AND ABNORMAL HEMATOPOIESIS IN THE MOUSE

A Dissertation

Presented for the

Doctor of Philosophy

Degree

The University of Tennessee, Knoxville

Mark D. Potter

August 1994

This work is dedicated to my wonderful, loving wife Laura, my beautiful daughter Chloe, and my entire family, for their constant support, understanding and encouragement.

ABSTRACT

Molecular and phenotypic analyses of allelic mutations that disrupt normal development are extremely useful tools for dissecting the roles particular genes play in development. Saturation mutagenesis of a large region surrounding the albino (*c*) locus of mouse chromosome 7, employing the point-mutagen *N*-ethyl-*N*-nitrosourea (ENU), has resulted in the identification of five independent mutations of a gene, designated *fitness 1* (*fit1*), which is necessary for normal pre- and postnatal growth and viability. By design of the mutagenesis strategy, *fit1*, as well as other ENU-induced mutations recovered in this screen, map within the extensive set of deletion mutations that surround the *c* locus. Therefore, given the inherent advantages of deletion mutations for rapidly mapping DNA probes and for gaining access to distant loci by cloning deletion breakpoints, *fit1* is a candidate for a positional-cloning strategy, which allows the molecular identification of a gene based on its map position rather than on functional information. Molecular characterization of the *fit1* gene, in conjunction with biological analysis of the *fit1* phenotype, should provide key insights into the processes involved in normal growth and development. Additionally, analysis of the five independent *fit1* mutations may provide information relevant to associating biological functions to specific DNA sequences.

The *fit1* gene has been mapped to a specific subregion of the *c* deletion complex, defined by the distal breakpoints of several deletion mutations. Molecular access to the *fit1* region was gained by cloning one of the deletion breakpoints associated with the proximal border of the *fit1* interval. Physical mapping of the *fit1* region, with this proximal probe and with an existing DNA probe that maps distal to *fit1*, has allowed determination of the maximum size of the *fit1* region, and has further distinguished the proximal border of the *fit1* locus and the distal border of at least three loci mapping proximal to *fit1*. Two yeast artificial chromosomes (YACs) were obtained, one of which spans an interval known to contain at least part of the *fit1* gene. Characterization of these YAC clones has provided additional DNA probes at the *fit1* locus, has narrowed the region containing at least part of the *fit1* gene, and has suggested several putative CpG island sites at the *fit1* locus.

Characterization of the *fit1* phenotype revealed that *fit1* mutants are growth retarded at least as early as 14.5 days of gestation and remain dwarfed throughout their shortened lifespan. Also, these growth analyses indicate that there is a range of severity among the five *fit1* mutations. Additionally, *fit1* mutants were found to be anemic, displayed numerous peripheral blood defects, and were deficient in early hematopoietic progenitor cell populations. Not only were erythroid and myeloid cells reduced, but the number of lymphoid lineage cells were also lower. These results implicate *fit1*

involvement in normal hematopoietic differentiation and suggest that, in conjunction with molecular analyses, further characterization of the *fit1* gene, and these five allelic presumed point mutations of the gene, will lead to an improved understanding of normal pre- and postnatal development and hematopoietic differentiation.

TABLE OF CONTENTS

LIST OF TABLES

LIST OF FIGURES

GENERAL APPENDIX

LIST OF ABBREVIATIONS

BFU-E	Burst forming unit-erythroid
BSA	Bovine-serum albumin
cDNA	Complementary DNA derived from reverse transcription of messenger RNA
CFU-E	Colony forming unit-erythroid
CFU-GM	Colony forming unit-granulocyte/macrophage
CFU-S	Colony forming unit-spleen
cM	Centimorgan (1% recombination)
CpG	Dinucleotide of deoxycytidine 5'-monophosphate (5') and deoxyguanosine 5'-monophosphate (3'), which occurs infrequently in mammalian genomic DNA
EDTA	Disodium ethylenediamine tetraacetate
ENU	*N*-ethyl-*N*-nitrosourea
ES cells	Embryonic stem cells
FAH	Fumarylacetoacetate hydrolase
FUT4	myeloid α-3-fucosyltransferase
Hct	Hematocrit
Hgb	Hemoglobin
Hpx	Hemopexin
HTF	*Hpa*II tiny fragments
kb	kilobase
LMP	Low-melting point
mb	Megabase

MW	Molecular weight
PBS	Phosphate Buffered Saline
^{32}P-dCTP	Deoxycytidine 5'[α-^{32}P] triphosphate
PCR	Polymerase chain-reaction
PFG	Pulsed-field gel
PFGE	Pulsed-field gel electrophoresis
poly-(A+) RNA	Eukaryotic RNA after enrichment for messenger RNAs containing long sequences of successive adenylate residues at the 3' end
RBC	Red blood cell
SV40	Simian virus-40
TE	10 m*M* Tris-Cl, 0.1 m*M* EDTA solution
UV	Ultraviolet
WBC	White blood cell
YAC	Yeast-artificial chromosome

I. INTRODUCTION

Development of a differentiated organism from an undifferentiated egg is a spectacular biological process directed by an enormous outlay of genomic information beginning during embryogenesis and continuing through adult life. A fundamental understanding of mammalian development will require the identification and cloning of genes encoding developmental information, determination of gene expression patterns and how that expression is regulated, as well as elucidation of the mechanisms by which encoded gene products direct cellular differentiation and specify ultimate cellular fates.

Mutations are Integral to Studying Mammalian Development

Even before knowledge of its molecular basis, the process of development was understood to be, in some manner, a heritable feature of all organisms. For centuries, livestock and crops were selected and bred for favorable characteristics, and organisms displaying unusual phenotypes were objects of fascination and, when possible, were maintained. Eventually, these "oddities of nature" were recognized as tools through which aspects of normal development could be studied [*e.g.*, Jacob, 1920; Silvers, 1979; Meyerowitz et al., 1989, (and references therein)].

Indeed, most of our current knowledge of mammalian development comes from characterization in experimental systems of genetic mutations that disrupt the normal course of development at different stages. The mouse has proven to an excellent model system within which to study mammalian development because of the existing wealth of heritable mutations, its genetic and biological similarity to humans, and the ease of manipulating it experimentally. The majority of genes cloned from the mouse genome have human homologs, and several heritable conditions identified in mice are believed to be phenotypically and biochemically similar to human disease conditions (Winter, 1988; Darling and Abbott, 1992; Smithies, 1993; Searle et al., 1994). Therefore, characterization of heritable mutations in the mouse provides an important resource for studying the functional and physical composition of the mammalian genome and should lead to improved understanding of genetic conditions affecting humans.

Introduction to Positional Cloning

Our understanding of mammalian development has improved greatly since the advent of recombinant DNA technology, which has enabled the cloning and molecular characterization of a number of developmentally important genes. The majority of the genes cloned thus far has been identified through techniques relying on knowledge

of the basic biochemical process affected by the gene. Unfortunately, for most existing mutations in mammals, very little such information exists.

Recent advances in a number of genetic-mapping and molecular techniques have made it possible to isolate genes with no prior knowledge of the gene product, beginning solely with the expressed phenotype. This approach, referred to as "positional cloning" (previously called "reverse genetics"), has been successfully used to isolate several genes, including many involved in serious human disorders (reviewed in Collins, 1992).

Positional-cloning strategies may utilize a variety of techniques; however, all are primarily centered around a common course: (1) establishing a chromosomal position for the gene of interest; (2) obtaining closely linked DNA clones; (3) chromosome "walking" or "jumping" into the region of interest; and (4) identification of a candidate transcript(s). A correct map position, "appropriate" spatial and temporal expression patterns, and altered gene expression in individuals displaying the mutant phenotype of interest may provide indirect evidence that the sought-after gene has been cloned. Definitive proof may eventually be gained by correction-of-phenotype experiments utilizing transgenic mice and/or experiments utilizing homologous recombination in embryonic stem (ES) cells to generate mice displaying the mutant phenotype.

It should be noted that any one, or all, of these steps can represent difficult tasks and, in general, positional-cloning

approaches are labor intensive, time consuming, expensive, and depend somewhat on serendipity. However, despite inherent difficulties, and given the variety of techniques now available, it is likely that any positional-cloning project can succeed, provided with sufficient time and effort. This is evidenced by the recent cloning of the gene responsible for Huntington's disease, which culminated at least ten years of effort (Huntington's Disease Collaborative Research Group, 1993).

Chromosomal Rearrangements Facilitate Positional Cloning

One factor that greatly enhances the likelihood of isolating a gene by positional cloning is the existence of chromosomal rearrangements defining or delimiting the locus of interest. Deletions, translocations, and inversions have proven to be valuable genetic tools for gaining molecular access to particular chromosomal regions and/or to specific genes (*e.g.*, Royer-Pokora et al., 1986; Monaco et al., 1986; Wallace et al., 1990; Herrmann et al., 1990; Rose et al., 1990; Groden et al., 1991). In fact, with only a few exceptions (Rommens et al., 1989), most successful positional-cloning strategies have relied on chromosomal rearrangements.

Overlapping deletion mutations are particularly useful reagents for both physical and functional characterization of large chromosomal regions (Rinchik and Russell, 1990).

Complementation analyses with overlapping deletions allow the assignment of particular functions to specific subregions of the deletion complex. In addition, panels of deletions facilitate the mapping of loci defined by DNA probes, as well as newly identified intragenic mutations, with respect to deletion breakpoints. Also, mapped DNA probes may be used to identify and clone deletion breakpoints, thereby providing access to genetic loci at or near the ends of deletions and allowing rapid chromosome jumping of potentially large (megabase) distances (*e.g.*, Klebig et al., 1992a). Thus, the development of functional and physical maps of regions spanned by deletion mutations is greatly facilitated, and the ability to rapidly map DNA probes and to chromosome-jump large distances, suggests any locus mapping within a complex of deletions as being amenable to a positional-cloning strategy.

The albino (*c*) Deletion Complex

Mutagenesis experiments utilizing the mouse specific locus test (SLT) (Russell, 1951) have provided a rich resource of deletion mutations surrounding seven recessive marker loci throughout the mouse genome. The best characterized of the SLT-deletion complexes is the 6- to 11-cM region surrounding the *albino* (*c*) locus in mouse chromosome 7. Genetic analyses utilizing 34 overlapping *c* deletions (Russell, 1982), and later histological analyses of mice

homozygous for a subset of deletion mutations (Niswander et al., 1988; 1989), have been used to identify at least 14 complementation groups collectively defining at least 9 functional units or loci. These loci, as well as other genetic markers and a subset of the albino deletions are shown in Fig 1*. A detailed description of the phenotypes associated with these complementation-defined loci can be found in Rinchik and Russell, 1990 (and references therein); a brief description of a selected subset of these loci will be given below.

The *hepatocyte-specific developmental regulation-1* (*hsdr-1*) locus, originally defined by mice homozygous for the c^{14CoS} or c^{3H} deletions, is defined phenotypically by perinatal death of deletion homozygotes (Erickson, 1968). *hsdr-1* mutants have defective expression of several liver-specific enzymes during late gestation (reviewed in Gluecksohn-Waelsch, 1979). Originally thought to encode a *trans*-acting liver-specific regulatory protein, the gene responsible for the *hsdr-1* phenotype has recently been shown to encode the fumarylacetoacetate hydrolase (*Fah*) gene (Klebig et al., 1992b; Ruppert et al., 1992; Kelsey et al., 1993). The locus has subsequently been redesignated *Fah*, and will appear as such in all figures except Fig 1.

* All figures and tables are in the Appendix unless otherwise noted.

Mice homozygous for the c^{20FATw} deletion, as well as compound heterozygotes of certain other deletions, are slightly growth-retarded and have decreased overall viability (Lewis, 1978; Russell et al., 1982). Additionally, male mutants have defects in spermiogenesis and are sterile; however, female mutants can conceive progeny, but spontaneously abort at mid-gestation (Lewis, 1978). Based on the displayed phenotype, this locus has been designated the *juvenile development and fertility* or *jdf* locus.

Two separate loci located distal to *c* appear to be necessary for early embryonic development. Mice homozygously deleted for the *embryonic ectoderm development* (*eed*) locus (c^{11DSD}, $c^{5FR60Hg}$, or c^{2YPSj} deletion homozygotes) die at embryonic day 8.5 (designated "day E8.5") (day of vaginal plug detection is designated E0.5) from an apparent failure to form the embryonic ectoderm (Niswander et al., 1989), whereas homozygous removal of the more distal *extraembryonic ectoderm development* (*exed*) locus (c^{6H} or $c^{4FR60Hd}$ deletion homozygotes) results in embryonic death a full day earlier, at day E7.5, due to a failure of the extraembryonic ectoderm to form (Niswander et al., 1989).

Thus, the loci identified in the *Fes-Hbb* region through complementation analyses affect a wide range of developmentally important functions, and cloning and characterization of the genes responsible for these phenotypes should contribute to our understanding of mammalian development. A number of DNA probes have been mapped to the *Fes-Hbb* region (summarized in

Rinchik and Russell, 1990; Holdener et al., 1993); the inherent advantages of overlapping deletion mutations for physical mapping and gene isolation suggest that these loci could be efficiently identified by positional cloning.

It is important to note that complementation-defined loci within this region are identified by phenotypes resulting from homozygous deletion of an interval of DNA, and are defined only by regions of overlap among deletions. Therefore, these phenotypes could result from the deletion and/or disruption of more than one gene. Additionally, phenotypes expressed very early in development may be masking the effects of later-acting genes that may also be deleted or disrupted by a particular deletion. Thus, other strategies must be utilized to complete the functional maps of regions characterized through complementation analyses with overlapping deletions.

Refining the Functional Map of the *c* Region by ENU Saturation-Mutagenesis

A saturation-mutagenesis experiment designed to refine the functional map of the 6- to 11- cM region of mouse Chr 7 spanned by the *c* deletions has recently been concluded (Rinchik et al, 1990; Rinchik and Carpenter, in preparation). The mutagenesis protocol utilized the spermatogonial point mutagen *N*-ethyl-*N*-nitrosourea

(ENU) in conjunction with a breeding strategy designed to identify genes by hemizygously expressing newly induced recessive point mutations opposite the large c^{26DVT} deletion. Once identified, newly identified loci were mapped to specific subregions of the *c* deletion complex by *trans*-complementation analyses with the overlapping *c* deletions. This mutagenesis strategy, described in detail in Rinchik et al, 1990, will be briefly reviewed below.

BALB/cRl males (G_0 generation), homozygous for the albino mutation of the tyrosinase gene (*c*/*c*), were treated with the presumed point mutagen ENU and then mated to wild-type (C57BL/10Rl X C3Hf/Rl)F_1 females (+/+). G_1 offspring generated from these crosses (+ +/*c* *) (where * represents any newly induced point mutation) all carry a mutagenized paternal genome including a mutagenized Chr 7 marked with the albino mutation. Such G_1 females were then mated to mice (c^{ch} +/c^{26DVT}) heterozygous for a 6- to 11-cM deletion surrounding the *c* locus. The genotypic classes of progeny generated from these crosses could be categorized based on pigmentation (detectable at birth through eye color and later by coat color): + +/c^{ch} + and + +/c^{26DVT} mice display wild-type pigmentation, c^{ch} +/*c* * are light chinchilla and are carriers of any newly induced point mutations, and *c* */c^{26DVT} offspring are albino. Additionally, the *c* */c^{26DVT} class will hemizygously express any newly induced recessive point mutation that maps within the region spanned by the c^{26DVT} deletion. Therefore, the albino class of progeny were observed at birth and at weaning for unusual appearance or behavior. The

absence of albino progeny in matings producing 30 or more offspring was also of note: this indicated a newly induced lethal mutation had been recovered. Once identified, any newly induced mutation could be recovered and maintained through the light chinchilla class (c^{ch} +/c *) or the G_1 parent (+ +/c *).

The mutagenesis strategy described above is primarily a screen for mutations expressed up to weaning age and, therefore, detects genes with roles in early development. A total of 31 independent heritable mutations defining at least eight complementation groups and specifying six previously unidentified loci in the *Fes-Hbb* region have resulted from these mutagenesis experiments (Rinchik et al 1990; Rinchik and Carpenter, 1993; Rinchik and Carpenter, in preparation). Included among the newly identified loci are at least five defined by mutations resulting in prenatal lethality [*l(7)1Rn*, *l(7)2Rn*, *l(7)3Rn*, *l(7)4Rn* and *l(7)6Rn*], mutations at the previously defined *shaker 1* (*sh1*) locus and complementation-defined *eed* locus [*l(7)5Rn*], and mutations causing growth retardation and reduced viability [*fitness 1* (*fit1*)]. Therefore, cloning and characterization of genes identified through these experiments should provide insights into a variety of pathways essential for normal development.

By design of this hemizygosity screen, any newly identified recessive mutation must map within the region spanned by the c^{26DVT} deletion. Furthermore, each new locus can be mapped to a more specific subregion of the *c* deletion complex through *trans*-

complementation crosses to mice heterozygous for various *c* deletions. A specific map position defined by deletion breakpoints, the availability of several DNA probes in the *c* region, and the inherent advantages of deletion mutations as tools for chromosome walking and/or jumping suggests that any newly identified gene resulting from the saturation-mutagenesis experiments should be amenable to positional-cloning strategies. Additionally, since ENU-induced mutations are presumably point mutations (and therefore intragenic) (*e.g.*, Popp et al., 1983; Batzer et al., 1988; Pastink et al., 1989), characterization of the mutant phenotypes associated with newly recovered mutations should provide crucial insights into the increasingly important task of associating biological functions with specific DNA sequences.

The *fit1* Locus and Growth-Retardation Syndromes

Five independent, non-complementing mutations identified through the mutagenesis experiments result in growth retardation and reduced viability and define a locus designated *fitness-1* (*fit1*). Mice homozygous or hemizygous for any of the five *fit1* mutations (designated $fit1^{494SB}$, $fit1^{764SB}$, $fit1^{3452SB}$, $fit1^{4226SB}$, and $fit1^{4397SB}$) are growth retarded and have shortened lifespans. Several mutations causing retarded growth or dwarfism have been described in the mouse and are thought to be representative of a number of disorders

in humans (Green, 1989). Although few genes causing dwarfism have been characterized, several different mutant phenotypes have been biologically and biochemically analyzed, and these studies have indicated that the causes of dwarfism can be diverse and complex.

For example, mice homozygous for mutations in the hypothyroid gene (*hyt*; Chr 12) are dwarfed, infertile, mildly anemic, have elevated serum cholesterol, undetectable serum thyroxine, and elevated serum thyroid-stimulating hormone (TSH) (Green, 1989). The phenotype is thought to be due to unresponsiveness of the mutant thyroid glands to TSH. These animals have been used as thyroid-deficient models in investigations of the effects of thyroxin on development of various systems (Beamer et al., 1981; Beamer and Cresswell, 1982).

Mutations in the cartilage matrix deficiency gene (*cmd*; Chr 7) also cause dwarfism in homozygotes. Mutant animals have an unusually short trunk and limbs, a cleft palate, and die shortly after birth (Rittenhouse et al., 1978; Green, 1989). Studies have shown that these mice fail to synthesize the core protein of cartilage-characteristic proteoglycan (Kimata et al., 1981; Brennan et al., 1983). This syndrome resembles the lethal condition achondrogenesis, and other osteochondrodysplasias in man.

Mice homozygous for the Hertwig's anemia gene (*an*; Chr 4) are dwarfed at birth, anemic, and rarely live beyond a few days after birth (Green, 1989). Any survivors remain anemic, are sterile, and have significantly reduced white blood cell counts (Bannerman et al.,

1973). Hematopoietic precursor populations decrease with maturation, and transplantation studies indicate that the mutation is cell autonomous (Bernstein, 1975). Abnormal mitotic figures have been detected in several hematopoietic tissues and is thought to result in the loss of germ cells during development (Eppig and Barker, 1983).

Snell's dwarf (*dw*; Chr 16) homozygotes show marked growth retardation and are sterile. The small size is due to a defective anterior pituitary in which there is a deficiency of growth hormone (GH)-producing cells. These animals are models for several human disorders including familial pan-hypopituitarism, growth hormone deficiencies, and Laron-type dwarfism. Recently, it has been shown that the *dw* gene encodes the POU-domain [*Pit-1*, *Oct-1*, *Oct-2*, *unc-86* (Herr et al., 1988)] transcription factor, *Pit-1* (Camper et al., 1990; Li et al., 1990). Indications are that this transcription factor is necessary for the differentiation of the somatotroph, lactotroph, and thyrotroph cell types present in the anterior pituitary.

As demonstrated by the examples above, growth retardation can be the result of mutations affecting a wide range of systems. Mutations causing dwarfism could conceivably affect transcriptional or translational processes, hormone synthesis, structural proteins, storage or release systems, hormone receptors and post-receptor signals, metabolizing enzymes, etc. Thus, phenotypic characterization of *fit1* mutants, as well as cloning and characterization of the *fit1* gene, could provide insights into any of a

wide variety of developmental pathways and could provide insights into similar human disease conditions.

A Strategy for the Molecular and Phenotypic Characterization of the *fit1* Locus.

The *fit1* locus has been mapped by *trans*-complementation analyses to a specific subregion of the *c*-deletion complex defined by the distal breakpoints of the c^{3DENb}, c^{AL}, and c^{202G} deletions (proximally) and the c^{11DSD} and $c^{24R145L}$ deletions (distally) (Potter et al, submitted; see Section V.). Several DNA probes have recently been mapped to the proximal region of the *c*-deletion complex near the proximal breakpoints of some of the deletions defining the *fit1* interval (Rinchik and Russell, 1990). Thus, one possible strategy for gaining molecular access to the *fit1* locus is to use existing DNA probes to identify and clone the breakpoints of any of the deletions defining the *fit1* interval. Derivation of probes from the distal end of the $c^{24R145L}$ and/or c^{11DSD} deletions would provide a probe(s) mapping distal to or within the *fit1* locus, whereas cloning any one of the c^{3DENb}, c^{AL}, or c^{202G} deletion breakpoints would provide a probe(s) proximal to the locus. Once molecular access to the region is obtained, long-range mapping experiments utilizing pulsed-field gel electrophoresis (PFGE) can be used to estimate the physical size of the *fit1* interval (as defined by deletion breakpoints). The physical

size of the *fit1* region will dictate the most appropriate methods for isolating potential candidate cDNAs from the interval (reviewed in Parrish and Nelson, 1993).

Analysis of the *fit1* mutant phenotype will be important for determining the normal function of the *fit1* gene in development. Also, biological characterization of *fit1* mutants could be useful in the search for the *fit1* gene, by providing information pertaining to the stages of development and the tissues in which the gene product might act. Continued analysis of the biology of the *fit1* phenotype, in conjunction with molecular analysis of the gene, should also provide insight into an early-acting pathway essential to normal early development. It should be noted that, through a limited number of initial experiments, it may prove difficult to define the primary underlying defect of a "reduced fitness" syndrome. Growth retardation can result from a number of different genetic and environmental conditions, and even when specific abnormalities are demonstrated between mutant and normal animals, it is many times not possible to determine whether these differences are directly attributable to a mutation or are indirect manifestations of the primary defect. Therefore, since growth retardation could be caused by disruption of any one of a number of different pathways (Green, 1989), initial analyses should be designed to examine several different systems. Characterization of mutant growth patterns and macro- and microscopic observations of a variety of tissues from mutant animals should contribute to characterization of the mutant

phenotype, and preliminary indications from these types of initial studies should lead to further, specific, in-depth analyses necessary to define the primary defect.

II. MATERIALS AND METHODS

Mice

All stocks used in this study were bred at the Biology Division of Oak Ridge National Laboratory. The *albino* deletion mutations [designated Df(*c*)] used in the complementation analyses are maintained in the heterozygous state opposite the chinchilla allele (c^{ch}) of the albino (*c*) locus. Deletion heterozygotes [c^{ch}/Df(*c*)] display a light-chinchilla coat color, in contrast to the darker, full-chinchilla coat color in c^{ch}/c^{ch} mice. Additionally, ENU-induced *fit1* mutations generated from the saturation-mutagenesis experiments (Rinchik et al., 1990; Potter et al., submitted) are maintained opposite the c^{ch} allele on a chromosome marked with the *c* mutation (i.e. c^{ch} +/*c fit1*). For the experiments described in this report, the *fit1* mutations were maintained by mating carriers to either the 47BS inbred strain, which is homozygous for the chinchilla allele (c^{ch} +/c^{ch} +), or the outbred FR-*p* c^{ch} *fr*/*p* c^{ch} *fr* strain, which is homozygous for mutations at three linked loci: the pink-eyed dilution mutation (*p*), the chinchilla allele at *c*, and the frizzy mutation (*fr*) (the genetic distances between these loci are: *p*--14cM--c^{ch}--10-20cM--*fr*). Mice homozygous for these three loci have a distinctive appearance, described as a "light orange", creamy-colored fur with kinky vibrissae. Thus, *fit1* mutations are also maintained in such a way that carriers are readily identified by coat color. For those mated to

the 47BS strain, such crosses (c^{ch} +/c *fit1* X c^{ch} +/c^{ch} +) yield light-chinchilla progeny that presumably carry the *fit1* mutation (c^{ch} +/c *?fit1*) as well as mice that are dark chinchilla in color (c^{ch} +/c^{ch} +). For those carriers mated to the FR strain, crosses (c^{ch} +/c *fit1* X *p* c^{ch} + *fr*/*p* c^{ch} + *fr*) also generate light-chinchilla, presumed carriers (+ *c fit1* +/*p* c^{ch} + *fr*) and, in the F_1 generation, chinchilla mice (+ c^{ch} + +/*p* c^{ch} + *fr*). However, the advantage of mating *fit1* carriers to the FR stock becomes apparent in subsequent generations. + *c fit1* +/*p* c^{ch} + *fr* carriers mated to *p* c^{ch} + *fr*/*p* c^{ch} + *fr* animals should generate two classes of mice: *p* c^{ch} + *fr*/*p* c^{ch} + *fr* (which display the distinctive FR phenotype) and *p* c^{ch} + *fr*/+ *c fit1* + (light-chinchilla with normal vibrissae). Only an unlikely double crossover event could generate a light chinchilla mouse from this cross that did not carry the *fit1* mutation (*p* c^{ch} + *fr*/+ *c* + +). Additionally, other recombinant classes are detectable: *p* c^{ch} + *fr*/+ *c ?fit1 fr* (light chinchilla color, kinky vibrissae) and *p* c^{ch} + *fr*/*p* c^{ch} *?fit1* + (FR coat color, but normal vibrissae). These progeny may or may not still carry the *fit1* mutation, and, although progeny testing could determine this (by mating to c^{ch} +/c^{26DVT} mice and looking for dwarfed albinos, see below), these recombinant classes were discarded.

Presumed *fit1* carriers (from either the 47BS line or the FR line) were confirmed by mating them to c^{ch} +/c^{26DVT} deletion heterozygotes. The c^{26DVT} deletion mutation removes a 6- to 11-cM segment surrounding the *c* locus, and, by design of the mutagenesis

strategy, must include the *fit1* locus (Rinchik et al., 1990). If albino offspring (*c fit1/c*^{26DVT}) exhibiting the *fit1* dwarfing phenotype were obtained when a presumed *fit1* carrier (*c*^{ch} *+/c ?fit1*) was mated to a *c*^{ch} *+/c*^{26DVT} animal, then that carrier was considered proved to carry *fit1*. Presumed carriers generated from the 47BS matings were tested each generation; however, since presumed carriers resulting from FR matings could only lose the *fit1* mutation through a rare double crossover event, these mice were only tested every third generation.

Complementation analyses were performed by mating such proved carriers of the prototypic *fit1* mutation, designated 494SB, (*c*^{ch} *+/c fit1*^{494SB}) to mice carrying specific *c* deletions [*c*^{ch} +/Df(*c*)]. One quarter of the offspring from such a cross should be albino and carry the *c fit1*^{494SB} chromosome opposite a *c* deletion chromosome [*c fit1*/Df(*c*)].

Growth Analyses

The methods used in gathering data to define the growth parameters of *fit1* mutants and their normal littermates were adapted, with modifications, from Hughes and Tanner, (1970). Tested carriers (from the 47BS lines) of each of the five *fit1* mutations (*c*^{ch} *+/c fit1*^{494SB}, *c*^{ch} *+/c fit1*^{764SB}, *c*^{ch} *+/c fit1*^{3452SB}, *c*^{ch} *+/c fit1*^{4226SB}, and *c*^{ch} *+/c fit1*^{4397SB}) were mated to mice heterozygous for the *c*^{26DVT}

deletion (c^{ch} +/c^{26DVT}). Pregnant females were checked daily for litters; at birth the number of offspring was recorded for individual litters, and each offspring was sexed and genotyped. At birth, genotypes were based on eye pigmentation: c^{ch} +/c^{ch} +, full eye pigmentation; c^{ch} +/*c fit1* or c^{ch} +/c^{26DVT}, light eye pigmentation; and *c fit1*/c^{26DVT}, no eye pigmentation. Subsequent to coat appearance, genotypes were based on coat color: c^{ch} +/c^{ch} +, full chinchilla; c^{ch} +/*c fit1* or c^{ch} +/c^{26DVT}, light chinchilla; and *c fit1*/c^{26DVT}, albino (and dwarfed). Since *fit1* mutants are smaller, "less fit", and are not able to compete for suckling as well as normal littermates, the litter sizes were reduced to four or five pups to enhance the survival of the *fit1* mutants. Also, reducing the litter sizes to a common number may minimize variability among litters due to different numbers of offspring (Hughes and Tanner, 1970). Although measurements were made for offspring of all genotypes, in the data presented in this study, only homozygous wild-type mice (c^{ch} +/c^{ch} +) are considered as a "control". Additionally, in reducing litter sizes, heterozygous wild-type mice [(c^{ch} +/*c fit1*) and (c^{ch} +/c^{26DVT}), which are phenotypically indistinguishable] were preferentially discarded. Each of the remaining offspring were subsequently identified by a number marked on the belly with a "VWR Lab Marker" (VWR Scientific, San Francisco, CA). The weight, nose-to-rump (body length), and rump-to-tip of tail (tail length) measurements were recorded for each animal on the day of birth and then every other day thereafter up to at least 32 days of age,

or until the *fit1* mutant(s) in each litter died (usually much earlier than 32 days). Weights were measured on a Mettler AE 100 Analytical Balance (Switzerland) or an American Scientific Products DTL 2500G Balance (Denver, CO). Body and tail length measurements were made by grasping each mouse by the scruff of the neck with one hand and grasping the tail with the thumb and forefinger of the other hand; the mouse is then held with body and tail straight and placed firmly to a metric rule.

The weights of 14.5-day (E14.5) fetuses were recorded only for $fit1^{4397SB}$ mutants and their normal littermates. Males carrying the $fit1^{4397SB}$ mutation (c^{ch} +/c $fit1^{4397SB}$) were mated to c^{ch} +/c^{26DVT} females; females were checked daily for vaginal plug. Detection of vaginal plug was denoted as E0.5, and on E14.5, pregnant females were sacrificed and uterine contents were examined. Each animal was classified as either a *fit1* mutant or as a wild-type fetus based upon eye pigmentation: c $fit1^{4397SB}/c^{26DVT}$ fetuses have no eye pigmentation, whereas c^{ch} +/c^{ch} +, c^{ch} +/c^{26DVT}, and c^{ch} +/c $fit1^{4397SB}$ fetuses all have eye pigmentation. Homozygous wild-type fetuses can be distinguished from the two classes of heterozygous wild-type fetuses; the eye pigmentation of homozygous wild-type fetuses is darker than that of the heterozygous wild-type fetuses (by virtue of the expression of two copies of the c^{ch} allele in homozygotes, versus one copy in the heterozygous wild-types). However, in these analyses, no attempt was made to distinguish these classes of wild-

type fetuses and the weights of these groups was assumed not to differ significantly.

Histology

All tissues, unless otherwise noted, were removed at sacrifice to a solution of 10% buffered formalin [10% formaldehyde in distilled water, buffered with sodium phosphate monobasic (NaH_2PO_4) and sodium phosphate dibasic (Na_2HPO_4) to pH 7.0]. Tissues were then embedded in paraffin, cut into 5-10μm sections, mounted on glass slides and stained with hematoxylin and eosin. Stained tissues were then examined by light microscopy.

Blood films were prepared by removing blood from the intraorbital sinus of anesthetized *fit1* mutants and wild-type littermates. For anesthesia, mice were placed in a small chamber containing Metofane® (Methoxyfluorane, Pittman-Moore Inc., Washington Crossing, NJ) for approximately 2-4 minutes. The blood was then either placed directly on #1 coverslips and spread, or transferred to a microtainer tube containing 5 μl 1.5% EDTA and then spread on a #1 coverslip. Air-dried blood films were stained with Wright's stain and mounted on glass slides for examination by light microscopy.

Hematology

Blood samples were taken from *fit1* mutants and normal littermates as described above. Hematocrit values were determined manually for some mice by centrifugation of blood in microhematocrit capillary tubes. The majority of hematocrit and hemoglobin values were determined by analysis on an Ortho ELT-15 laser-based Hematology Analyzer (Ortho Diagnostics), modified to optimize the analysis of mouse blood (Popp et al., 1986).

White blood cell counts were performed by diluting peripheral blood in Turk's WBC diluting solution (1% Crystal violet, 1% acetic acid, in distilled water) on a standard hemocytometer. For reticulocyte counts, peripheral blood was removed to New Methylene Blue, smeared on coverslips, and counter stained with Wright's stain.

For all *in vitro* progenitor cell assays, single-cell suspensions of spleen and bone marrow tissues in αMEM media (Difco, Detroit Michigan) were cultured in 0.8% Alpha Methylcellulose-Complete Ready-Mix, containing methylcellulose, fetal calf serum, bovine serum albumin, erythropoietin and conditioned medium in alpha medium plus nucleosides (Terry Fox Laboratory, British Columbia, Canada). For CFU-E analyses, 0.1 ml aliquots of a 4 X 10^5 cells/ml solution (for both spleen and bone marrow tissues) were plated in 96-well culture plates and incubated at 37°C and 5% $C0_2$ in air for two days. For bone marrow BFU-E experiments, 1-ml aliquots of a 5 X 10^4

cells/ml solution were plated in 6-well culture plates and cultured at 37°C and 5% CO_2 in air for 7-10 days. BFU-E analysis for spleen cells was carried out as described for bone marrow with the exception that 1-ml aliquots of a 5 X 10^5 cells/ml solution were plated. Five wells were plated for each sample, and the values presented are based upon the mean number of progenitors obtained from counting 2-4 wells of each sample.

The spleen colony assay was performed as described (Till and McCulloch, 1961) to assess the number of CFU-S in the bone marrow of *fit1* mice and wild-type controls. Single-cell suspensions of bone marrow cells in calcium- and magnesium-free phosphate-buffered saline (PBS) were prepared and the total bone marrow cellularity determined. For CFU-S analysis, groups of irradiated *scid/scid* mice (0.7 Gy/min, for a total of 2.5 Gy) received either 1 X 10^5 wild-type cells in PBS per mouse, 2 X 10^5 *fit1* cells per mouse, or PBS only (this served as a radiation control group), and were kept in isolation for 14 days. At that time, all mice were sacrificed, spleens were removed, fixed in Telly's fixative (100 parts 70% ethanol, 5 parts formaldehyde, 5 parts acetic acid), and CFU-S colonies were enumerated.

Flow-cytometry studies were performed with spleen and bone marrow cells in PBS supplemented with 0.1% sodium azide and 0.1% bovine serum albumin that had been incubated on ice with 1 mg anti-mouse monoclonal antibodies to Thy 1 and B220 (CD45R). The antibodies were labeled by the manufacturer (Pharmingen) with phycoerythrin (PE) (B220) or fluoroisothiocyanate (FITC). After

incubation with antibodies, cells were washed three times with the PBS solution to remove unbound antibody.

Genomic DNA Isolation, Southern-Blot Analyses, and Pulsed-Field Gel Electrophoresis

High-molecular weight DNA was prepared from either adult liver or spleen and was analyzed by Southern blotting and hybridization as previously described (Rinchik et al., 1989; Klebig et al., 1992b; Rinchik et al., 1993). Preparation of genomic DNA, electrophoresis protocols, blotting of gels, and hybridizations suitable for pulsed-field gel electrophoresis (PFGE) were as previously described (Klebig et al., 1992b). Specific electrophoresis conditions for individual PFGs are described in figure legends.

Hybridization Probes

All DNA probes used in this study are described in Table 1. The purification of DNA clones, recovery of insert DNA fragments, and radiolabeling of DNA fragments for use as hybridization probes were done using standard protocols (Ausubel et al., 1989; Maniatis et al., 1982). Whole cosmid clones used as DNA probes were preassociated at 65° C for 120 minutes with total mouse genomic

DNA, sonicated to an average fragment size of 200 bp, added to a final concentration of 0.5 mg/ml.

Yeast Artificial Chromosome (YAC) Clones

The YAC clones used in this study, designated D6E7 and D18H2, were isolated from the Princeton Mouse YAC library (Burke et al., 1991), and were obtained as a generous gift from T. Magnuson and B. Holdener (Holdener et al., in preparation).

Yeast DNA was prepared in agarose plugs, and in liquid preparations, as described (Smith et al., 1986). Complete digestion of yeast DNA agarose blocks was performed as described above for mouse genomic DNA in agarose blocks (Klebig et al., 1992b). Partial digests of yeast DNA blocks was performed as described in Burke et al., (1987).

Cosmid Library Construction and Libraries Screened

Separate cosmid libraries were constructed from YACs D6E7 and D18H2 partially digested DNAs in a *Pvu*II-*Bam*HI-digested pCOS2EMBL vector (Ehrich et al., 1987) using standard procedures (Ausubel et al., 1989; Maniatis et al., 1982). Briefly, for each library, approximately 100 μg of yeast DNA was partially digested with the

*Mbo*I restriction enzyme and size selected by gel electrophoresis. Fractions of partially digested yeast DNA that contained fragments suitable in size for cloning into cosmids (30-45 kb) were pooled, phosphatased by incubation with calf alkaline phosphatase, and cloned into the pCOS2EMBL vector. Cosmid-insert ligations were packaged *in vitro* (Gigapack Gold; Stratagene) using standard protocols (Ausubel et al., 1989; Maniatis et al., 1982), and were plated in DH5αmcr- cells (BRL).

Additional libraries screened were: (1) a cosmid library (D. Johnson, unpublished) made from a mixture of 129/Rl and C3Hf/Rl splenic DNA, partially digested with *Sau*3A, and cloned in a *Sma*I-*Bam*HI-digested c2RB vector (Bates and Swift, 1983); (2) a cosmid library (M. Mucenski, unpublished) constructed with *Mbo*I partially digested 129/Sv splenic DNA cloned into a *Pvu*II-*Bam*HI cut pCOS5EMBL vector (Ehrich et al., 1987); (3) a cDNA library (L. Stubbs, unpublished) made from size-selected, E14.5 whole-fetus mRNA, prepared by standard procedures (Ausubel et al., 1989) and cloned in λgt10 phage vector (Stratagene); and (4) a cDNA library made from E8.5 whole-embryo mRNA, described elsewhere (Fahrner et al., 1987).

Northern Blot Analysis

The Northern blots screened contained poly-(A+) RNA prepared, electrophoresed, and blotted by standard procedures (Ausubel et al., 1989; Aviv and Leder, 1971). Northern blots of *fit1* mutant (*c fit1/c*^{26DVT}) and littermate control (c^{ch} +/c^{ch} +) poly-(A+) RNA were graciously prepared by C. Culiat. Additionally, a Northern blot of poly-(A+) RNA from E14.5 fetuses was kindly provided by D. Johnson. Two Northern blots containing poly-(A+) derived from adult spleen tissues and skin were generously provided by P. Blair.

Exon Amplification Analyses

The pSPL1 vector has been described (Buckler et al., 1991). Additionally, all exon amplification methods, including cell culture, cloning, electroporation, RNA isolation, and RNA/PCR amplification, were performed as described (Buckler et al., 1991).

III. RESULTS: PHENOTYPIC CHARACTERIZATION

fit1 Mutants are Retarded in Growth Postnatally

The *fit1* mutations were originally detected in the saturation mutagenesis screen because progeny carrying a mutagenized Chr 7 opposite the c^{26DVT} deletion were dwarfed as compared to other G_2 littermates (Rinchik et al., 1990). Other than the observed growth retardation at the time of weaning and an observed reduced fitness or viability [most mutants die by weaning age (D.A. Carpenter, M.D.P., E.M. Rinchik personal observation)], nothing was known about the *fit1* phenotype.

To define the growth characteristics of *fit1* mutants, carriers of each of the five *fit1* mutations (c^{ch} +/c $fit1^m$, where *m* represents any one of the *fit1* alleles: 494SB, 764SB, 3452SB, 4226SB, or 4397SB) were mated to c^{ch} +/c^{26DVT} deletion heterozygotes, and the resulting *fit1*-mutant (c $fit1^m/c^{26DVT}$) and wild-type (c^{ch} +/c^{ch} +) progeny were weighed at birth and every other day thereafter through 30-32 days of age. Also at the time of weighing, additional growth parameters, the nose-to-rump (body) and rump-to-tip of tail (tail) lengths, were recorded for each animal.

The measured weights of *fit1* and wild-type mice (Fig 3 and Table 2) show that all *fit1* mutants are growth retarded at birth, as compared to normal littermates, and remained dwarfed throughout

the recording period. Interestingly, there appears to be a range of severity of growth retardation among the five alleles of *fit1*. Mutants expressing the *fit1*^{4397SB} allele are more severely growth retarded than mice expressing any of the other four alleles. Based on these weight measurements (Table 2), *fit1*^{4397SB} mutants are estimated to be, on average, 61.1% the size of normal littermates at birth, and an average of 20.4% of the normal size at weaning (26-30 days of age). In contrast, mutants expressing the *fit1*^{4226SB} allele appear to be the least growth retarded of the five *fit1* mutants. *fit1*^{4226SB} mutants are estimated to be an average of 75.0% of normal at birth and 56.3% of normal size at weaning (Table 2). The remaining three alleles are intermediate to these extremes, with *fit1*^{494SB} mutants usually more severely affected than either *fit1*^{764SB} or *fit1*^{3452SB} mutants. Therefore, *fit1* mutants are growth retarded at birth, but the degree of growth retardation, as compared to a normal littermate, apparently increases with age (see Fig. 3).

Body length and tail length have previously been used as growth parameters, and the body length plotted versus tail length as one parameter of shape, or proportionality (Hughes and Tanner, 1970). The body length and tail length measurements of *fit1* mutants and littermate controls (Tables 3 and 4, respectively, and Figs. 4 and 5, respectively) also demonstrate growth retardation of all the *fit1* mutants. These data also suggest that *fit1*^{4397SB} mutants are the most severely affected and that *fit1*^{4226SB} mutants are the least affected. The mean body length of mice expressing the *fit1*^{4397SB}

mutation is approximately 81.1% that of controls at birth, and 63.5% of control body length at weaning age (26 days), whereas the mean body length of *fit1*^{4226SB} mutants is 90.9% and 82.6% of control at birth and weaning age, respectively. The mean tail lengths reflect a similar pattern: *fit1*^{4397SB} mutants are 74.8% (birth) and 63.4% (weaning) of control and *fit1*^{4226SB} mutants are 86.6% (birth) and 83.5% (weaning) of control. Additionally, the body length versus tail length plot, as a measure of proportionality, does not show significant differences between *fit1* mutants and normal littermate controls (Fig 6). Therefore, these data support the observation that *fit1* mutants are growth retarded, and also suggest that *fit1* mutants are proportionately dwarfed. Based on these weight, body, and tail measurements, the *fit1* mutations may be ordered with respect to the severity of growth retardation as follows (listed in order of most-severely affected to least-severely affected): 4397SB > 494SB > 764SB > 3452SB $\geq$ 4226SB > control.

Mice expressing any of the *fit1* mutations died at various times from birth up to, or shortly after, weaning age (D.A. Carpenter, M.D.P. personal observation) and, therefore, the lifespan for *fit1* mutants appears to be shortened, although extremely variable. In concordance with the observed range of severity of growth retardation among the five *fit1* alleles, the more severely growth retarded animals (mutants expressing the *fit1*^{4397SB} or *fit1*^{494SB} alleles) usually died earlier than those less severely affected (mutants expressing the *fit1*^{764SB}, *fit1*^{3452SB} or *fit1*^{4226SB} alleles).

fit1 Mutants are Growth Retarded *in utero*

The data reported above showing that *fit1* mutants are smaller at birth suggests that *fit1* mutants may also be growth retarded *in utero*. Intrauterine growth retardation (IUGR) is a significant problem in humans and can result from a number of genetic and/or environmental insults (reviewed in Evans, 1983). Therefore, determining whether *fit1* mutants are dwarfed *in utero* would not only provide further information about the function of the *fit1* gene, but could also suggest *fit1* mutants be considered a model of at least one type of IUGR.

Mice heterozygously carrying the c^{26DVT} deletion (c^{ch} $+/c^{26DVT}$) were mated to tested carriers of the $fit1^{4397SB}$ mutation (c^{ch} $+/c$ $fit1^{4397SB}$) and checked daily for vaginal plugs. Pregnant females were sacrificed at 14.5 days (E14.5) of gestation (date of vaginal plug detection is designated as E0.5), and the uterine contents were examined. *fit1* mutants are easily distinguishable at this point of gestation due to the expression of the closely linked albino mutation (see Materials and Methods). Each embryo was removed from the uterus, classified genotypically (mice lacking eye pigmentation, c $fit1/c^{26DVT}$; those with eye pigmentation, c^{ch} $+/c^{ch}$ $+$, c^{ch} $+/c^{26DVT}$, or c^{ch} $+/c$ *fit1*; note that c^{ch} $+/c^{26DVT}$ and c^{ch} $+/c$ *fit1* mice are indistinguishable; see Materials and Methods), and weighed. The results from these analyses, shown in Fig. 7, indicate that $fit1^{4397SB}$

mutants are an average of 70.2% the size of normal littermates at E14.5. A representative E14.5 *c fit1*^{494SB}/*c*^{26DVT} mutant and a wild-type littermate, which show this IUGR, are shown in Fig. 8. Thus, the *fit1* gene is not only necessary for postnatal growth and viability, but also for proper intrauterine growth. It should be noted that, as indicated above, *fit1* mutants, although dwarfed *in utero*, apparently become more severely affected, relative to controls, as development progesses from birth to weaning age.

Macroscopic and Microscopic Observations of *fit1* Mutants

In a further effort to identify a possible underlying cause of *fit1* growth retardation, necropsies of *fit1* mutants and littermate controls were performed. (These investigations were initiated under the guidance of V. Godfrey, D.V.M.) Macroscopic observation of the internal structure of *fit1* mutants revealed that the organs appear normally developed, but are proportionately smaller as compared to organs of normal littermates. One exception was that splenomegaly was observed in most *fit1* animals. The data in Table 5 show that, on average, spleens from *fit1* mutants compose approximately 2.0% of the mutant body weight, whereas the mean weight of normal littermate spleens is 0.42% of mean control body weight.

Enlargement of the spleen (splenomegaly) can result from a number of conditions, including infectious, metabolic, circulatory, endocrine, neoplastic, and mechanical disorders; therefore, an

observation of splenomegaly is not itself indicative of a particular condition, and warrants further investigation (Wintrobe et al., 1974; Miale and Rywlin, 1977; Leeson and Leeson, 1981). Microscopic investigation of the structure of *fit1* spleen tissue, as well as other *fit1* mutant tissues including the endocrine and hematopoietic organs, are necessary to gain further insights into the pathology of the *fit1* phenotype.

Therefore, histological sections of *fit1* mutant tissues, including peripheral blood smears, were observed for any apparent abnormalities. Mature red blood cells (RBCs) in the peripheral blood are usually circular in shape, uniform in diameter, and their biconcave shape leads to darker staining at the periphery and a "ringed" appearance (Fig. 9A; Hayhoe and Flemans, 1970). The peripheral blood also usually contains a small number ($\leq$1-2% in adult mice, and a slightly higher percentage in weaning-aged mice) of reticulocytes, a mature RBC precursor that retains the remnants of darkly staining ribosomal RNA for 1-2 days in the periphery. In contrast, the peripheral blood of *fit1* mutants displays a wide range of RBC size (anisocytosis), shape (poikilocytosis), and depth of staining (hypochromia) (Fig. 9B). Additionally, there appears to be a significantly increased number of reticulocytes and a significantly decreased number of white blood cells (WBCs) in *fit1* peripheral blood (Table 6).

No obvious abnormalities were observed in weaning-aged *fit1* mutant endocrine organs (V. Godfrey, personal communication;

data not shown). However, consistent with the observed splenomegaly and the peripheral blood defects, sections from *fit1* mutant spleens were found to have increased hematopoietic activity (see Fig. 10). Histological sections from a normal spleen (c^{ch} +/c^{ch} +) (Fig. 10A) reveal the characteristic organization of the tissue into areas of white pulp, which is the site of lymphoid cell production (T and B cells), and the surrounding areas of red pulp, which are the sites of erythropoiesis. In splenic sections prepared from *fit1*^{4397SB} mutants, hyperplasia of the regions surrounding the white pulp is obvious as compared to controls (Fig. 10B). This hyperplasia presumably represents a response to an increased demand for mature RBCs. Areas of white pulp, however, are smaller and less distinct; this may be due either to the extensive red-pulp hyperplasia "overrunning" the white pulp areas or to a deficiency of lymphoid cell production.

The primary site of hematopoiesis in adult mammals is the bone marrow. Although some hematopoietic activity is normal in the spleens of adult animals, the finding of increased extramedullary hematopoiesis in *fit1* spleen tissue suggested that *fit1* bone marrow should also be examined for abnormalities of hematopoiesis. In normal marrow, hematopoietic cells of all lineages, although primarily of erythroid and myeloid lineages (*e.g.*, erythrocytes, granulocytes, megakaryocytes, etc), and all stages of differentiation within each lineage may be found dispersed throughout the tissue. Bone marrow from a *fit1*^{4397SB} mutant appears similar to wild-type

littermate bone marrow (Fig 11A and 11B), although the overall size of a *fit1*-mutant femur is much smaller than that of an age-matched wild-type littermate. However, evidence of splenic hyperplasia suggests that the ratio of myeloid-to-erythroid cells in *fit1* bone marrow (approximately 50:50 in normal marrow) might be elevated (Wintrobe et al., 1974). Although an accurate estimate of this ratio requires analysis of bone marrow cell suspensions, observations of a limited number of histological sections from *fit1*^{4397SB} femurs indicate that, perhaps, there are more myeloid cells present than erythroid cells, and that the myeloid-to-erythroid ratio may be elevated (Fig. 11; data not shown). This finding supports the observation of increased hematopoietic activity in mutant spleen tissue, and suggests that the *fit1* mutant condition is causing an increased demand for hematopoietic cell production.

Conditions of hematopoietic stress may also induce extramedullary hematopoiesis at sites other than the spleen, including the liver (Wintrobe et al., 1974). Since increased hematopoietic activity was detected in *fit1* mutant spleen tissue, mutant liver tissue was also examined for signs of extramedullary hematopoiesis. However, no obvious signs of hematopoietic activity were detected in *fit1* liver tissue (data not shown).

The splenomegaly, possible bone marrow abnormalities, and the peripheral blood abnormalities seen in *fit1*^{4397SB} mutants (Figs. 9, 10, 11), suggests that the *fit1* mutant phenotype may result from defects in hematopoiesis (Wintrobe et al., 1974). Indeed,

splenomegaly accompanies several anemic conditions. Additionally, several mutations resulting in anemia have been identified in the mouse, and many of these also cause growth retardation (Russell, 1979; Green, 1989).

fit1 Mutants are Anemic

"Anemia" is traditionally defined as a reduced concentration of hemoglobin (hgb) or a reduced volume of packed red blood cells [hematocrit (hct)] (Wintrobe et al., 1974). Therefore, to confirm whether *fit1* mutants are anemic, hematocrit values and hemoglobin levels were determined for both mutants and littermate controls. The data shown in Fig. 12 confirm that all *fit1* mutants are moderately to severely anemic; *fit* 1^{4397SB} mutants are extremely anemic, as compared to normal littermates, with an average hematocrit of 16.7% (compared to 44.7% for normal littermates) (Fig. 12A). The hemoglobin levels of *fit1* mutants also reflect the severe nature of the anemia (Fig. 13B). Control mice (c^{ch} +/c^{ch} +) had hgb levels of 14.2 ± 1.2 g/dl, whereas *fit*1^{4397SB} mutants had a value of 5.7 ± 1.1 g/dl. Also, mean hct and hgb values for each of the *fit1* mutant groups displayed a range of severity among the five *fit1* mutations (Fig. 12), and the severity of anemia correlates with the degree of growth retardation seen among mutants carrying the five *fit1* alleles.

Erythroid and Myeloid Progenitors are Reduced in *fit1* Tissues

From the data above, it is unclear whether the *fit1* mutations cause a defect specific to the mature red blood cell, to the pathway leading to the mature cell, *i.e.,* erythroid precursors, or perhaps to an even earlier progenitor cell common to erythroid, myeloid, and/or lymphoid lineages. Hematopoietic progenitors of erythroid and other myeloid lineages can be assayed by *in vitro* culture methods in which single-cell suspensions of hematopoietic tissue are resuspended in a semisolid media (methylcellulose) containing the necessary factors for cells with sufficient proliferative potential to form identifiable colonies of erythroid, granulocyte/macrophage, and mixed (erythroid, granulocyte/macrophage, and megakaryocyte) lineages (Pluznik and Sachs, 1965; Bradley and Metcalf, 1966; Humphries et al., 1981; Ogawa 1983). To determine the number of erythroid, as well as other myeloid, progenitors in hematopoietic tissues from *fit1* mutants, as compared to normal littermate tissues, bone marrow and spleen cells from weaning-age $c\ fit1^{4397SB}/c^{26DVT}$ mutants and $c^{ch}+/c^{ch}+$ wild-type littermates were assayed by *in vitro* methylcellulose cultures. The data in Fig. 13A and 13B show that both a late-stage [the Colony Forming Unit-Erythroid (CFU-E)] and an earlier-stage erythroid progenitor [Burst Forming Unit-Erythroid (BFU-E)] are reduced in $fit1^{4397SB}$ adult hematopoietic tissues. The number of CFU-E per 10^5 cells in both the bone marrow and spleens

of *fit1*^{4397SB} mutants is less than 20% that of the number in wild-type littermates. Likewise, the number of BFU-E per 10^5 cells in adult tissues of *fit1*^{4397SB} mutants is less than 20% that of controls. Additionally, a myeloid progenitor of granulocytes and macrophages, the CFU-GM (Colony Forming Unit-Granulocyte/Macrophage), is also reduced in *fit1*^{4397SB} tissues, although apparently not as severely as the erythroid progenitors (42.5% and 32.2% that of controls in the bone marrow and spleen, respectively) (Fig. 13A and 13B). Methylcellulose experiments performed with *fit1*^{4397SB} tissues from earlier time points indicate that the hematopoietic defect is also apparent at 7 and 19 days of age (data not shown). These data suggest that both erythroid and myeloid differentiation is compromised by the *fit1*^{4397SB} mutation, at least as early as the BFU-E and CFU-GM stage.

If a hematopoietic defect is the primary cause of the *fit1* phenotype, and since *fit1* mutants are phenotypically distinguishable (*i.e.*, growth retarded) as early as E14.5, then the primary hematopoietic tissue at that stage of development (the fetal liver) might also be affected. The data in Fig. 14 demonstrate that, indeed, erythroid and myeloid precursors, as determined by methylcellulose assays, are also reduced in *fit1* mutant fetal liver at E14.5. The number of CFU-E in *fit1*^{4397SB} E14.5 liver is approximately 39% that of normal littermates, and BFU-E are apparently reduced to a greater extent (14.4% of control). The CFU-GM are also reduced, although not as severely as the erythroid progenitors (50.9% of control). These

data suggest that the *fit1* mutations also affect an early progenitor of erythroid and myeloid fetal hematopoiesis, at least as early as E14.5 of gestation.

Since the spleens of *fit1* mutants are sometimes enlarged (Table 5), the apparent decreased concentration of progenitor cells in the spleen may result from this increased cellularity (*i.e.*, the same number of progenitors may be distributed thoughout a larger number of cells, and therefore, the number of progenitors per 10^5 cells might appear lower). Therefore, it may be necessary to consider the total number of progenitors per spleen to determine if the actual number of progenitors is decreased. The results in Table 7 show that, although on average the *fit1*^{4397SB} spleens were more cellular (although not significantly, $p < 0.05$), the total number of spleen progenitors is reduced. When considering total number per spleen, the number of CFU-GM in *fit1*^{4397SB} spleens is approximately 45% that of the wild-type littermate number (Table 7). Since the total number of cells in the *fit1*^{4397SB} bone marrow and fetal liver is reduced (approximately 39.4% of the number of wild-type bone marrow cells, and 50.1% of the number of control cells in fetal liver) the total number of progenitors in those tissues remain reduced (Table 7).

CFU-S are Reduced in *fit1*^{4397SB} Bone Marrow

The fact that both an early erythroid progenitor and an early progenitor of other myeloid lineages are affected by the *fit1*^{4397SB} mutation suggests that perhaps an earlier, common progenitor may also be affected. Progenitors of the BFU-E and CFU-GM are not easily recognized in *in vitro* methylcellulose assays; therefore other assays are necessary to measure very early hematopoietic progenitors. Till and McCulloch (1961) found that bone marrow cells injected into the blood stream of heavily irradiated recipient mice initially home to the spleen, and those cells with sufficient proliferative potential form macroscopic clonal colonies (termed Colony Forming Unit-Spleen, or CFU-S) of multilineage cell types 7 to 14 days post-injection. The spleen colony assay is capable of measuring one of the earliest detectable hematopoietic progenitors (Till and McCulloch, 1961).

To test the hypothesis that an early progenitor common to both myeloid and erythroid lineages is affected in *fit1* mutants, CFU-S experiments were performed with *fit1*^{4397SB} bone marrow tissue. To avoid immune rejection of the non-congenic *c fit1*^{4397SB}/*c*^{26DVT} donor bone marrow cells, immunologically compromised *scid/scid* mice were used as recipients. Mutations in the *scid* gene result in a T and B cell deficiency (Fulop and Phillips, 1989, 1990). Groups of *scid/scid* mice were irradiated with 2.5 Gy of X-rays (see Materials and

Methods) to destroy endogenous hematopoietic cells, and were injected with either 2 X 10^5 bone marrow cells derived from a 30-day-old *fit* 1^{4397SB} mutant (*c fit*1^{4397SB}/*c*^{26DVT}), or 1 X 10^5 bone marrow cells from a wild-type littermate (c^{ch} +/c^{ch} +). (Twice as many *fit*1^{4397SB} cells were injected to ensure that at least some colonies would likely be present in recipient spleens, since there was an indication from the *in vitro* progenitor assays that the number of progenitors in *fit1* mutants is significantly reduced). Fourteen days post injection, all mice were sacrificed, spleens were removed, and spleen colonies were enumerated. Based on the number of macroscopic colonies found on the spleens of *scid* mice injected with *c fit*1^{4397SB}/*c*^{26DVT} bone marrow cells, and the number of cells injected, *fit*1^{4397SB} mutants are estimated to have 2.4 ± 0.65 CFU-S per 10^5 bone marrow cells (Table 8). This represents 35.3% of the estimated number of CFU-S per 10^5 bone marrow cells from the wild-type littermate (6.8 ± 1.9 CFU-S per 10^5 bone marrow cells). Additionally, if the total number of CFU-S per femur is calculated, then the total number is clearly reduced in *fit1* mutants (Table 8). These results show that hematopoiesis is affected at least as early as the CFU-S stage by the *fit*1^{4397SB} mutation.

In addition to being fewer in number, the CFU-S that developed from *c fit*1^{4397SB}/*c*^{26DVT} injected cells were smaller and different in morphology than those that developed from wild-type cells (Fig. 15A, 15B). This suggests that not only are there fewer CFU-S in *c fit* 1^{4397SB}/*c*^{26DVT} bone marrow, but also that those that are present are

not able to proliferate as well in a normal microenvironment as compared to normal (c^{ch} +/c^{ch} +) bone marrow cells. Histological sections from the spleen colonies reveal cells of mixed lineages in the wild-type spleen: erythrocyte, megakaryocyte, granulocyte, and macrophage lineages are represented. Although these lineages are also represented in the *fit1*-derived spleen colonies, fewer cells of the erythroid lineage appear to be present, and a larger number of megakaryocytes may be present (Fig. 15B; data not shown).

Lymphoid Lineages are Also Affected by *fit1* Mutations

Since the data above suggest that the *fit1*^{4397SB} mutation affects hematopoiesis at least as early as the CFU-S stage, that the germinal centers in *fit 1*^{4397SB} mutant spleen tissue may be abnormal, and that *fit1* mice have lower numbers of circulating WBCs (Table 6), it is possible that the lymphoid lineages may also be affected by the *fit1* mutations. To establish a preliminary measure of the lymphoid cell populations in *fit1*^{4397SB} mutants, *fit1*^{4397SB} hematopoietic tissues were analyzed by flow cytometry with monoclonal antibodies specific to B cells [CD45R (B220)] and T cells (Thy-1). The data in Table 9 show that the number of B cells in both *fit1*^{4397SB} mutant bone marrow and spleen tissues is significantly reduced. The number of B220-positive cells found in *fit1*^{4397SB} bone marrow is approximately 50% of that found in wild-type bone marrow, and the number of B220-positive

cells in the *fit1*^{4397SB} spleen is only 30% of that found in wild-type spleen. Additionally, the number of Thy-1-positive cells in *fit1*^{4397SB} spleen tissue was also found to be reduced; however, the difference from the control was not statistically significant. [It should be noted that, although the spleens of *fit1* mutants may be enlarged (Table 5), the total cellularity of the spleen tissues analyzed here was not significantly different between *fit1*^{4397SB} mutants and wild-type controls, and therefore it was not necessary to consider the total number of antibody-positive cells per spleen.] These data suggest that the B cell population is significantly reduced in *fit1* mutant spleen and bone marrow, and that the T cell population may also be slightly reduced. Therefore, the lymphoid lineage of hematopoietic differentiation is, either directly or indirectly, affected by the *fit1* mutations.

IV. DISCUSSION: PHENOTYPIC CHARACTERIZATION

Series of allelic mutations that induce subtle changes in gene function and/or expression, thereby resulting in a range of phenotypic variations, are extremely useful tools for deciphering the roles specific genes play in development. The studies reported here represent the initial phenotypic characterization of five independent mutations of a gene, designated *fitness 1* (*fit1*), recovered through a saturation-mutagenesis strategy employing the spermatogonial super mutagen, *N*-ethyl-*N*-nitrosourea (ENU). ENU is thought to induce primarily small intragenic mutations (*e.g.*, Popp et al., 1983; Batzer et al., 1988; Pastink et al., 1989), and, therefore, the five *fit1* mutations most likely represent independent, single-amino acid changes that result in a phenotype displaying defects in growth, viability, and hematopoiesis. The results of these phenotypic analyses of *fit1* mutants show that the gene is necessary for normal growth and viability both *in utero* and postnatally. Additionally, these studies have shown that *fit1* mutants have peripheral blood defects, are anemic, and have a deficit of hematopoietic progenitor cells. The range of phenotypic severity among the five *fit1* alleles, demonstrated by the results of this study, suggests that each of the *fit1* mutations has altered the functional capacity and/or the expression of the *fit1* gene product to varying degrees. Consequently, characterization of the *fit1* phenotype, as well as molecular

characterization of the *fit1* gene, should eventually lead specifically to an increased understanding of the systems affected by this gene (*i.e.*, hematopoiesis, growth, viability, etc.), and more generally to a better understanding of the biological functions associated with specific DNA sequences.

The *fit1* Gene is Required For Pre- and Postnatal Growth And Viability

The *fit1* mutations were originally detected in the saturation mutagenesis screen because mice carrying a mutagenized Chr 7 opposite a large *c* deletion were smaller when compared to littermates (Rinchik et al., 1990). Characterization of the growth patterns of mice displaying dwarfing syndromes can sometimes provide insights into the particular system affected. For example, mice with defects in some endocrine functions (*e.g.*, Snell's dwarf, *dw*; Ames dwarf, *df*; little, *lit*; hypothryoidism, *hyt*) appear normal at birth, but they become dwarfed during postnatal development (Beamer et al., 1981; Cheng et al., 1983; Green, 1989). In contrast, dwarfism resulting from structural abnormalities [*e.g.*, cartilage matrix deficiency, *cmd*; chondrodysplasia, *cho*; cartilage anomaly, *can*) is sometimes detectable *in utero* and usually results in a disproportionate dwarfism (Johnson and Wise, 1971; Rittenhouse et al., 1978; Green, 1989). Also, certain anemias (*e.g.*, flexed-tail, *f*,

Hertwig's anemia, *an*), or mutations affecting certain growth factors (*e.g.*, insulin-like growth factor-2, *Igf2*) can result in mice growth retarded *in utero* (*i.e.*, smaller at birth) (Russell, 1979; Green, 1989). .

The data in Figs 3, 4, and 5, and Tables 2, 3, and 4 show that all of the *fit1* mutants are significantly growth retarded at birth and remain so throughout their shortened lifespan. The average weight, body length, and tail length of all of the *fit1* mutants are significantly reduced at birth and remain so throughout the measured time period when they are compared to wild-type littermates. Mice expressing the $fit1^{4397SB}$ allele are 61.1% of control weight at birth, and are 20.4% the weight of controls at 26-30 days of age (Table 2; Fig. 3). In contrast, mice expressing the $fit1^{4226SB}$ allele are 75.0% of normal weight at birth, and are 56.3% of normal at weaning age (Table 2; Fig. 3). Mice expressing the other *fit1* alleles are intermediate to these extremes (Table 2; Fig. 3). Therefore, these results suggest that there is a range of severity among the five *fit1* alleles.

Other growth measurements, such as tail length and body length, also support the conclusion that *fit1* mutants are growth retarded and that there exists a range of severity among the five alleles. For example, $fit1^{4397SB}$ mutants are 81.1% of the control body length at birth and 63.5% of control at weaning age (Table 3), whereas $fit1^{4226SB}$ mutants are 90.9% of normal body length at birth and 82.6% of normal at weaning age (Table 3). Mice expressing the remaining *fit1* mutations again display body lengths intermediate to these extremes (Table 3; Fig. 4). Additionally, the mean tail lengths reflect

a similar pattern (Table 4; Fig. 5). Based upon these data, the *fit1* mutations may be ordered with respect to severity of growth retardation as follows (listed in order of most severely affected to least severely affected): $fit1^{4397SB} > fit1^{494SB} > fit1^{764SB} > fit1^{3452SB} \geq fit1^{4226SB} >$ control.

These results also suggest that, since *fit1* mutants were smaller at birth, mice expressing *fit1* mutations might be growth retarded *in utero*. Indeed, weight measurements of E14.5 fetuses, revealed that $fit1^{4397SB}$ mutants are also significantly smaller at this stage of development (Fig. 7). E14.5 fetuses expressing the $fit1^{4397SB}$ mutation are 70.2% of the mean weight of normal littermates. This indicates that the *fit1* gene is not only necessary for postnatal growth and viability, but is also necessary for normal growth *in utero*. Additionally, since mutations affecting endocrine organs usually result in only postnatal dwarfing, these findings suggest that the *fit1* mutations most likely do not affect an endocrine function, at least those specific to the pituitary gland (Beamer et al., 1981; Cheng et al., 1983; Leiter et al., 1987; Green, 1989). However, these data do not exclude other endocrine factors from being involved, and previously unknown, prenatal functions regulated by the pituitary gland could also be affected.

Intrauterine growth retardation (IUGR), which can result from a number of environmental and genetic conditions, is a significant problem in humans and is associated with a great deal of infant morbidity and mortality (Evans et al., 1983; Kramer et al.,

1990; Pollack and Divon, 1992). However, human IUGR is difficult to study directly due to ethical constraints; therefore, animal models of IUGR have been sought for experimental study. Since *fit1* mutants are growth retarded *in utero*, these mutants may be useful as a model of one type of IUGR. The significance of the *fit1* mutants as models of IUGR may become more apparent as the specific underlying defect of *fit1* mutants is determined.

Another growth parameter that can provide insights into the system(s) affected in cases of growth retardation is proportionality (Johnson and Wise, 1971; Rittenhouse et al., 1978; Green, 1989). Many mutations affecting genes that encode structural components of muscle, cartilage, or bone, for example, cause disproportionate dwarfing (Green, 1989). One measurement of proportionality, defined as uniformity of shape over time, is a plot of the body length versus tail length (Hughes and Tanner, 1968). A plot of the mean body lengths versus mean tail lengths of fit1 mutants, compared to a plot of the mean body length versus mean tail length of the controls (Fig. 6) shows that *fit1* mutants are proportionately dwarfed. However, the $fit1^{4397SB}$ body length versus tail length plot does vary somewhat from the control and $fit1^{4226SB}$ line; however, this variation, which could reflect a true difference from controls and other *fit1* mutants, is probably due more to the extreme variability seen in the viability and growth of $fit1^{4397SB}$ mutants, and may not be truly reflective of the proportionality of $fit1^{4397SB}$ mutants. Since fewer $fit1^{4397SB}$ mutants survive long after birth, fewer mutants are

available for measurement at later time points; therefore, those animals that do survive may not be representative of the true growth pattern. Indeed, when only the first five to six points of the *fit1*^{4397SB} mutant body vs. tail line are considered, the slope is not significantly different than that of the control or *fit1*^{4226SB} mutant line.

Alternatively, the growth pattern (shape or proportionality) of *fit1*^{4397SB} mutants may be different from that of controls. However, based on the measurements of the other *fit1* mutants and on other gross observations, the *fit1* mutations most likely cause a proportional dwarfism. These findings, therefore, suggest that the dwarfism seen in *fit1* mutants is resulting from something other than a gross structural abnormality, which is usually manifested in a disproportionate dwarfism (Johnson and Wise, 1971; Rittenhouse et al., 1978; Green, 1989).

It is interesting to note that mutants hemizygous for each of the *fit1* alleles, although significantly growth retarded at birth, become even more growth retarded over time (Figs. 3, 4, and 5). *fit1*^{4397SB} mutants begin postnatal life 61.1% the weight of their normal littermates, but by weaning age, those still alive are 20.4% of control size (Fig. 3). The same pattern is seen in all other *fit1* mutants, but apparently the change is not as severe as that observed in *fit1*^{4397SB} mutants. For example, *fit1*^{4226SB} mutants are 75.0% of control weight at birth, but are only 56.3% of control weight at weaning (Fig. 3; Table 2). Additionally, the *in utero* weight data for *fit1*^{4397SB} mutants also indicate that these mutants are significantly

smaller at least as early as E14.5 (70.2% of control) (Fig. 7), but that by birth these mutants are already more growth retarded (61.1% of control weight) (Fig. 3). The body-length and tail-length measurements reflect a similar pattern (Figs. 4 and 5; Tables 3 and 4). The significance of this apparent increase in growth retardation is unknown. The degree of growth retardation over time may be a direct manifestation of the *fit1* mutations, and the *fit1* gene may play an increasingly important role in growth as development progresses. It is also possible, however, that the increase in growth retardation is simply an indirect consequence of the *fit1* mutations. For example, since *fit1* mutants are smaller and less viable, they are unable to compete for suckling as efficiently as normal littermates (M.D.P., D.A. Carpenter personal observation). This might explain the fact that less severely affected *fit1* mutants do not experience as dramatic a decrease in growth rate over time as the more severely affected $fit1^{4397SB}$ mutants. Less severely affected $fit1^{4226SB}$ mutants, while being less "fit" than normal littermates (and, therefore, at a competitive disadvantage), are better able to compete than more severely affected $fit1^{4397SB}$ mutants. Additionally, at increasingly older ages, *fit1* mice remain small and less active and, therefore, are still less competitive for food and water. Thus, malnutrition could be a secondary contributing factor to the early mortality seen in *fit1* mutants. Indeed, culling litter sizes to reduce suckling competition, and making food available on the cage floor, apparently increases the viability of *fit1* mutants (M.D.P., personal observation). However,

this hypothesis may not be able to explain the decreased growth rate in *fit1*^{4397SB} mutants from E14.5 to birth. Although, fetal position within the uterine horn can affect fetal size and viability (Evans et al., 1983), *fit1* mutants and normal littermates, on average, should be equally nourished *in utero*. Thus, the fact that *fit1* mutants are smaller *in utero* underscores the conclusion that the *fit1* gene is important in normal prenatal development.

It should also be noted that *fit1* mutants suffer from an anemia (discussed below), and that the severity of the anemia correlates with the degree of growth retardation seen among mice expressing each of the *fit1* mutations (see Fig. 12). The growth retardation seen in many cases of anemia is thought to result from an overall metabolic inefficiency due to hypoxia (Wintrobe et al., 1974). Additionally, the underlying cause of the anemia may have other manifestations that result in stunted growth, such as the dysphagia and disruption of other biochemical processes associated with iron-deficiency anemias (Wintrobe et al., 1974). Further analyses would be required to discern whether the *fit1*-associated growth retardation directly results from anemia.

The results of these growth analyses, therefore, indicate that the *fit1* gene is necessary for pre- and postnatal growth and viability. It also is likely that, since *fit1* mutants are proportionately dwarfed, the *fit1* mutations do not affect a gene necessary for any gross anatomical structures, such as muscle tissue, cartilage, or bone. Additionally, since *fit1* mutants are dwarfed *in utero*, it is unlikely

that these mutations affect growth regulation via the pituitary gland, in which case mutants might be expected to be normal in size at birth.

Therefore, these analyses have provided the initial characterization of the growth patterns of mice expressing mutations of the *fit1* gene, and have provided initial insights into possible explanations of the primary defect. Further phenotypic analyses, described below, have given a better understanding of the pathology in *fit1* mutants.

fit1 Mutants Are Anemic

No gross structural abnormalities were detected in macroscopic or microscopic analyses of *fit1* mutant endocrine organs (V. Godfrey, D.V.M., personal communication). Additionally, no obvious abnormalities, perhaps indicative of the primary *fit1* defect, were detected in necropsies of *fit1* mutants (V. Godfrey, D.V.M., data not shown). However, splenomegaly was frequently, although not always, observed. Indeed, on average, spleens from *fit1* mutants constitute a greater percentage of the total body weight than do spleens of normal littermates (Table 5). In normal mice, the spleen functions as an important reticuloendothelial organ, acts as a store for red blood cells and platelets, and filters the blood to remove foreign particles, bacteria, and degenerating leukocytes and erythrocytes

(Leeson and Leeson, 1981). Enlargement of the spleen can result from a number of causes, including extramedullary hematopoiesis (EMH), often observed in cases of extreme anemia (Wintrobe et al., 1974). During periods of hematopoietic stress, if the medullary site (adult bone marrow) cannot compensate for the increased cellular demands, hematopoiesis may shift to extramedullary sites, such as the spleen, liver, and less frequently to the lymph nodes, kidney, adipose tissue, and other sites (Wintrobe et al., 1974). Histological sections of *fit1* mutant spleen tissue reveal that the red pulp of the *fit1* spleen shows an apparent hyperplasia, whereas, the white pulp areas, which are sites of lymphoid cell production, are smaller (Fig. 10). Splenic hyperplasia suggests that there is an increased demand for erythroid cells in *fit1* mutants, and that the *fit1* bone marrow is not able to completely meet this demand. Indeed, *fit1* mutant bone marrow, although not strikingly abnormal, may have fewer erythroid precursors (Fig. 11). This finding is consistent with the EMH seen in *fit1* spleen tissues: if there is an increased demand for mature RBCs, and the *fit1* bone marrow tissue is not able to supply the needed cells, EMH would be expected in the spleen and perhaps other tissues. It is interesting to note, however, that given the degree of EMH seen in *fit1* mutant spleen tissue, no signs of EMH are found in the liver tissues of *fit1* mutants (data not shown). The hematopoietic potential of the adult mouse liver has been documented (Aldler and Trobaugh, 1978; Pfrimmer et al., 1978) and EMH is not uncommon in the liver during conditions of hematopoietic stress

(Wintrobe et al., 1974). However, the significance of the lack of EMH in the *fit1* mutant liver remains to be determined.

Thus, these results suggest that hematopoiesis may be disrupted in *fit1* mutants. Blood is a unique connective tissue made up of an intercellular fluid containing a variety of cell types that are required for an extensive array of functions, including oxygenation of body tissues, transportation of nutrients, mediation of immune responses, and clot formation (Leeson and Leeson, 1981). A tremendous number of cells are required for these functions; indeed, it is estimated that in an average human, close to 1×10^{12} blood cells must be replaced every day (Ogawa, 1993). When the balance of maintaining the mature blood-cell populations is disrupted, and either a deficit or surplus of cells results, pathogenesis can ensue. Evidence of EMH in *fit1* mutant spleen tissue suggests that the normal balance of the mature blood-cell populations may be disrupted. Concurrent with histological analyses of *fit1* hematopoietic tissues, *fit1* mutant peripheral blood was also examined for any obvious abnormalities. Normal RBCs have a uniform size, shape, and pigmentation (Fig. 9A); however, *fit1* mutant RBCs appear hypochromic, are fewer in number, and vary abnormally in size (anisocytosis) and shape (poikilocytosis) when compared to those found in normal littermates (Fig 9B). Hypochromia, seen as increased central pallor in the mature RBC, usually results from a failure of hemoglobin synthesis, due to a lack of iron, defective globin synthesis, or defective porphyrin synthesis

(Wintrobe et al., 1974). The observed anisocytosis and poikilocytosis in *fit1* blood can also be indicative of defective iron metabolism or globin synthesis, a specific red blood cell membrane defect, as well as a number of other genetic and/or environmental stresses (discussed below) (Wintrobe et al., 1974).

The striking peripheral blood defects, in conjunction with the splenic hyperplasia, suggested that *fit1* mutants may suffer from an anemia. "Anemia" is traditionally defined as a lowered packed red cell volume, or hematocrit (hct), and/or decreased levels of hemoglobin (hgb) (Wintrobe et al., 1974). *fit1*^{4397SB} mutants had a mean hct value of 16.7% (vs. 44.7% for controls) and a mean hgb value of 5.7 g/dl (vs. 14.2 g/dl for controls) (Fig. 12). Mutants carrying each of the other *fit1* alleles were also anemic (Fig. 12). Interestingly, the hct and hgb values ranged in severity among the five groups of *fit1* mutants, and the range of severity correlates with the degree of growth retardation seen in each group [*i.e.*, *fit1* mutants most severely growth retarded (*fit1*^{4397SB} mutants) are also the most severely anemic, and those least severely growth retarded (*fit1*^{4226SB}) are the least anemic] (Fig. 12). This correlation is intriguing, since a number of anemias have been described in the mouse that also result in growth retardation (Russell, 1979; Green, 1989).

In addition to hct and hgb levels, the white blood cell (WBC) count and the reticulocyte count were determined for *fit1* peripheral blood. WBC numbers are significantly reduced in *fit1* mutants, as compared to controls, whereas the *fit1* peripheral blood contains a

highly elevated number of reticulocytes (Table 6). Reticulocytes are immature RBCs that contain ribosomes, and they usually compose 1-2% of the population of circulating blood cells. However, *fit1*^{4397SB} mutants have extremely high numbers of reticulocytes (Table. 6). In cases of extreme anemia, or other conditions of increased RBC demand, reticulocytes may be released into the blood stream at an increased rate as the hematopoietic system strives to compensate for the increased demand for red cells. This observation, together with the observed splenic hyperplasia, indicates that blood-forming cells of *fit1* mutants are attempting to produce RBCs rapidly. Therefore, this is further evidence that the normal production of blood cells is defective in *fit1* mutants.

It should be noted, however, that "anemia" is not a specific diagnosis, and, while a number of diseases result from defects of the blood and blood-forming tissues, perhaps more frequently disorders of other systems cause defects in the blood as a secondary consequence (Wintrobe et al., 1974). Additionally, the hematopoietic system is composed of a complex hierarchy of differentiating and proliferating cells. Thus, specific hematopoietic defects may affect various stages of hematopoietic differentiation, from a single class of mature cells, to multipotent progenitors (*i.e.*, multiple lineages or cell types), to the pluripotent stem cell. For example, the results above suggest that not only are RBCs reduced in *fit1* mice, but that the WBCs, another hematopoietic lineage, is also reduced. Therefore, the finding of anemia, although intriguing, necessitates

further characterization of the *fit1* phenotype in order to gain insight into the primary defect.

Hematopoiesis Is Defective In *fit1* Mutants

As noted above, the hematopoietic system is required to produce continually a large number of mature, highly differentiated cells. As evidenced by the peripheral blood profile (Fig. 9), the mature RBC population is obviously affected by the *fit1* mutations; however, it is possible that the developmental pathway leading to the production of the mature RBC is also affected by the *fit1* mutations.

A generally accepted model of the hierarchical pathway of hematopoietic differentiation is shown in Fig. 16. Briefly, a small number of pluripotent stem cells, with extensive proliferative and differentiation potential, exist in a quiescent state. These cells may then differentiate to form larger numbers of multipotent progenitor cells. Multipotent progenitor cells are capable of limited self-renewal and can give rise to a restricted set of cell lineages. The progeny of multipotent progenitors are further lineage- and self-renewal-restricted, and produce larger numbers of more-differentiated, committed precursors, until ultimately large populations of fully differentiated, mature cells are derived. The stem-cell population is much smaller than the number of progenitor cells, which, in turn, are less frequent than the mature cell population. Therefore, in the

pathway from pluripotent stem cell to mature, completely differentiated progeny, self-renewal capacity and differentiation potential decreases and numbers of cells increase dramatically. The differentiation pathway and the factors regulating it are relatively well characterized for progenitors and the mature cells produced by them (Demetri, 1992); however, since stem cells and very early progenitors exist in such low numbers and are not morphologically distinct, much less is known about their developmental program.

In adults, the primary site of hematopoietic differentiation is the bone marrow. However, during mammalian development, hematopoietic differentiation occurs at different sites (reviewed in Dick, 1991; Tavassoli, 1991). Hematopoietic precursors first migrate from the primitive-streak region of the blastoderm and initiate the foci of extraembryonic hematopoiesis in blood islands of the yolk sac. In the mouse, this occurs by approximately E8 of gestation and proceeds through E10. By E10 of murine development, hematopoiesis shifts to the fetal liver. Concommitant with the shift to the fetal liver, hematopoiesis in the yolk sac begins to decline, and the fetal liver remains the major site of hematopoiesis during fetal life. The spleen also displays hematopoietic activity in the mouse, beginning at E15, and continuing throughout gestation and, to some extent, into adult life. By E17-E18, hematopoiesis is initiated in the bone marrow; however, it is limited to granulopoiesis, while the fetal liver and spleen continue to provide erythropoietic function (Tavassoli, 1991). Beginning shortly after birth, the bone marrow gains erythropoietic

function and becomes the major site of hematopoiesis in the adult. Although very little is known of how these site changes are accomplished and regulated, it is believed that the microenvironment of the tissues involved, as well as some components of the extracellular matrix, play an important role in the receptiveness of one or another tissue to hematopoeisis (Tavassoli, 1991).

Due to their low numbers and lack of morphological distinction, hematopoietic stem cells and early progenitor cells have primarily been defined through *in vitro* and *in vivo* assays that essentially measure the proliferative and differentiation capacity of individual cells. These assays are based on the ability of a particular progenitor cell, provided with the proper regulatory factors, to form recognizable colonies of single or multiple lineages.

For example, colonies of hematopoietic cells can be successfully generated in *in vitro* cultures (Pluznik and Sachs, 1965; Bradley and Metcalf, 1966; Ogawa, 1983). Cells from hematopoietic tissues are resuspended in a semisolid culture supplemented with conditioned media. Progenitors are identified by morphological characteristics of the developing colony and by the time of appearance of the colony. Colonies representing progenitors of erythroid, granulocyte and macrophage, megakaryocyte, eosinophilic, and of multilineage capacity have been identified (Dick, 1991). These colonies may also be placed within the developmental continuum of the hematopoietic differentiation pathway based upon their time of appearance in culture, differentiation capacity, and ability to self-

replicate. Therefore, those colonies appearing early in culture and having a restricted differentiation potential represent a relatively late-staged progenitor, whereas one appearing later in culture and having multiple lineage capacity would represent an earlier-staged progenitor.

These *in vitro* assays have allowed the identification of several additional progenitors within the hematopoietic differentiation pathway, and represent an extremely useful method for both quantification and characterization of hematopoietic cells under different physiological and genetic conditions. In fact, the nomenclature for hematopoietic progenitors is based on the "colony forming unit" (CFU), followed by a designation of the particular lineage of the progenitor. Examples of some of these progenitor colonies include the following:

-Burst Forming Unit-Erythroid colonies (BFU-E) are early erythroid progenitors that grow in clustered arrays of hundreds to thousands of hemoglobinized cells. BFU-E appear 7-10 days after initiation of *in vitro* colony assays.

-Colony Forming Unit-Erythroid colonies (CFU-E) are a more mature erythroid progenitor than the BFU-E. CFU-E appear *in vitro* 2 days after initiation of cultures and appear as small clusters of 8-64 or more hemoglobinized cells.

-Colony Forming Unit-Granulocyte, Macrophage colonies (CFU-GM) are early myeloid progenitors that appear

7-10 days after in vitro cultures are established. CFU-GM may contain up to hundreds of cells committed to form granulocytes and macrophages.

To assess whether the *fit1* mutations affect hematopoietic differentiation, or whether the *fit1* defect is restricted to mature RBCs, *fit1* mutant bone marrow and spleen were assayed in *in vitro* hematopoietic progenitor cell assays. Both CFU-E and the earlier erythroid-progenitor, BFU-E, were significantly reduced in 30-day-old *fit1* mutant hematopoietic tissues (Fig. 13). Interestingly, in addition to these erythroid progenitors, an early myeloid progenitor, the CFU-GM, is also significantly reduced in adult *fit1* mutant hematopoietic tissues (Fig. 13). However, the reduction in CFU-GM is not as great; the number of CFU-E and BFU-E in adult *fit1* hematopoietic tissues is less than 20% of the number found in controls, whereas the CFU-GM are 42.5% and 32.2% that of controls in bone marrow and spleen, respectively. Therefore, the *fit1* mutations affect erythroid differentiation at least as early as the BFU-E, and also affect myeloid differentiation at least as early as the CFU-GM stage (see Fig. 16). Additionally, since the *fit1* dwarfing phenotype is evident *in utero*, fetal liver was also assayed in *in vitro* assays. These results were similar to those found in adult tissues: all colonies were significantly reduced, however, the CFU-GM were not as greatly reduced as the CFU-E and BFU-E (Fig. 14). Thus, hematopoiesis is defective in *fit1*

mutants at least as early as E14.5, and the defect is also present in adult hematopoietic tissues as well.

The significance of the apparently greater reduction of erythroid progenitors as compared to CFU-GM is unknown. The *fit1* gene product may play a more prominent role in erythroid differentiation than in myeloid-cell development. Also, evidence suggests that there is a great deal of functional redundancy among molecules regulating hematopoiesis (Bass and Beckner, 1992; Kishimoto et al., 1992; Stahl and Yancopoulos, 1993). Therefore, absence or alteration of the *fit1* gene product may have more profound consequences on erythroid development than on myeloid development due to another molecule(s) that can functionally take the place of *fit1* in myeloid cells. However, the indication that the *fit1* mutations affect both early erythroid and myeloid differentiation suggests that the *fit1* gene plays a role in early hematopoietic differentiation, and that perhaps an earlier, common progenitor is affected.

One of the earliest assays for hematopoietic cells developed is the *in vivo* spleen colony forming unit assay (CFU-S assay) (Till and McCulloch, 1961). The CFU-S assay represents a useful assay for quantifying one of earliest detectable hematopoietic progenitors. It was discovered that hematopoietic cells derived from bone marrow (although other hematopoietic tissues may be used), injected into the blood stream of heavily irradiated recipient mice, initially home to the spleen, and cells with sufficient proliferative potential form

macroscopic, clonal colonies of multilineage cell types seven to 14 days post-injection. Each spleen colony (CFU-S) was originally thought to represent the proliferative result of a single stem cell (Till and McCulloch, 1961); however, substantial evidence now exists suggesting that these colonies, while representing an early progenitor, does not represent the stem-cell population (Ploemacher and Brons, 1989; Jones et al., 1990). CFU-S display terminal differentiation in the erythrocyte, macrophage, granulocyte, and megakaryocyte lineages and can undergo limited self-renewal. Evidence from CFU-S studies indicate that, within the structured continuum of the hematopoietic stem-cell environment, the most primitive cells have the greatest long-term repopulating ability and are the most resistant to proliferation and differentiation. Therefore, in terms of the CFU-S, those colonies forming 12-14 days post-injection are more primitive progenitors than those appearing 7 or 8 days post-injection. Despite the fact that the assay probably does not directly measure the stem-cell population, the CFU-S assay provides a technique with which to define and quantify one of the earliest stages of hematopoiesis, and this assay remains an important tool in characterization of the hematopoietic system.

CFU-S assays performed with *fit1* mutant bone marrow cells revealed that the number of CFU-S are also significantly reduced in *fit1* mutants as compared to normal littermates (Fig. 8). Bone marrow cells from a 30-day old *c* $fit1^{4397SB}/c^{26DVT}$ mouse produced only 35.3% the number of CFU-S, as compared to control cells (c^{ch}

$+/c^{ch}$ + littermate bone marrow), fourteen days post-injection. Additionally, the colonies formed by *fit1* mutant cells were smaller and different in morphology than control-derived colonies (Fig. 15). These results demonstrate that the *fit1* mutations disrupt normal hematopoiesis at a very early stage (see Fig. 16).

Since *fit1* mutant cells behave abnormally when placed in the presumably "normal" microenvironment of a recipient mouse, the *fit1* mutation is likely a cell-autonomous defect and is intrinsic to the mutant cells. Further support for this conclusion could be provided by additional transplantation experiments. If the *fit1* defect is cell autonomous, and the *fit1* hematopoietic microenvironment is normal, then transplantation of normal hematopoietic cells into *fit1* mutants would be expected to function normally and alleviate the *fit1* associated anemia. To perform this experiment, however, the normal donor-derived cells must be of the same genetic background as that of the recipient, in order to avoid immunological rejection of the donor cells. A congenic line carrying the $fit1^{494SB}$ mutation has been made (Rinchik and Carpenter, unpublished); however, the inherent reduced viability and fertility of this inbred line, coupled with the additional burden of expressing the *fit1* mutation, resulted in no *fit1* mutants being born from crosses of heterozygotes (c^{ch} $+/c$ $fit1^{494SB}$ X c^{ch} $+/c$ $fit1^{494SB}$) and in crosses of congenic carriers to outbred mice carrying the c^{26DVT} deletion (c^{ch} $+/c$ $fit1^{494SB}$ X c^{ch} $+/c^{26DVT}$) (M.D.P. personal observation). Therefore, this experiment could not be performed in this study. [The CFU-S experiment was

possible since non-congenic *fit1*^{4397SB}/*c*^{26DVT} cells were transplanted into immunologically compromised *scid/scid* mice. Mice homozygous for the *scid* mutation lack a functional immune system, and, therefore, will not reject the donor cells (Fulop and Phillips, 1989).]

The finding that CFU-S formed by *fit1* mutant cells are smaller suggests that not only are fewer progenitors present, but those that are present may be functionally compromised. Indeed, other anemias described in the mouse have cellular defects resulting in a reduced ability of stem cells to proliferate (Russell, 1979). Cells from human patients suffering from Fanconi's anemia display a longer-than-average doubling time in culture, and they are very sensitive to ultraviolet radiation and certain chemicals (Weksburgk et al., 1979). The primary defect in these cells has been postulated to involve DNA repair and/or replication. Additionally, many unusual mitotic figures are seen in bone marrow cells from mice with mutations in the Hertwig's anemia gene (*an*) (Russell et al., 1985). These mitotic defects are thought to result in a steady decrease in hematopoietic cell numbers as these cells attempt to divide and differentiate, a situation that eventually results in anemia. The underlying cause resulting in the apparent failure of *fit1*-derived cells to proliferate as well as normal cells has not been determined.

The results of the hematopoietic progenitor-cell assays suggest that multiple lineages of hematopoietic differentiation are affected by the *fit1* mutations, at least as early as the CFU-S stage (see Fig. 16).

Histological evidence that the germinal centers of the spleen are abnormal (Fig. 10), and the data suggesting that fewer WBCs are in the *fit1* periphery (Table 6), suggest that perhaps the *fit1* mutations also affect lymphoid differentiation. To test this hypothesis, the expression of monoclonal antibodies that recognize antigens specific for B cells (B220) and T cells (Thy-1) in *fit1* hematopoietic tissues was assayed by flow cytometry. A significant reduction of $B220^+$ cells were found in $fit1^{4397SB}$ mutant bone marrow and spleen (Table. 9). The B220 antigen is found on both pre-B cells and mature B cells (Coffman and Weissman, 1981). Since only 50% and 30% of the number of $B220^+$ cells are found in *fit1* mutant bone marrow and spleen, respectively, the *fit1* mutations must, therefore, also affect the B cell population. Additionally, the number of Thy-1-positive cells in $fit1^{4397SB}$ spleen tissue was also reduced. Although observed Thy-1 reduction was not statistically significant from control, it was consistently found, and may, in fact, represent a true reduction of the $Thy\text{-}1^+$ population. The Thy-1 antigen is primarily associated with expression on T lymphocytes (Reif and Allen, 1964; Basch and Berman, 1982), but is also found at low levels on stem cells (Basch and Berman, 1982; Spangrude et al., 1988). The B cell and T cell populations are within the lymphoid lineage, and the branch of hematopoietic differentiation that distinguishes the lymphoid lineage (B cells and T cells) from other lineages occurs very early in this pathway (see Fig. 16). Therefore, these results not only suggest that the *fit1* mutations affect lymphoid lineages of hematopoiesis, but,

together with the data demonstrating that erythroid and myeloid lineages are affected as well, suggest that the *fit1* mutations affect hematopoiesis very early in the differentiation process, perhaps even at the stem-cell level.

However, it should be noted that, in mice in which the stem-cell population has been reduced (by irradiation for example), there may be a "competition" for stem cells (Hellman and Grate, 1968). In such animals an increased demand for erythrocytes causes a reduction in the number of other hematopoietic cells. Therefore, if the *fit1* mutations are affecting the stem-cell pool, as well as specifically creating an increased demand for RBCs, then the reduction of myeloid progenitors and lymphoid cells may be an indirect consequence of the mutations. However, in mice with a normal stem-cell population, however, exaggerated demand of a particular cell type stimulates an increase in all cell lineages (Gaylor et al., 1969). Thus, the *fit1* gene may indeed be directly responsible for some aspect of differentiation of erythroid, myeloid, and lymphoid cells.

What Is The Primary Defect In *fit1* Mutants?

The phenotypic studies of mice expressing the *fit1* mutations have shown that the *fit1* gene is necessary for normal adult and fetal hematopoiesis in the mouse. Hematopoiesis is disrupted in *fit1*

mutants at least as early as the CFU-S stage, and cells representative of all three hematopoietic lineages (erythroid, myeloid, and lymphoid) are significantly reduced. Moreover, the circulating RBCs of *fit1* mutants are hypochromic and display varying degrees of anisocytosis and poikilocytosis. In addition to these hematopoietic defects, *fit1* mutants are growth retarded *in utero* and remain dwarfed throughout their shortened lifespan. Therefore, the *fit1* gene plays a crucial role in fetal and adult growth, viability, and hematopoiesis.

It should be noted, however, that a number of genetic and environmental insults can result in anemia. Indeed, mutations at over 17 genetic loci on at least 10 different chromosomes have been identified that result in some type of anemia in affected mice (Russell, 1979; Green, 1989). Mutations affecting structural proteins, metabolic enzymes, DNA repair enzymes, signaling pathways, iron metabolism, renal function, etc., can all produce anemias with phenotypic manifestations similar to those seen in *fit1* mice. Therefore, despite the information gained from the initial biological characterization of the mice expressing the *fit1* mutations, the underlying defect causing the anemia in *fit1* mutants remains unknown. However, the data collected in this study have provided insights into possible causes of the *fit1* phenotype, and should provide direction to future analyses that may lead to discovery of the role of the *fit1* gene.

For example, the RBC membrane cytoskeleton is composed of a complex meshwork of proteins beneath the lipid bilayer, and mutations affecting any one of a number of these RBC cytoskeletal proteins can result in anemias characterized by abnormal RBC morphology (reviewed in Davies and Lux, 1989). Thus, the abnormal morphology of *fit1* mutant RBCs suggests that the *fit1* mutation could be affecting a RBC membrane cytoskeleton protein. Although the functions of many of these proteins are not well defined, mutations affecting these proteins are thought to disrupt the mechanical stability of the RBC membrane. The associated anemia results from removal of the defective RBCs from circulation and the inability of the hematopoietic tissues to maintain the cell populations. Unlike the *fit1* mutant condition, however, bone marrow hyperplasia is usually evident and, importantly, other hematopoietic lineages are not affected (Wintrobe et al., 1974). Despite these phenotypic differences, the *fit1* mutations could possibly be affecting a RBC cytoskeletal protein, and future experiments could be directed toward further characterization of the RBC membrane of *fit1* mutants.

Other anemias that present some clinical manifestations similar to the *fit1*-associated anemia are those resulting from abnormalities of the glycolytic metabolic pathway. The most common of such anemias is pyruvate kinase (PK) deficiency (Wintrobe et al., 1974).

RBCs rely on energy derived from ATP for vital functions, such as maintenance of cationic gradients. Since RBCs do not contain

mitochondria, they cannot utilize mitochondrial oxidative phosphorylation to maintain ATP levels, but must rely on regeneration of ATP from glycolysis. One of the consequences of diminished ATP levels is thought to be disruption of cationic gradients within the cells, and subsequent RBC membrane distortion can occur (Wintrobe et al., 1974). Mutations affecting PK, or other glycolytic enyzmes, can result in RBC poikilocytosis, anisocytosis, and increased numbers of reticulocytes, similar to that seen in *fit1* mutants. However, in contrast to *fit1* mutants, PK-deficiency results in bone marrow hyperplasia, general macrocytosis (larger RBCs), and, since cells other than RBCs possess additional mechanisms for generating ATP, usually only mature RBCs are affected. Thus, despite some similarities, it is unlikely that the *fit1* mutations affect a glycolytic pathway enzyme.

Another group of hereditary anemias, characterized by ineffective erythropoiesis, multinuclear erythroblasts, and varying degrees of anisocytosis and poikilocytosis, are the congenital dyserythropoietic anemias (CDAs). The molecular defect responsible for at least one of the CDAs (CDA type II) has been identified as a mutation in a gene encoding an enzyme necessary for the synthesis of asparagine-linked oligosaccharides in erythroid cells (Fukuda et al., 1990). As a result of this deficiency, the hydrophobicity of certain glycoproteins within the RBC membrane is increased, and they become clustered and abnormally distributed within the membrane, resulting in the characteristic morphological defects (Fukuda et al.,

1990). The anisocytosis and poikilocytosis seen in *fit1* mutant blood is similar to that seen in CDA patients. Additionally, the CDA phenotype is present at birth, and CDA patients sometimes experience growth retardation (Wintrobe et al., 1974). However, apparently only RBCs are affected by CDA; the WBC and platelet populations are normal (Wintrobe et al., 1974). Also, no unusual nuclear structure has been observed in sections of *fit1* mutant bone marrow (M.D.P., personal observation). However, future analyses could include a closer investigation of the nuclear structure of erythroid precursors of *fit1* bone marrow cells.

Of all the examples of systems cited above that, when disrupted, result in a phenotype resembling the *fit1* phenotype, perhaps the most similarities exist between the *fit1* mutant phenotype and iron-deficiency anemias. Iron is an indespensable component in a large number of biochemical reactions, including the transport of oxygen by hemoglobin, electron-transfer reactions, DNA synthesis, the decomposition of noxious derivatives of oxygen, etc. (reviewed in Aisen, 1977). Therefore, iron deficiency can produce a range of phenotypic consequences, including anemia. Iron-deficiency anemias are characterized by a poverty of hemoglobin, resulting in hypochromic RBCs. In extreme cases, RBCs may appear as mere rings. Additionally, RBCs may be microcytic, although a range of cell sizes may be seen (anisocytosis), and a moderate number of poikilocytes are usually present (Wintrobe et al., 1974). There is increased destruction of RBCs and their precursors,

and not only are RBC populations affected, but myeloid and lymphoid cell populations may also be reduced (Ricketts and Cavill, 1977; Chandra et al., 1977). All of these characteristics appear to be similar to the *fit1* mutant phenotype.

A mutation in the laboratory rat, recovered through X-ray mutagenesis experiments and designated Belgrade Laboratory rat anemia (*b*) (Sladic-Simic et al., 1963), results in iron deficiency, and *b/b* rats display a phenotype similar to that seen in *fit1* mutants. Rats homozygous for the *b* mutation are growth retarded at birth and remain smaller throughout a shortened lifespan (Sladic-Simic et al., 1966). Additionally, the peripheral blood of *b/b* rats is characterized by microcytosis, anisocytosis, poikilocytosis, and an increased number of reticulocytes. Since hemoglobin synthesis predominates in the later stages of erythropoiesis, it has been proposed that the *b* mutation, and other iron deficiences, may not affect early stages of erythropoiesis (Edwards et al., 1986). However, hematopoietic progenitor cell assays in *b/b* rats have demonstrated that both CFU-E and the earlier progenitor BFU-E are severely reduced (Pavlovic-Kentera et al., 1989). Additional studies have indicated that granulopoiesis and megakaryocytopoiesis are also affected by the *b* mutation, and that T lymphocytes are also defective in *b/b* rats (Stojanovic et al., 1990; Biljanovic-Paunovic et al., 1992; Rolovic et al., 1985; 1991). The apparent effect of iron deficiency on such a wide range of hematopoietic cells, including progenitors, has been proposed to be due to the general importance of iron for cellular

proliferation (Pavlovic-Kentera et al., 1989). Alternatively, it has also been proposed that the abnormalities seen in *b/b* rats result from an acquired disorder of the hematopoietic stem cell due to the deleterious effect of prolonged hypoxia (Rolovic et al., 1991).

Therefore, based upon the studies of *fit1* mutants presented here, a number of striking similarities exist between iron deficiency anemias, particularly the *b/b* anemia phenotype, and the *fit1* mutant phenotype. These similarities suggest that the *fit1* mutations could affect iron metabolism and that at least some future investigations of *fit1* mutants should address this possibility. For example, kinetic studies of iron metabolism in the *b/b* rat have indicated that iron delivery to tissues is deficient in affected rats, and that this is due to defective transport of iron from endosomes within *b/b* reticulocytes (Edwards et al., 1986; Garrick et al., 1993).

Thus, these are some examples of future directions that may be initiated to investigate the *fit1* mutant phenotype, based upon the results of the phenotypic analyses presented here. As noted above, anemias with characteristics similar to those observed in the *fit1* phenotype can be caused by defects to a number of different pathways. Therefore, similarities of the *fit1* phenotype to other anemic conditions should provide insights into future experiments that may point to the primary defect in these mice, and, in conjunction with the eventual cloning of the *fit1* gene, will contribute to our understanding of mammalian hematopoiesis.

V. GENETIC AND PHYSICAL MAPPING OF THE *fitness 1* (*fit1*) LOCUS WITHIN THE *Fes-Hbb* REGION OF MOUSE CHROMOSOME 7

Introduction

The phenotypic analyses performed in this study have provided some indication of the biological function of the *fit1* gene. However, despite the accumulated phenotypic information, the specific defect in *fit1* mice remains unknown. Although continued phenotypic analyses should provide further insights into the specific action(s) of the *fit1* gene, perhaps the most information about the function of this gene in mammalian development will come from molecular cloning and characterization of the gene itself.

The following section has been submitted to *Mammalian Genome* as a research article (Potter et al., submitted) entitled "Genetic and physical mapping of the *fitness 1* (*fit1*) locus within the *Fes-Hbb* region of mouse chromosome 7". The manuscript describes mapping of the *fit1* gene, identification and cloning of a deletion breakpoint (c^{AL}) which defines the proximal border of the *fit1* gene, derivation and mapping of a DNA probe (RN302) from the distal end of the c^{AL} deletion, and initial physical mapping of the *fit1* region through the use of the RN302, and another DNA probe (pA4.2c11) that maps distal to *fit1*. This manuscript represents the initial work necessary for the molecular characterization of the *fit1* locus.

Submitted to: *Mammalian Genome*

Genetic and Physical Mapping of the *fitness 1* (*fit1*) Locus Within the *Fes-Hbb* Region of Mouse Chromosome 7

Mark D. Potter[1,2], Mitchell L. Klebig[2], Donald A. Carpenter[2], and Eugene M. Rinchik[2]

[1]University of Tennessee-Oak Ridge Graduate School of Biomedical Sciences and [2]Biology Division, Oak Ridge National Laboratory, P.O. Box 2009, Oak Ridge, Tennessee 37831-8077, USA

Offprint requests to: E.M. Rinchik. Present address:

Sarah Lawrence College
1 Mead Way
Bronxville, NY 10708

Abstract

Mutations at the *fit1* locus affect normal pre- and postnatal development by retarding growth and reducing viability. We report mapping of the *fit1* locus, by *trans*-complementation crosses to mice carrying deletions of the albino (*c*) locus in Chromosome (Chr) 7, to a subregion of the *c*-deletion complex within the *Mod2--sh1* interval. The locus, which is currently defined by five *N*-ethyl-*N*-nitrosourea (ENU)-induced mutations, was found to map in a subregion between the *eed* and *exed* loci. A restriction fragment containing a deletion breakpoint that genetically defines the proximal border of *fit1* was cloned, providing a DNA probe (RN302), from the distal end of this deletion, that should map proximal to *fit1*. Long-range mapping with this probe, and with a DNA probe that maps distal to the *fit1* interval, established that the region containing at least part of the *fit1* gene is 530 kb or less. Positioning of *fit1* between deletion breakpoints, and the isolation and mapping of a DNA probe proximal to it, should facilitate the cloning and molecular characterization of *fit1*, as well as of the *eed* locus and the tightly linked *l(7)5Rn* and *l(7)6Rn* loci.

Complementation analyses among overlapping deletion mutations surrounding the albino (*c*) locus in mouse chromosome (Chr) 7 have led to the identification of a number of loci within the *Fes-Hbb* region necessary for pre- and postnatal development (Fig. 1*; reviewed in Rinchik and Russell, 1990; Holdener and Magnuson, 1993). One method being used to refine the functional map of this region is a saturation-mutagenesis strategy employing the presumptive point-mutagen *N*-ethyl-*N*-nitrosourea (ENU) (Rinchik et al. 1990). This mutagenesis and breeding protocol generates mice carrying a mutagenized Chr 7 marked with the *c* mutation opposite a Chr 7 carrying a 6- to 11-cM deletion of the *c* locus. Thus, any new, recessive, ENU-induced mutation that maps within the region spanned by the large *c* deletion will be expressed.

Initial results from these on-going experiments identified two mutations of a gene, designated *fitness1* (*fit1*), that is necessary for normal growth and viability (Rinchik et al. 1990). Mice hemizygous or homozygous for the prototype mutation, $fit1^{494SB}$, are 30-70% the size of their normal littermates at weaning age, and remain dwarfed throughout their shortened lifespan (Rinchik et al. 1990; M.D.P. and E.M.R., unpublished results). Additionally, *fit1* mutants are

*All figures and tables for Section V are found in the Appendix immediately following this section.

noticeably smaller at least as early as day 14.5 of gestation (M.D.P. and E.M.R. unpublished results). Characterization of the *fit1* gene and of *fit1* mutants should provide insights into aspects of normal prenatal growth requirements as well as into any one of a number of processes necessary for proper pre- and postnatal growth and viability (Evans et al. 1983).

An important step necessary for the identification of the *fit1* gene at the molecular level is to define a more precise map position for the locus. By design
of the hemizygosity screen used to identify this ENU-induced mutation (Rinchik et al. 1990), the *fit1* locus, as well as any other locus identified in the screen, can be mapped to a specific subregion within the *Fes-Hbb* region through a series of complementation crosses with overlapping *c*-locus deletion mutations (e.g., Rinchik and Carpenter, 1993; Rinchik et al. 1993a). Because the *c* deletions provide useful tools for rapidly mapping DNA probes and for gaining access to loci at the ends of deletion mutations (by cloning of restriction fragments containing deletion breakpoints) (e.g., Klebig et al. 1992a; Rinchik et al. 1993b), locating genes within intervals of the deletion complex by complementation analyses is an important first step in molecular isolation of the gene by positional-cloning strategies.

This report describes the mapping of the *fit1* locus to the *Mod2--exed* interval of the *c*-deletion complex, as well as the cloning of a

restriction fragment containing the site of a deletion breakpoint that is closely linked and proximal to the *fit1* gene. We also describe a long-range physical map of the *fit1* region, which suggests that at least part of this gene lies within a 530-kb region between the distal breakpoints of the c^{202G} and c^{11DSD} deletions.

Materials and Methods

Mice

All stocks used in this study were bred at the Biology Division of Oak Ridge National Laboratory. The albino deletion mutations [designated *Df(c)*] used in the complementation analyses are maintained in the heterozygous state opposite the chinchilla allele (c^{ch}) of the albino (*c*) locus. Deletion heterozygotes [$c^{ch}/Df(c)$] display a light-chinchilla coat color, in contrast to the darker, full-chinchilla coat color in c^{ch}/c^{ch} mice. Additionally, ENU-induced *fit1* mutations generated from the saturation-mutagenesis experiments (Rinchik et al. 1990) are maintained opposite the c^{ch} allele on a chromosome marked with the *c* mutation (i.e., c^{ch} +/*c fit1*). For the experiments described in this report, the $fit1^{494SB}$ mutation was maintained by mating carriers to the 47BS inbred strain, which is homozygous for the chinchilla allele (c^{ch} +/c^{ch} +). Thus, *fit1* mutations are also maintained in such a way that carriers of *c* are readily identified by

coat color. Such crosses (c^{ch} +/c^{ch} + X c^{ch} +/c *fit1*^{494SB}) yield light-chinchilla progeny that presumably carry the *fit1* mutation (c^{ch} +/c *?fit1*) as well as mice that are chinchilla in color (c^{ch} +/c^{ch} +).

Such presumed *fit1* carriers (c^{ch} +/c *?fit1*^{494SB}) were confirmed by mating them to c^{ch} +/c^{26DVT} deletion heterozygotes. The c^{26DVT} deletion mutation removes a 6- to 11-cM segment surrounding the *c* locus, and, by design of the mutagenesis strategy, must include the *fit1* locus (Rinchik et al. 1990). Obtaining albino offspring (*c fit1*^{494SB}/c^{26DVT}) from this test cross that display the *fit1* dwarfing phenotype proved that the presumed *fit1* carrier does indeed carry the mutation.

Complementation analyses were performed by mating such proved *fit1* carriers (c^{ch} +/c *fit1*^{494SB}) to mice carrying specific *c* deletions [c^{ch} +/*Df*(*c*)]. One quarter of the offspring from such a cross should be albino and carry the *c fit1*^{494SB} chromosome opposite a *c* deletion chromosome [*c fit1*/*Df*(*c*)]. If the dwarfing phenotype appeared in the albino progeny of these crosses, that combination was considered to be non-complementing.

Southern Blot Analysis, Pulsed-Field Gel Analysis, and DNA Probes

High-molecular-weight DNA was prepared from either adult liver or spleen and was analyzed by Southern blotting and hybridization as previously described (Rinchik et al. 1989, 1993b;

Klebig et al. 1992b). Preparation of genomic DNA, electrophoresis protocols, blotting of gels, and hybridizations suitable for pulsed-field gel analysis (PFGE) were previously described (Klebig et al. 1992b).

Probe pA4.2c11 is a 4.2-kb *Asp718* fragment containing the distal breakpoint of the c^{11DSD} deletion (Sharan et al. 1991). A 2.9-kb *Kpn*I-*Sph*I fragment isolated from this clone defines the *D7Cwr11D* locus.

Cloning the c^{AL} Deletion-Breakpoint Fusion Fragment and Isolation of pRN302

Isolation of the clone pRN286 and identification of the c^{AL} deletion-breakpoint fusion fragment are described in the text. Genomic DNA was prepared from a c^{AL}/c^{112K} animal, digested to completion with *Bam*HI, and size-fractionated on a 10-40% sucrose gradient. Fractions containing the 8.2-kb *Bam*HI size-altered fragment recognized by the pRN286 probe were identified by Southern blot hybridization, and were cloned into the NM1151-λABS phage vector (Poutska et al. 1987). Approximately 4.8 X 10^5 recombinant phage were screened; seven positives were selected and one of these was screened to purity. A 1.8-kb *Bam*HI-*Pst*I fragment, representing the distal end of the c^{AL} deletion, was subsequently subcloned into pBSK+ (Stratagene) and designated pRN302.

Results

Mapping the *fit1* Locus by Complementation Analyses

The *fit1* locus maps within the segment encompassed by the c^{26DVT} deletion, a 6- to 11-cM deletion surrounding the *c* locus (see Fig. 1) (Rinchik et al. 1990). To define the map position of the *fit1* locus more precisely, mice carrying the $fit1^{494SB}$ mutation (c^{ch} +/*c* $fit1^{494SB}$) were mated to mice carrying various *c* deletions [c^{ch} +/*Df*(*c*)]. If at least a portion of *fit1* maps within the interval spanned by a particular deletion, the albino progeny [*c* $fit1^{494SB}$/*Df*(*c*)] will be dwarfed as compared to their normal chinchilla and light-chinchilla siblings.

The results of these crosses (Table 1) show that the c^{112K} deletion complements *fit1*, but the $c^{24R145L}$ and c^{11DSD} deletions do not; thus *fit1* cannot map proximal to *c*, and must map near the *eed* locus. Three deletions (c^{AL}, c^{3DENb}, and c^{202G}) that include at least a part of the *eed* locus, do complement *fit1*; therefore, *fit1* must map distal to *eed*. Because the $c^{24R145L}$ and c^{11DSD} deletions fail to complement *fit1*, but do complement for the *exed* phenotype (Niswander et al. 1989; Sharan et al. 1991), the *fit1* locus must map proximal to *exed*. Therefore, *fit1* maps distal to both *Mod2* and *eed*, within a subregion defined proximally by the distal breakpoints of the

c^{AL}, c^{202G}, and c^{3DENb} deletions and distally by the c^{11DSD}, $c^{5FR60Hb}$, c^{2YPSj}, and $c^{24R145L}$ deletions (Table 1).

Cloning the c^{AL} deletion breakpoint and mapping of probe RN302

It is evident from the mapping results presented in Table 1 that the identification and cloning of any of the deletion breakpoints defining the *fit1* interval would be useful for gaining molecular access to the *fit1* locus, as well as to loci necessary for prenatal development located both proximal and distal to these deletion breakpoints (see Fig. 1) (Sharan et al. 1992; Rinchik and Carpenter, 1993). Sharan et al. (1991) have reported cloning the c^{11DSD} breakpoint and the isolation of a DNA probe, pA4.2c11, from the distal end of this deletion. Mapping of this probe, which defines the *D7Cwr11D* locus, revealed that the $c^{4FR60Hd}$, $c^{5FR60Hb}$, and c^{2YPSj} deletions remove *D7Cwr11D*. Therefore, the c^{11DSD} distal breakpoint is more proximal than the $c^{4FR60Hd}$, $c^{5FR60Hb}$, and c^{2YPSj} distal breakpoints. However, mapping pA4.2c11 with respect to $c^{24R145L}$, the remaining deletion defining the distal border of the *fit1* interval, revealed that *D7Cwr11D* is not deleted by $c^{24R145L}$ and that pA4.2c11 detects size-altered fragments on Southern blots and pulsed-field-gel blots in $c^{24R145L}$ DNA. Figure 2 shows that pA4.2c11 hybridizes, as expected, to both wild-type and size-altered fragments in BstEII-digested c^{ch}/c^{11DSD} DNA. It also hybridizes to a 15.1-kb size-altered

fragment in addition to the 24.2-kb wild-type fragment in $c^{ch}/c^{24R145L}$ DNA. The pA4.2c11 probe likewise detects size-altered fragments in $c^{ch}/c^{24R145L}$ DNA digested with several other enzymes (Fig. 5; data not shown). These results suggest that the $c^{24R145L}$ deletion distal breakpoint is proximal to the c^{11DSD} deletion and that it is 15.1 kb or less from *D7Cwr11D*.

Based on genetic analyses alone, the distal breakpoints of the deletions defining the proximal border of the *fit1* interval (c^{202G}, c^{AL}, and c^{3DENb}) are indistinguishable: all three complement *fit1*, all three elicit the *eed* phenotype when homozygous, and all three fail to complement ENU-induced mutations at two loci [*l(7)5Rn* and *l(7)6Rn*] necessary for prenatal development (Rinchik and Carpenter, 1993). Thus, a DNA probe derived from the distal end of these deletions would be useful in determining the order of their breakpoints, which would further delimit the interval containing the *fit1* locus. The most distally extending deletion of this group defines the proximal genetic border and provides a proximal physical-map landmark for the *fit1* gene. Further, cloning of any of these breakpoints provides a DNA probe with which to initiate molecular analyses of the region.

The c^{202G} and c^{AL} deletions have been shown to extend proximally from *c*, deleting the fumarylacetoacetate hydrolase (*Fah*) locus, but not the *msd* locus (Russell et al., 1982; Klebig et al. 1992a)(see Fig.1). Using a probe (RN226.1) derived from the *Fah* locus (Klebig et al. 1992a), we isolated a cosmid clone, designated RN224, from 129/Rl DNA (Fig. 3A). The end fragments of RN224 were

subcloned and used as probes to screen a panel of *c* deletions by Southern-blot analysis. Fig. 3B shows that, as expected, one end-subclone (RN259) of the cosmid is deleted by the c^{112K}, c^{AL}, c^{26DVT}, and c^{202G} deletions. However, the other end (RN254), while being deleted in c^{112K} and c^{202G}, is not deleted by either the c^{AL} or c^{26DVT} deletions; RN254 is also deleted by other deletions reported by Klebig et al. (1992A) to include *Fah* (data not shown). These results indicate that the proximal breakpoints of the c^{AL} and c^{26DVT} deletions map somewhere within the DNA contained within the wild-type cosmid RN224. Thus, a DNA probe isolated from RN224 can be used to identify a restriction fragment carrying the c^{AL} deletion breakpoint in genomic DNA of the mutant, providing a molecular clone mapping near the proximal border of the *fit1* locus.

To identify such a restriction fragment containing the c^{AL} deletion-breakpoint, DNA probes derived from RN224 were used to screen c^{AL}/c^{112K} DNA by Southern blot analyses. A 1.7-kb *Kpn* I fragment from the RN224 cosmid, designated RN286 (Fig. 3A), was found to hybridize to a 14-kb *Bam*HI fragment in control DNAs, but hybridized to a size-altered 8.2-kb *Bam*HI fragment in c^{AL}/c^{112K} DNA (Fig. 3C). RN286 also detected a polymorphism between control and c^{AL}/c^{112K} DNAs digested with *Xba* I (Fig. 3C). The 8.2-kb *Bam*HI size-altered fragment was, therefore, then cloned from c^{112K}/c^{AL} DNA (see Materials and Methods). Subsequently, a 1.8-kb *Bam*HI-*Pst*I fragment of this 8.2-kb *Bam*HI fragment (Fig. 4A) was subcloned and designated RN302.

The *D7Rn5* locus, identified by the RN302 probe, was mapped by screening Southern blots of genomic DNA from *Mus musculus*-*Mus spretus* F_1 hybrids carrying various *c* deletions (Johnson et al. 1989). RN302 hybridizes to a 4.0-kb *Bam*HI fragment in *M. spretus* DNA and to an 8.5-kb *Bam*HI fragment in *M. musculus* DNA. Fig. 4B shows that the 8.5-kb *Mus musculus*-specific band is, as expected, absent in $c^{26DVT}/+^{Spt}$ DNA, and is also absent in $c^{202G}/+^{Spt}$, $c^{24R145L}/+^{Spt}$, and $c^{11DSD}/+^{Spt}$ DNA. However, the fragment is present in $c^{3DENb}/+^{Spt}$ DNA [RN302 also detects, as expected, the 8.2-kb rearranged fragment in $+^{Spt}/c^{AL}$ DNA]. These results indicate that *D7Rn5* indeed maps distal to *c*, is not deleted by the c^{3DENb} deletion, but is deleted by the c^{202G} deletion. Therefore, the distal breakpoint of the c^{3DENb} deletion lies proximal to the distal breakpoints of the c^{AL} and c^{202G} deletions, and defines the distal border of the interval containing the *eed*, *l(7)5Rn*, and *l(7)6Rn* loci (Rinchik and Carpenter, 1993). Similarly, because the c^{202G} deletion includes *D7Rn5* (i.e., the c^{AL} distal breakpoint), the c^{202G} distal breakpoint defines the proximal border of the *fit1* interval, and, therefore, at least a portion of the *fit1* gene must lie between the distal breakpoints of the c^{202G} and $c^{24R145L}$ deletions.

Physical Mapping of the *fit1* Interval.

The availability of DNA probes from the *D7Rn5* and *D7Cwr11D* loci, which flank the *fit1* interval, suggested that long-range physical mapping, using the RN302 and pA4.2c11 probes, respectively, could be used to estimate the size of the region containing *fit1*. Therefore, the RN302 and pA4.2c11 probes were used to screen panels of wild-type DNAs, as well as DNAs from mice carrying the c^{202G}, c^{AL}, c^{11DSD}, and $c^{24R145L}$ deletions, that had been digested with rare-cutting enzymes and separated by pulsed-field gel electrophoresis. RN302 and pA4.2c11 identify a ~1.5 Mb wild-type fragment in DNAs digested with *Not*I, and a common 530-kb fragment in *Eag*I-digested DNAs (Fig. 5). Because the c^{202G} deletion is known to remove the *D7Rn5* locus (defined by probe RN302) (Fig. 4), the pA4.2c11 probe should detect rearranged fragments when hybridized to *Not*I- and *Eag*I-digested DNAs from c^{ch}/c^{202G} and c^{ch}/c^{AL} mice (as well as c^{11DSD} and $c^{24R145L}$ DNAs). Figure 5 shows that, as expected, rearranged fragments were observed in these deletion DNAs digested with *Not*I, and that rearranged fragments were detected in c^{ch}/c^{11DSD}, $c^{ch}/c^{24R145L}$, and c^{ch}/c^{AL} DNAs digested with *Eag*I.

No size-altered fragment was apparent in c^{ch}/c^{202G} DNA digested with *Eag*I, and it was assumed that the rearranged fragment in c^{ch}/c^{202G} DNA is either too large to be detected under these PFGE conditions, or that it is approximately the same size as the wild-type *Eag*I fragment. However, the rearranged fragments

detected by pA4.2c11 in *Not*I-digested $c^{ch/c11DSD}$, $c^{ch/c24R145L}$, and $c^{ch/cAL}$ DNAs appear to be identical in size to those seen in the same DNAs digested with *Eag*I (Fig. 5). The DNA sequence recognized by *Not*I differs by only one base pair flanking either side of the *Eag*I restriction enzyme recognition site, and, therefore, these sites commonly coincide. The *Eag*I and *Not*I sites flanking the c^{11DSD}, $c^{24R145L}$, c^{202G}, and c^{AL} deletions apparently coincide and, therefore, the rearranged fragments detected by pA4.2c11 in these deletion DNAs are the same size in *Eag*I- and *Not*I- digested DNAs (Fig. 5). This suggests that pA4.2c11 may detect a rearranged fragment in *Eag*I-digested $c^{ch/c202G}$ DNA that is approximately the same size (530 kb) as the wild-type *Eag*I fragment and the *Not*I rearrangement.

Based on these results, the maximum distance separating the *D7Cwr11D* and the *D7Rn5* loci, 530 kb, is represented by the smallest common restriction fragment (*Eag*I) detected by pA4.2c11 and RN302. Additionally, the maximum distance from pA4.2c11 to the distal breakpoint of the c^{202G} deletion is represented by the smallest rearranged fragment detected in $c^{ch/c202G}$ DNA by the pA4.2c11 probe [a 530-kb rearranged *Not*I (and presumably, *Eag*I) fragment]. Therefore, this 530-kb interval represents the smallest determined region within which at least a portion of the *fit1* gene must be contained (see Fig. 6).

Discussion

Through a strategy designed to refine the functional map of the *Fes-Hbb* region by recovering ENU-induced mutations at loci mapping within a large (6- to 11- cM) *c* deletion, Rinchik et al. (1990) reported the identification of a gene, *fit1*, that appears to be necessary for proper intrauterine and postnatal growth and survival (Rinchik et al. 1990). Mice homozygous or hemizygous for the *fit1* mutation are proportionately dwarfed as early as day 14.5 of gestation, and *fit1* mutants remain dwarfed throughout their shortened lifespan. They also exhibit a severe anemia and may have defects in hematopoiesis (M.D.P. and E.M.R. unpublished results). Because *fit1* mutants are dwarfed before birth, cloning and characterization of the *fit1* gene will provide insight into mid- to late-gestational events important in normal pre- and postnatal growth and viability (Evans et al. 1983). Additionally, because the *fit1* mutation, and any other ENU-induced mutations recovered in this mutagenesis screen, are presumably intragenic mutations, cloning and sequence analysis of genes identified in this manner will be of importance in correlating biological function with specific DNA sequences. It should also be noted that the ENU-mutagenesis screen has proved useful for identifying loci within the *c* region, such as *fit1*, that were previously not detectable in extensive complementation analyses with radiation-induced deletions (Russell et al. 1982; Rinchik et al., 1993a).

Complementation analyses with lethal *c* deletions demonstrated that *fit1* maps to a subregion of the *c*-deletion complex defined by the distal breakpoints of the c^{AL}, c^{202G}, and c^{3DENb} deletions (proximally) and the c^{11DSD} and $c^{24R145L}$ deletions (distally) (Table 1). Derivation of a probe from the distal end of the c^{AL} deletion has now allowed the ordering of the deletion breakpoints defining the *fit1* proximal border (Figs. 4B and 6). These results suggest that a portion of the *fit1* gene and/or controlling regions map between the c^{202G} and $c^{24R145L}$ distal breakpoints. Additionally, probe RN302 (from locus *D7Rn5*) and an existing DNA probe (pA4.2c11, from locus *D7Cwr11D*) that maps distal to *fit1* (Sharan et al. 1991), co-hybridize to common restriction fragments, as determined by PFGE, and pA4.2c11 detects a 530-kb size-altered fragment in c^{ch}/c^{202G} DNA digested with *Not*I and *Eag*I (Fig. 5). Thus, at least a portion of the *fit1* gene should be contained within a maximum distance of 530 kb. These data will facilitate positional-cloning strategies designed to isolate the *fit1* gene, because both the RN302 and pA4.2c11 probes can be used to initiate chromosome walks into the *fit1* region. In addition, because the distal c^{202G} deletion breakpoint maps distal to that of the c^{AL} deletion, the former provides a physical landmark in the chromosome-walking experiments. Thus, any transcripts identified in the *D7Rn5-D7Cwr11D* interval that map to loci within the c^{202G} deletion can be immediately excluded as candidates for *fit1*.

It is interesting to note that *fit1* maps distal to *Mod2*, and is complemented by the c^{20FATw} and c^{112K} deletions. Mice homozygous

for the c^{20FATw} deletion, or c^{20FATw}/c^{112K} or c^{6H}/c^{3H} compound heterozygotes, all lack the *juvenile development and fertility* (*jdf*) locus (see Fig. 1) and display an external phenotype similar to that displayed by *fit1* mutants: dwarfed mice with a shortened lifespan (Lewis et al. 1978; Russell et al. 1982). However, the complementation crosses in Table 1 clearly demonstrate that both the c^{20FATw} deletion, as well as the c^{112K} deletion (which includes *Mod2*, as well as *jdf*), complement the $fit1^{494SB}$ mutation. Thus, *fit1* is a locus distinct from *jdf*.

In addition to aiding in the physical mapping of *fit1*, mapping of the *D7Rn5* locus has further refined the subregion containing the *eed* locus as well as two loci, *l(7)5Rn* and *l(7)6Rn*, recently identified through the ENU saturation-mutagenesis strategy (Rinchik and Carpenter, 1993). The *eed* locus had previously been defined through complementation (Russell et al. 1982) and histological (Niswander et al. 1988, 1989) analyses, and is required for normal formation of the embryonic ectoderm shortly after implantation. Homozygous deletion of this locus results in death of the embryo at approximately day 8.5 of gestation (Niswander et al. 1989; Sharan et al. 1992). The mapping of *D7Rn5* demonstrates that the distal breakpoint of the c^{3DENb} deletion maps proximal to the distal breakpoints of the c^{AL} and c^{202G} deletions. The c^{3DENb} deletion aslo fails to complement ENU-induced mutations at *l(7)5Rn* and *l(7)6Rn* (Rinchik and Carpenter, 1993). This establishes the c^{3DENb} distal deletion breakpoint as the closest breakpoint on the distal side of *eed*. Thus

the isolation of the RN302 probe has further defined the subregion containing the *eed* locus and will facilitate initiation of molecular characterization of this subregion and of two more loci defined by ENU-induced mutations (Rinchik and Carpenter, 1993).

Mapping the *fit1* locus to a specific subregion of the *c* deletion complex, as well as derivation and mapping of *D7Rn5*/RN302, has expanded the functional and physical map of the *Fes-Hbb* region of mouse Chr 7 and will facilitate the eventual isolation of this gene. A defined physical interval containing at least part of the gene, flanking DNA markers, and the existence of deletion breakpoints that delimit the *fit1* region make a positional-cloning strategy feasible. Additionally, five independent alleles of *fit1*, varying widely in severity of effect, have now been recovered from the mutagenesis screen (E.M.R., M.D.P., and D.A.C. unpublished results). Characterization of each of these mutations with respect to any isolated candidate genes will facilitate the identification of alterations in candidate-gene expression or rearrangements at the DNA level.

LIST OF REFERENCES

Ausubel, F.M., Brent, R., Kingston, R.E., Moore, D.D., Seidman, J.G., Smith, J.A., and Struhl, K. (eds.): *Current Protocols in Molecular Biology: Volume 1*, John Wiley and Sons, New York, 1989.

Bates, P.F. and Swift, R.A.: Double *cos* site vectors: simplified cosmid cloning. *Gene* 26: 137-146, 1983.

Johnson, D.K., Hand, Jr., R.E., and Rinchik, E.M.: Molecular mapping within the mouse albino-deletion complex. *Proc Natl Acad Sci USA 86*: 8862-8866, 1989.

Evans, M.I., Mukherjee, A.B., and Schulman, J.D.: Animal models of intrauterine growth retardation. *Ob. and Gyn. Survey 38*: 183-192, 1983.

Holdener-Kenny, B., Sharan, S.K., and Magnuson, T.: Mouse albino deletion complex: from genetics to genes in development. *BioEssays 14*, 831-839, 1992.

Klebig, M.K., Russell, L.B., and Rinchik, E.M.: Murine fumarylacetoacetate hydrolase (*Fah*) gene is disrupted by a neonatally lethal albino deletion that defines the hepatocyte-specific developmental regulation 1 (*hsdr-1*) locus. *Proc Natl Acad Sci USA 89*: 1363-1367, 1992a.

Klebig, M.K., Kwon, B.S., and Rinchik, E.M.: Physical analysis of murine albino deletions that disrupt liver-specific gene regulation or mesoderm development. *Mammalian Genome 2*: 51-63, 1992b.

Lewis, S.E., Turchin, H.A., and Wojtowicz, T.E.: Fertility studies of complementing genotypes at the albino locus of the mouse. *J Reprod Fertil 53*: 197-202, 1978.

Niswander, L., Yee, D., Rinchik, E.M., Russell, L.B., and Magnuson, T.: The albino-deletion complex and early postimplantation survival in the mouse. *Development 102*: 45-53, 1988.

Niswander, L., Yee, D., Rinchik, E.M., Russell, L.B., and Magnuson, T.: The albino-deletion complex in the mouse defines genes necessary for development of embryonic and extraembryonic ectoderm. *Development 105*: 175-182, 1989.

Poustka, A., Pohl, T.M., Barlow, D.P., Frischauf, A.M., and Lehrach, H.: Construction and use of human chromosome jumping libraries from*Not*I-digested DNA. *Nature 325*: 353-355, 1987.

Rinchik, E.M., Russell, L.B., Copeland, N.G., and Jenkins, N.A.: Molecular genetic analysis of the *dilute-short ear* (*d se*) region of the mouse. *Genetics 112*: 321-342, 1986.

Rinchik, E.M., Machanoff, R., Cummings, C.C., and Johnson, D.K.: Molecular cloning and mapping of the ecotropic leudemia provirus *Emv-23* provides molecular access to the albino-deletion complex in mouse chromosome 7. *Genomics 4*: 251-258, 1989.

Rinchik, E.M., and Russell, L.B.: Germ-line deletion mutations in the mouse: tools for intensive functional and physical mapping of regions of the mammalian genome. *In* K.E. Davies and S.M. Tilghman (eds.); *Genome Analysis Volume 1*: Genetic and Physical

Mapping, pp. 121-158, Cold Spring Harbor Laboratory Press, Plainview, New York, 1990.

Rinchik, E.M., Carpenter, D.A., and Selby, P.B.: A strategy for fine-structure functional analysis of a 6- to 11-centimorgan region of mouse chromosome 7 by high-efficiency mutagenesis. *Proc Natl Acad Sci USA 87*: 896-900, 1990.

Rinchik, E.M., and Carpenter, D.A.: *N*-ethyl-*N*-nitrosourea-induced prenatally lethal mutations define at least two complementation groups within the embryonic ectoderm development (*eed*) locus in mouse chromosome 7. *Mammal. Genome 4*: 349-353, 1993.

Rinchik, E.M., Carpenter, D.A., and Long, C.L.: Deletion mapping of four loci defined by *N*-ethyl-*N*-nitrosourea-induced postimplantation-lethal mutations within the *pid-Hbb* region of mouse chromosome 7. *Genetics 135*: 1117-1123, 1993a.

Rinchik, E.M., Tonjes, R.R., Paul, D., and Potter, M.D.: Molecular analysis of radiation-induced albino (*c*)-locus mutations that cause death at preimplantation stages of development. *Genetics 135*: 1430-1443, 1993b.

Russell, L.B., Montgomery, C.S., and Raymer, G.D.: Analysis of the albino-locus region of the mouse IV. Characterization of 34 deficiencies. *Genetics 100*: 427-453, 1982.

Sharan, S.K., Holdener-Kenny, B., Ruppert, S., Schedl, A., Kelsey, G., Rinchik, E.M., and Magnuson, T.: The albino deletion complex of the mouse: Molecular mapping of deletion breakpoints that define

regions necessary for development of the embryonic and extraembryonic ectoderm. *Genetics 129*: 825-832, 1991.

Sharan, S.K., Holdener-Kenney, B., Threadgill, D.W., and Magnuson, T.: Genomic mapping within the albino-deletion complex using individual early postimplantation mouse embryos. *Mammal. Genome 3*: 79-83, 1992.

SECTION V.

APPENDICES

SECTION V.

APPENDIX A

TABLES

TABLE 1. Mapping the *fit1* locus by complementation analyses with albino deletions.[a]

DELETION	Number of Progeny Weaned	ALBINO OFFSPRING [c $fit1^{494SB}$/Df(c)] Normal	Dwarfed	COMPLEMENTATION
26DVT	25	1[b]	9	NO
20FATw	27	7	0	YES
11DSD	31	0	2	NO
4FR60Hd	29	0	5	NO
5FR60Hg	41	0	6	NO
2YPSj	45	0	4	NO
202G	55	9	0	YES
24R145L	21	1[b]	4	NO
AL	83	20	0	YES
3DENb	30	8	0	YES
112K	16	7	0	YES

[a] Mice heterozygous for a *fit1* mutation (c^{ch} +/c $fit1^{494SB}$) were mated to mice heterozygous for specific c deletions [c^{ch} +/Df(c)]. Mice were classified at weaning. Progeny of these crosses may be distinguished by coat color: c^{ch} +/c^{ch} + mice are chinchilla in color, c^{ch} +/c $fit1^{494SB}$ and c^{ch} +/Df(c) are a light-chinchilla color, and c $fit1^{494SB}$/Df(c) are albino. Albinos should comprise 25% of the progeny. In cases of non-complementation, the albino class will display the *fit1* dwarfing phenotype. Often, if the dwarfing were severe, albinos would die before weaning leading to a deficiency of the albino class.

[b] Normal albinos found in non-complementing combinations were presumed to be recombinants that had lost *fit1* from the c *fit1* chromosome. These normal albinos represent one of the two recombinant classes detectable; the other detectable recombinant class, c^{ch} $fit1^{494SB}$/Df(c) progeny, would be dwarfed but not albino. However, dwarfing in this phenotypic class could result sporadically from a cause unrelated to the $fit1^{494SB}$ mutation. Neither class of these rare presumed recombinants were progeny tested.

SECTION V.

APPENDIX B

FIGURES

FIGURE 1. A Genetic Map of the *Fes-Hbb* Region of Mouse Chromosome 7 Showing a Subset of Loci As Well As a Subset of the Albino Deletions.

Loci shown above the chromosome are: *Fes*, feline sarcoma virus protooncogene; *tp*, taupe; *Fah*, fumarlyacetoacetate hydrolase; *c*, tyrosinase; *Emv23*, integration site of the endogenous ecotropic murine leukemia provirus 23; *Mod2*, mitochondrial malic enzyme; *sh1*, shaker 1; and *Hbb*, globin (β chain) (Holdener et al. 1993). The loci indicated below the chromosome are defined by complementation analysis of overlapping *c* deletions (see Rinchik and Russell, 1990, for review). These loci are: *msd*, mesoderm deficient; *jdf*, juvenile development and fertility; *eed*, embryonic-ectoderm development; *exed*, extraembryonic-ectoderm development; and *pid*, preimplantation development. *l(7)5Rn* and *l(7)6Rn* are loci defined by ENU-induced lethal mutations mapping to the *eed* region (Rinchik and Carpenter, 1993).

The horizontal lines beneath the chromosome represent a subset of the deletions surrounding the *c* locus. The names of the specific deletions shown are abbreviated (*e.g.*, 26DVT = c^{26DVT}) and are listed above each line. No physical distance is implied by the lengths of the lines.

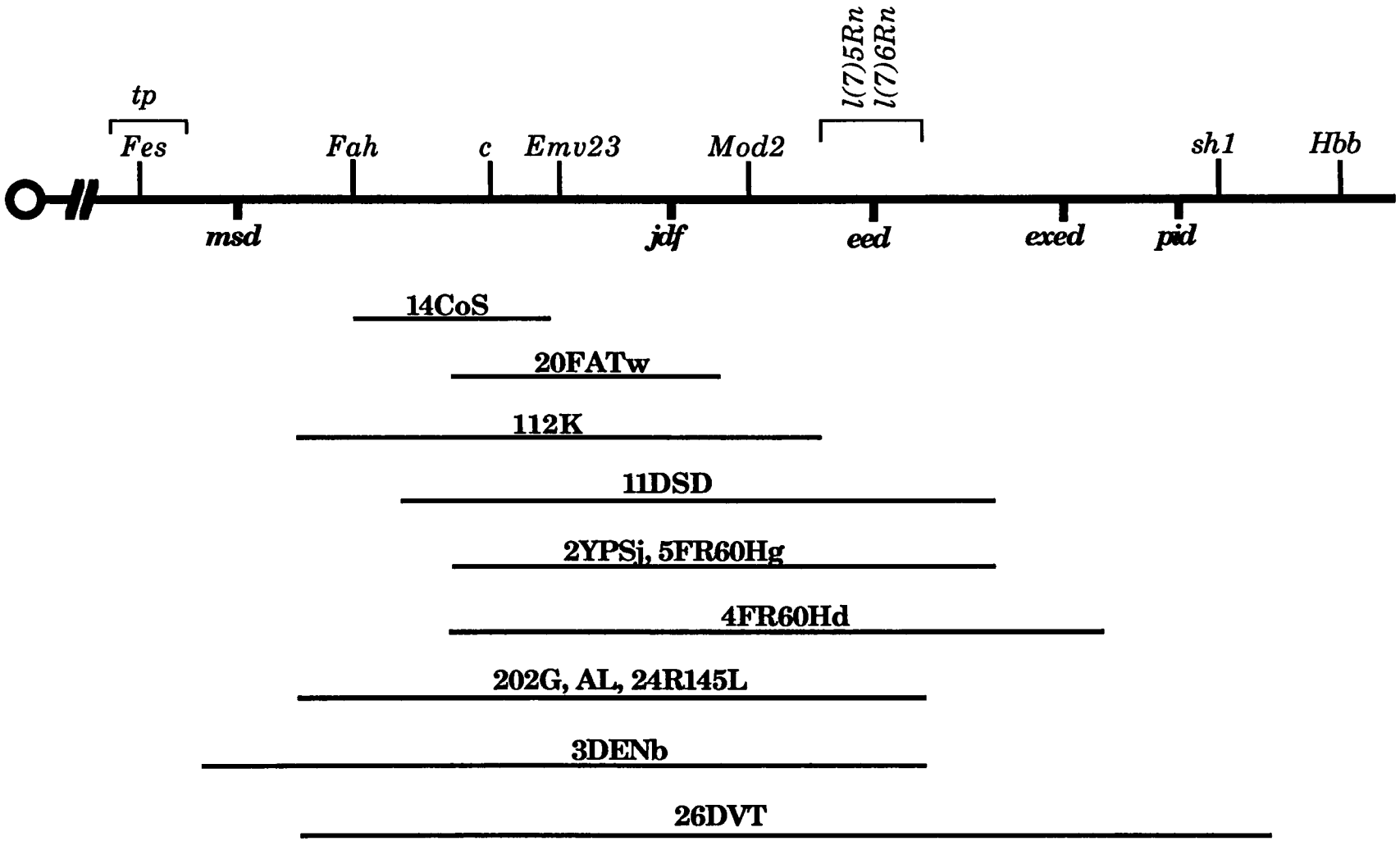
tp
Fes
Fah
c
Emv23
Mod2
l(7)5Rn
l(7)6Rn
sh1
Hbb
msd
jdf
eed
exed
pid
14CoS
20FATw
112K
11DSD
2YPSj, 5FR60Hg
4FR60Hd
202G, AL, 24R145L
3DENb
26DVT

FIGURE 2. Detection of the $c^{24R145L}$ Distal Deletion Breakpoint By the *D7Cwr11D* Clone pA4.2c11.

A Southern blot of *BstE*II-digested DNAs of the indicated genotypes was hybridized with pA4.2c11. Deletion DNAs are abbreviated as in Fig. 1 (*e.g.*, 11DSD = c^{11DSD}), and shall be abbreviated as such in all remaining figures. In addition to the size-altered fragment detected in $c^{24R145L}$ DNA (15.1 kb), a rearranged fragment (9.5 kb) representing the c^{11DSD} deletion breakpoint-fusion fragment is also detected by pA4.2c11.

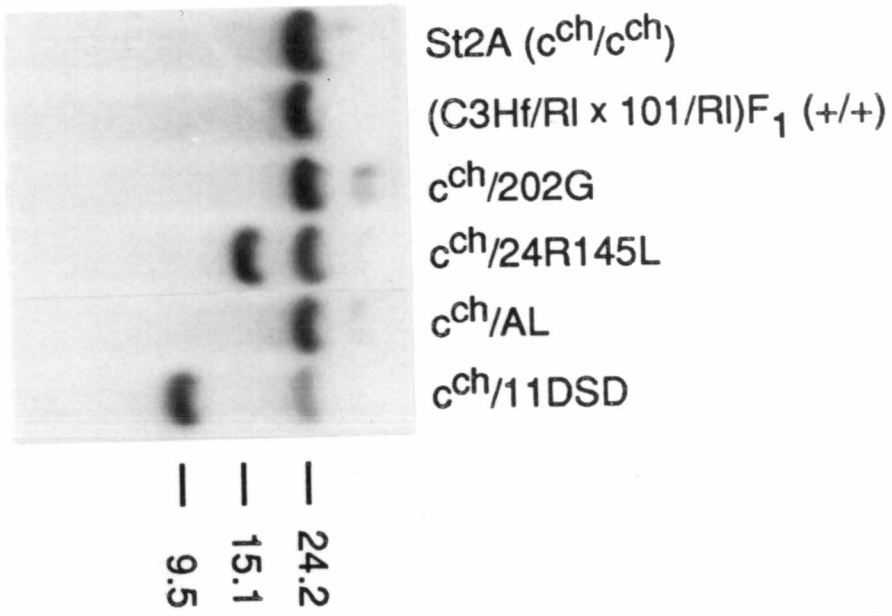
St2A (c^{ch}/c^{ch})
(C3Hf/Rl x 101/Rl)F_1 (+/+)
c^{ch}/202G
c^{ch}/24R145L
c^{ch}/AL
c^{ch}/11DSD
24.2
15.1
9.5

FIGURE 3. Identification of the c^{AL} Deletion Breakpoint-Fusion Fragment With a DNA Probe Isolated From An *Fah* Cosmid.

(A) Restriction map of cosmid clone RN224 isolated with a probe derived from the *Fah* locus. Probe RN254, shown as an open box, is a 4.9-kb *Hind*III-*Sal*I fragment; 0.9 kb of the clone is genomic mouse DNA and 4.0 kb is derived from the c2RB cosmid vector (Bates and Swift, 1983). RN259, shown as a filled box, is a 2.8-kb *Xba*I-*Sal*I fragment, of which 1.45 kb is genomic mouse DNA and 1.35 kb is vector-derived. DNA probe RN286, shown as a shaded box, is a 1.7-kb *Kpn*I fragment isolated from RN224 that detects the c^{AL} breakpoint. Restriction mapping (B = *Bam*HI; K = *Kpn*I) was performed as described (Ausubel et al. 1989). (B) A Southern blot of wild-type DNA (C3Hf/Rl and 101/Rl), stock 2A DNA (c^{ch}/c^{ch}), and DNAs from mice carrying the c^{112K}, c^{AL}, or c^{26DVT} mutations opposite the c^{112K} deletion, digested with *Bam*HI and hybridized consecutively with probes RN259 and RN254. DNA probe 94.1 is a 0.5-kb *Eco*RI-*Hind*III fragment from the *dilute* (*d*) locus in mouse chromosome 9 (Rinchik et al., 1986), and is used here as a DNA loading control. Fragment sizes (in kb) are shown to the right. (C) Southern blot of wild-type (C3Hf/Rl X 101/Rl)F_1 and c^{112K}/c^{AL} compound heterozygote DNAs, digested with either *Bam*HI (B) or *Xba*I (X), and hybridized with probe RN286.

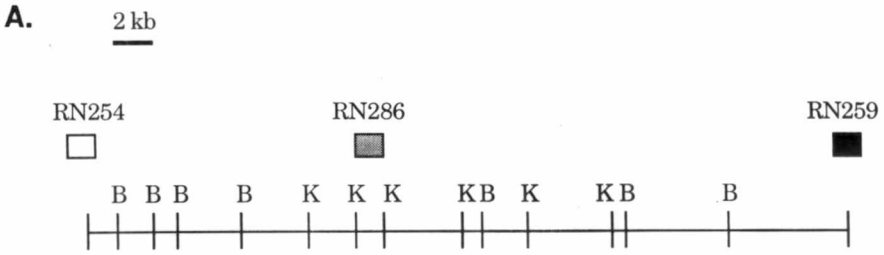
A.
2 kb
RN254
RN286
RN259
B B B B K K K K B K K B B

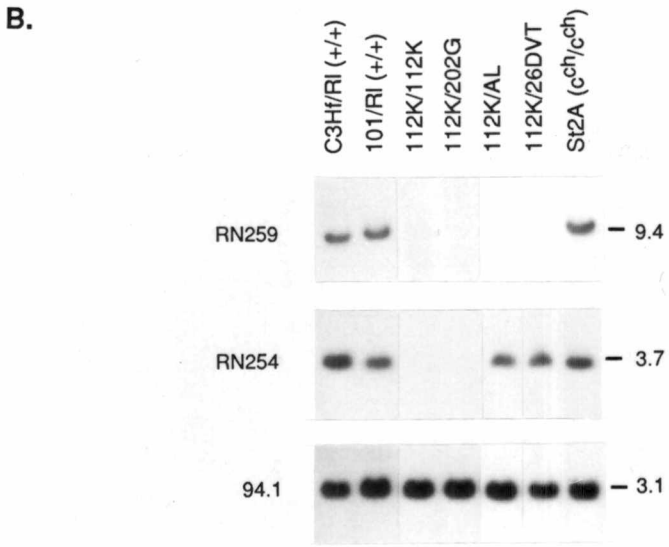
B.
C3Hf/RI (+/+)
101/RI (+/+)
112K/112K
112K/202G
112K/AL
112K/26DVT
St2A (cch/cch)
RN259
9.4
RN254
3.7
94.1
3.1

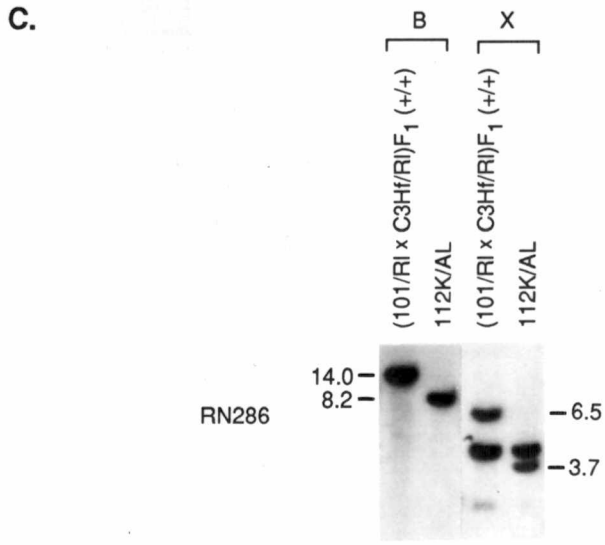
C.
B
X
(101/RI x C3Hf/RI)F1 (+/+)
112K/AL
(101/RI x C3Hf/RI)F1 (+/+)
112K/AL
RN286
14.0
8.2
6.5
3.7

FIGURE 4. Mapping the RN302 DNA Probe (*D7Rn5*) to a Specific Subregion of the *c*-Deletion Complex.

(A) Restriction map of the 8.2-kb deletion-breakpoint-fusion fragment cloned from c^{AL}/c^{112K} DNA with probe RN286 (see Fig. 3C). (B = *Bam*HI; P = *Pst*I). (B) Southern blots of *Bam*HI-digested DNAs of the indicated genotypes were hybridized with the RN302 probe. DNAs from *Mus musculus/Mus spretus* F_1 deletion heterozygotes [*Spt/Df(c)*], *M. musculus* deletion heterozygote dams [$c^{ch}/Df(c)$], and *M. spretus* homozygote sires (*Spt*) are shown. RN302 detects an 8.5-kb *Bam*HI fragment in *Mus musculus* DNA and a 4.0-kb fragment in *Mus spretus*. The absence of the *M. musculus*-specific fragment (8.5 kb) in *Mus spretus* deletion heterozygotes indicates that the *D7Rn5* locus is removed by the deletion.

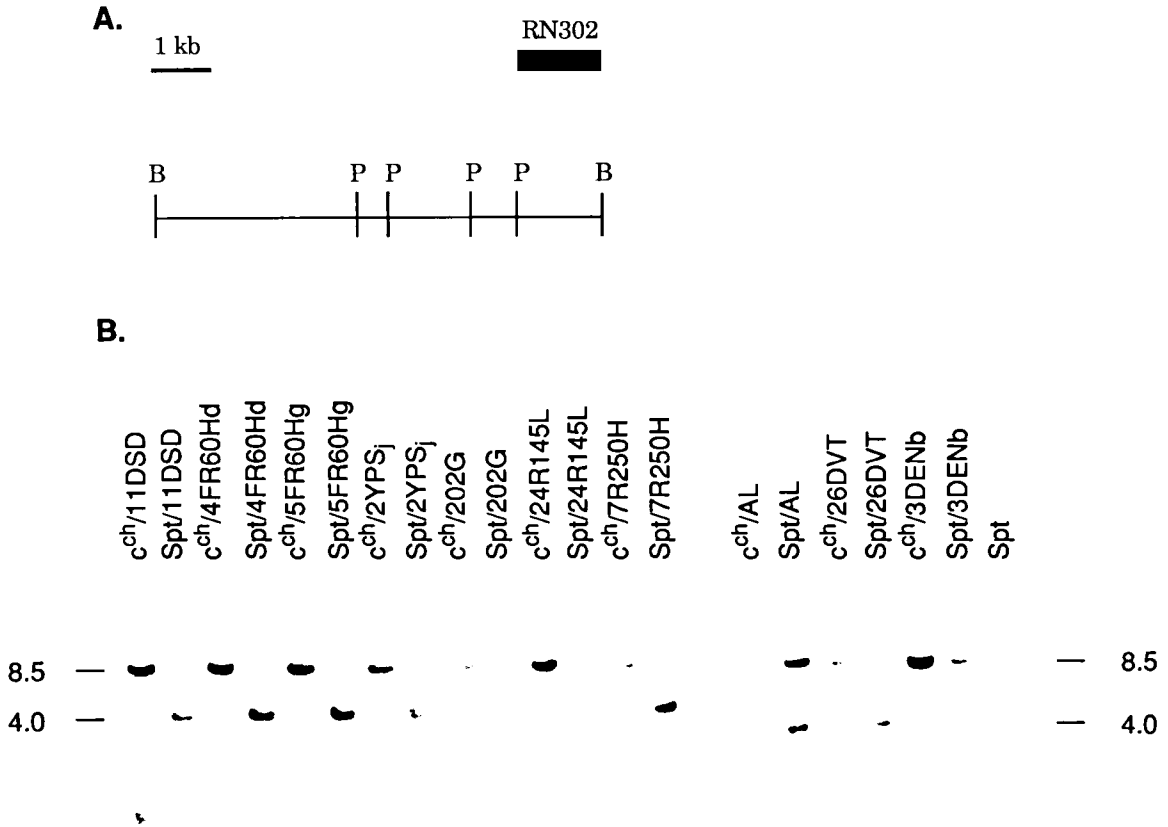
A.
1 kb
RN302
B
P
P
P
P
B
B.
c^ch/11DSD
Spt/11DSD
c^ch/4FR60Hd
Spt/4FR60Hd
c^ch/5FR60Hg
Spt/5FR60Hg
c^ch/2YPSj
Spt/2YPSj
c^ch/202G
Spt/202G
c^ch/24R145L
Spt/24R145L
c^ch/7R250H
Spt/7R250H
c^ch/AL
Spt/AL
c^ch/26DVT
Spt/26DVT
c^ch/3DENb
Spt/3DENb
Spt
8.5
4.0
8.5
4.0

FIGURE 5. Pulsed-Field Gel Analysis of the Region Containing the *D7Rn5* and *D7Cwr11D* Loci.

A PFGE blot of stock 2A (c^{ch}/c^{ch}) and (C3H/Rl X 101/Rl)F_1 control DNAs as well as c^{ch}/c^{11DSD}, $c^{ch}/c^{24R145L}$, c^{ch}/c^{202G} and c^{ch}/c^{AL} deletion-heterozygote DNAs, digested with the indicated enzymes and hybridized consecutively with the pA4.2c11 probe and the RN302 probe (E, *Eag*I; N, *Not*I). The molecular weight sizes of the bands are indicated in kilobases (kb). Digested DNAs were separated under the following conditions: 60- to 140- second pulse ramp, 180 volts, for 32 hrs. The wild-type *Not*I fragment detected by RN302 and pA4.2c11 was sized on blots of gels run under conditions designed to separate very large fragments (not shown). Also, a DNA band migrating at ~180 kb was seen in some hybridizations with both probes, and apparently represents non-specific hybridization.

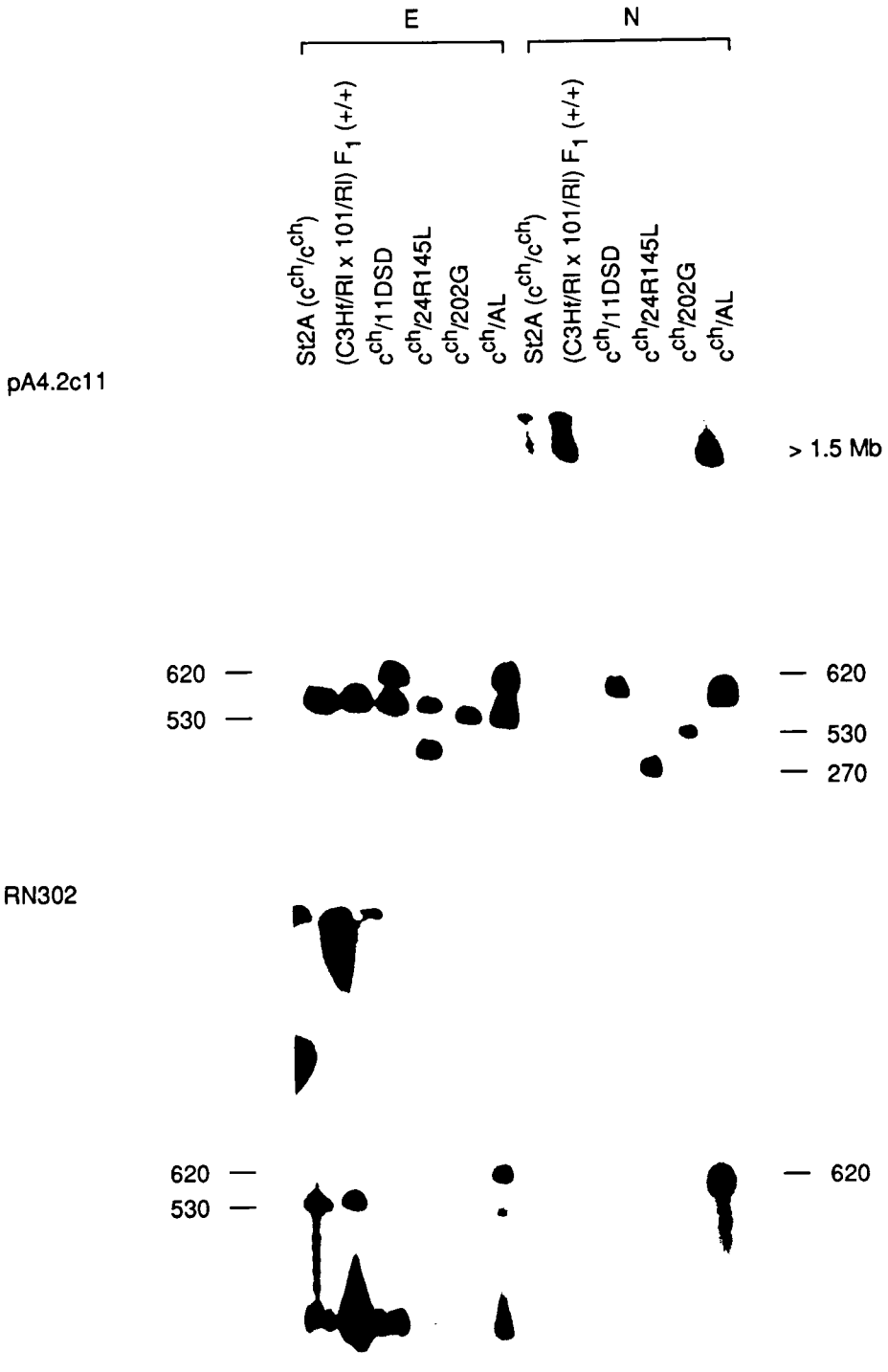
E
N
St2A (c^{ch}/c^{ch})
(C3Hf/Rl x 101/Rl) F_1 (+/+)
c^{ch}/11DSD
c^{ch}/24R145L
c^{ch}/202G
c^{ch}/AL
St2A (c^{ch}/c^{ch})
(C3Hf/Rl x 101/Rl) F_1 (+/+)
c^{ch}/11DSD
c^{ch}/24R145L
c^{ch}/202G
c^{ch}/AL
pA4.2c11
> 1.5 Mb
620
530
620
530
270
RN302
620
530
620

FIGURE 6. Summary of Complementation And Physical Mapping of *fit1*.

At least a portion of the *fit1* gene maps between the distal breakpoints of the c^{202G} and $c^{24R145L}$ deletions (gray box). The physical distance between the c^{202G} breakpoint and *D7Cwr11D* is estimated to be $\leq$ 530 kb (Fig. 5), and the distance from the $c^{24R145L}$ breakpoint to *D7Cwr11D* is $\leq$ 15.1 kb (Fig. 2).

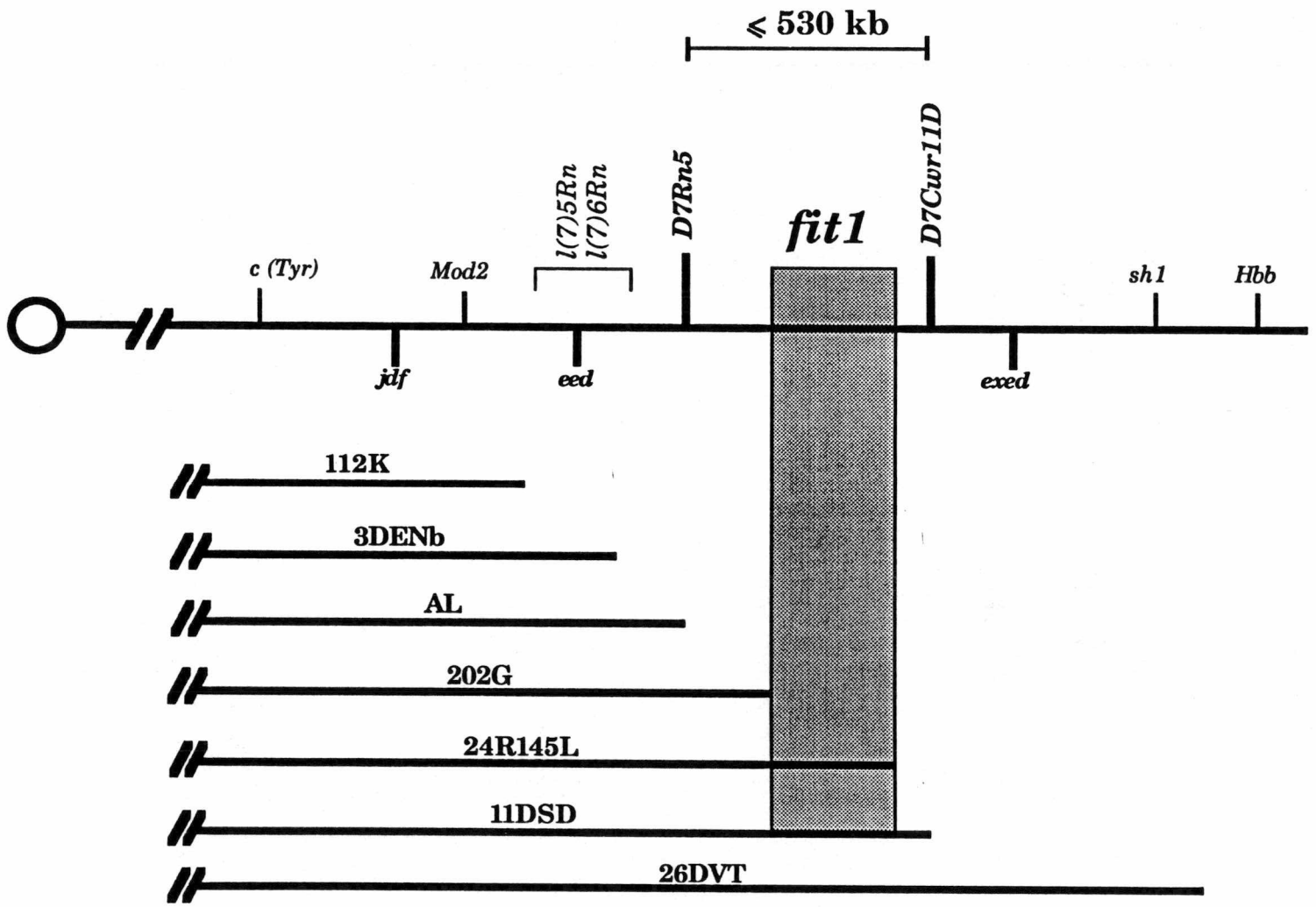
≤ 530 kb
D7Rn5
fit1
D7Cwr11D
l(7)5Rn
l(7)6Rn
c (Tyr)
Mod2
sh1
Hbb
jdf
eed
exed
112K
3DENb
AL
202G
24R145L
11DSD
26DVT

VI. CONTINUED MOLECULAR ANALYSIS OF THE *fit1* LOCUS

Two YAC Clones Map To The *fit1* Region

Most methods now available for isolating cDNAs from genomic DNA require large segments of cloned DNA from the region of interest (Parrish and Nelson, 1993). Therefore, the next step necessary for an attempt at isolating the *fit1* gene requires generating additional DNA clones from the *fit1* region.

Yeast Artificial Chromosomes (YACs) represent useful tools for the molecular analysis of large genomic regions, being capable of containing inserts up to 1 Mb in size (Burke et al, 1987). In an effort to characterize the *eed* and *exed* loci (see Fig 1), two YAC clones were isolated with the pA4.2c11 probe (locus *D7Cwr11D*) (Holdener-Kenney et al., in preparation). These YACs, designated D6E7 and D18H2, are 385 kb and 340 kb in size, respectively, and may extend proximally and/or distally to include all or part of the *fit1* locus. The proximal and distal ends of D6E7 and D18H2 were subcloned and mapped with respect to the *c*-region deletions, including the c^{11DSD} and c^{AL} deletions (Holdener-Kenney et al., in prep.). Importantly, one end of D6E7 was found to be deleted by the c^{202G} and c^{AL} deletions, whereas the distal end, as expected, was not deleted by c^{11DSD}, but was deleted by other *c*-region deletions known to extend further distally (e.g., $c^{5FR60Hg}$) (Holdener-Kenney et al., in prep.). These results indicate

that D6E7 includes both the *D7Cwr11D* and *D7Rn5* loci, and, therefore, spans the *fit1* interval from *D7Cwr11D* to the distal breakpoint of the c^{202G} deletion. This also narrows the maximum size of the *fit1* interval from 530 kb to the size of D6E7, which is 385 kb.

The proximal end of D18H2 was found to be present in the c^{AL} and c^{202G} deletion chromosomes, but is deleted by c^{11DSD}; the distal end is not deleted by c^{11DSD}, but is removed by $c^{5FR60Hg}$ (Holdener-Kenney et al., in prep.). Therefore, D18H2 does not span the interval from *D7Cwr11D* to the distal breakpoint of the c^{202G} deletion (the interval containing at least part of the *fit1* gene). Holdener-Kenney et al. (in prep.) have shown that D6E7 and D18H2 overlap by a maximum of 19 kb surrounding the *D7Cwr11D* locus; therefore, D18H2 must extend a minimum of ~320 kb distal to *D7Cwr11D*. However, since the complementation mapping data for *fit1* do not rule out the possibility that part of the gene could map beyond the distal breakpoint of the c^{11DSD} deletion (Table 1, Section V), then characterization of D18H2, as well as D6E7, should facilitate efforts to identify the *fit1* gene.

Physical Characterization of D6E7 and D18H2

To characterize further the physical map of the *fit1* region, and perhaps to identify sites containing putative CpG "islands" (often associated with the 5' end of transcripts, and less often, with the 3'

end) (Bird, 1987; Gardiner-Garden et al., 1987), rare-cutter restriction-enzyme maps were constructed for both D6E7 and D18H2. Each YAC was digested to completion with several enzymes that cut mammalian DNA infrequently (*Bss*HII, *Mlu*I, *Eag*I, *Cla*I, *Not*I, *Nru*I, *Ksp*I, and *Nar*I; *Cla*I and *Ksp*I digests were not performed on D18H2), as well as partially digested with the same enzymes by varying both the amount of enzyme and the time of digestion (see Materials and Methods). Digestion products were separated by PFGE, and the resulting gels were blotted and hybridized sequentially with right- and left-end vector specific sequences (Burke et al., 1987), and with pA4.2c11 and RN302 (see Materials and Methods; Table 1). Examples of these hybridizations are shown in Fig. 17. Restriction maps were constructed by sizing the partially digested products that hybridized with each end probe; the size of each fragment represents the distance from the end of the YAC [specified by the particular end-probe being used (*i.e.*, right- or left-end specific probe)] to a restriction site for that particular enzyme contained within the cloned YAC insert. The size difference between partially digested fragments hybridizing to a particular end-probe represents the distance between two restriction enyzme sites for that particular enzyme. Tables 10 and 11 show the sizes of partial fragments identified with both YAC end-probes for both D6E7 and D18H2, respectively. By performing this type of analysis for several different enzymes, each particular restriction enzyme map may be overlayed, resulting in the construction of a multi-enzyme restriction

map. Other DNA probes, such as RN302 and pA4.2c11, may also be placed on the restriction map by hybridizing them to the blots of partially digested YAC DNAs. A restriction map of YACs D6E7 and D18H2, as well as the approximate positions of RN302 and pA4.2c11, is shown in Fig 18.

Hybridization of partially digested D6E7 DNAs with pA4.2c11 revealed a pattern identical to that seen with the pYAC4 left-end probe, whereas hybridization of pA4.2c11 to partially digested D18H2 DNAs showed a pattern identical to that seen with the pYAC4 right-end probe (Fig. 17; data not shown). These data suggest that pA4.2c11 is located very near the distal end of D6E7 and near the proximal, overlapping end of D18H2. Indeed, Holdener-Kenney et al., (in prep.), have shown that D6E7 and D18H2 overlap by a maximum distance of 19 kb; therefore, pA4.2c11 must map within 19 kb of the distal end of D6E7 and 19 kb of the proximal end of D18H2. Additionally, RN302 hybridized to partially digested D6E7 DNAs yields a pattern identical to the pYAC4 right-end probe (Fig. 17; data not shown). Therefore, based upon hybridization patterns, RN302 and pA4.2c11 map within the opposite end fragments of D6E7, representing a maximum distance of 385 kb between the two probes. Since RN302 may map anywhere within the ~70-kb *Eag*I fragment at the proximal end of D6E7, and, as noted above, pA4.2c11 maps within 20 kb of the distal end of D6E7, then the minimum distance between RN302 and pA4.2c11 is ~295 to 315 kb. Since the c^{202G} deletion is known to remove RN302 (Fig. 4, Section V), the distance from

pA4.2c11 to the distal breakpoint of the c^{202G} deletion (the *fit1* interval) must be less than the RN302-pA4.2c11 distance.

Potential CpG Islands Within the *fit1* Region

Small regions of DNA containing a high density of unmethylated CpG dinucleotides, identified by rare-cutting restriction enzymes that contain CpG dinucleotides in their recognition sequences, have been shown, in many cases, to be associated with the 5' ends of genes (Bird, 1986, 1987). These "CpG-islands" (also referred to as "HTF-islands"), which can extend over 0.5 to several kb of DNA, may also be found associated with the 3' ends of some genes, as well as within transcribed sequences (Gardiner-Garden and Frommer, 1987). Identification of CpG-islands provides a useful technique for assaying a large region of DNA for potential coding regions, and DNA probes derived from CpG island sites have been successfully used to isolate genes (reviewed in Parrish and Nelson, 1992). Statistical analyses have shown that certain enzyme sites (*Not*I, *Bss*HII, *Eag*I, and *Sst*II) are more frequently found in CpG islands, while others (*Mlu*I and *Nru*I) are more often found outside island sites (Bird, 1989). Based upon those observations, clusters of rare-cutter sites have been classified as "strong" potential island sites if at least three of the four frequently found enzyme sites are present in a cluster, whereas those

containing two are classified as a "moderate" site (Tassone et al., 1992).

The rare-cutter restriction maps constructed for YACs D6E7 and D18H2 indicate possible CpG-island sites within the *fit1* interval (Fig. 18). D6E7, which spans the *fit1*-containing region, contains no "strong" island sites; however, there are possible "moderate" candidate CpG island sites. A cluster of at least four rare-cutter sites is located ~240-245 kb proximal to pA4.2c11. *Ksp*I and *Mlu*I sites are coincident approximately 245 kb from the distal end of D6E7, and approximately 5 kb proximal to this site are coincident *Bss*HII and *Nar*I sites. *Ksp*I is an isoschizomer of *Sst*II; therefore, this cluster may be considered a "moderate" island, since both a *Bss*HII site and *Ksp*I site are present. No other clusters identified in D6E7 could be considered a "moderate" site. However, at least two other *BssH*II sites in this YAC map near, or coincide with, other rare-cutter sites. Approximately 65 kb from the distal end of D6E7 a *Bss*HII site is located near a *Cla*I site (within ~10 kb). Additionally, an *Eag*I site maps ~20 kb proximal to this *Cla*I site. Another *Bss*HII site, approximately 145 kb from the distal end, apparently coincides with a *Cla*I site. In addition, a third potential island site is located appoximately 70 kb from the proximal end of D6E7, where an *Eag*I site maps near a *Cla*I site (within ~5 kb).

The restriction map of D18H2 reveals a "strong" CpG island site approximately 130 kb from the proximal end of the YAC (and pA4.2c11) (Fig. 18). This island contains at least 4 to 5 rare-cutter

sites, including *Bss*HII, *Eag*I, and *Not*I. A second "moderate" site is located approximately 90 kb from the proximal end of D18H2; it contains both a *Bss*HII and an *Eag*I site. No other potential CpG island sites were identified within D18H2. Therefore, D18H2 contains at least one "strong" CpG island site, and at least one "moderate" site.

It should be also noted, however, that due to DNA methylation patterns, the restriction maps of D6E7 and D18H2 may not be completely representative of the genomic DNA restriction map of this region. Restriction enzyme sites present in cloned DNAs may not be functional sites in genomic DNA, since sites in genomic DNA may be methylated, a condition that inhibits restriction enzyme digestion. For example, the restriction map of D6E7 (Fig. 18) indicates three *Eag*I sites between pA4.2c11 and RN302; however, genomic long-range mapping results suggest that pA4.2c11 and RN302 hybridize to a common 530-kb *Eag*I fragment (Fig. 5, Section V). Therefore, it is likely that the three *Eag*I sites between pA4.2c11 and RN302 are methylated in genomic DNA.

Localization of the c^{202G} Deletion Breakpoint

Physical mapping of D6E7 indicates that the distance between RN302 and pA4.2c11 is a maximum of 295-315-kb (Fig. 18). Thus, although the distance from pA4.2c11 to the c^{202G} deletion distal

breakpoint is not known, it is presumably less than 295-315 kb. Since the approximate physical distance from pA4.2c11 to specific restriction enzyme sites within D6E7 is known, localization of the c^{202G} distal deletion breakpoint with respect to specific restriction-enzyme sites within D6E7 would be useful for estimating more precisely the distance from pA4.2c11 to the distal breakpoint of the c^{202G} deletion (the interval containing at least part of *fit1*), and for subsequent attempts to isolate candidate transcripts from this region. For example, the "moderate" candidate CpG island site within D6E7, located approximately 140 kb from the proximal end of the YAC, could be associated with the *fit1* gene. However, the position of the distal breakpoint of the c^{202G} deletion, with respect to this CpG island, is not known. If the c^{202G} deletion removes this CpG island, then this island is not likely to be associated with the *fit1* gene, since c^{202G} complements the *fit1* mutations (and, therefore, cannot delete any part of it). Thus, refining the position of the c^{202G} distal-deletion breakpoint will facilitate further analyses of the *fit1* interval, and could determine if the candidate CpG island in D6E7 could be associated with *fit1*.

Since genomic PFGE analyses indicate that RN302 and pA4.2c11 hybridize to a common 530-kb *Eag*I fragment (Fig. 5, Section V), one strategy that was useful for localizing the c^{202G} distal breakpoint within this interval is long-range mapping utilizing pA4.2c11 and RN302 with DNAs doubly digested with *Eag*I and one of the rare-cutting enzymes that, according to the restriction map of

D6E7, cuts only once in the interval between the two probes (*e.g.*, *Ksp*I, *Mlu*I, and *Nar*I). If the c^{202G} deletion removes the internal enzyme site, then pA4.2c11 should, for example, detect a size-altered fragment in *Eag*I + *Ksp*I doubly digested c^{ch}/c^{202G} DNA. The distance from pA4.2c11 to the distal breakpoint of the c^{202G} deletion would then be a maximum distance equal to the size of the rearranged fragment, or equal to a distance less than the distance from pA4.2c11 to the chosen restriction site (*Ksp*I, for example), as determined from the restriction map of D6E7. If the c^{202G} deletion does not remove the internal restriction site, then the miminum distance from pA4.2c11 to the c^{202G} distal-deletion breakpoint would equal the distance from pA4.2c11 to that internal restriction site (again, as estimated from the restriction map of D6E7).

A PFGE blot of wild-type DNAs, as well as of DNAs from mice carrying the c^{202G} and c^{AL} deletions, digested with *Eag*I and *Ksp*I, was hybridized with the pA4.2c11 and RN302 DNA probes. As shown in Fig. 19, pA4.2c11 hybridizes to a ~340-kb *Eag*I + *Ksp*I fragment in all of the DNAs, and no size-altered fragment is detectable in c^{ch}/c^{202G} DNA. Therefore, the c^{202G} deletion most likely does not remove the single *Ksp*I site located between pA4.2c11 and RN302. According to the restriction map of D6E7 (Fig. 18), this *Ksp*I site is approximately 245 kb proximal to pA4.2c11; therefore, the distal breakpoint of the c^{202G} deletion is a minimum of 245 kb from the pA4.2c11 probe, and presumably, the c^{202G} deletion does not remove the putative "moderate" CpG island at this site (Fig. 18).

Additionally, since the genomic *Eag*I + *Ksp*I fragment detected by pA4.2c11 is ~340 kb, and since it is known that the *Ksp*I site is ~245 kb proximal to pA4.2c11, then it would be predicted that an *Eag*I site would be located ~95 kb distal to pA4.2c11. The restriction map of D18H2 (Fig. 18) shows that, indeed, an *Eag*I site is located ~90 kb distal to pA4.2c11. Also, if *Ksp*I does cut only once between pA4.2c11 and RN302, then the size of the *Eag*I + *Ksp*I-fragment detected by probe RN302, when added to the *Eag*I + *Ksp*I-fragment size detected by pA4.2c11 (~340 kb), should equal the size of the *Eag*I fragment detected by RN302 and pA4.2c11 (~530 kb). Fig. 19 shows that RN302 does detect a 190-kb *Eag*I + *Ksp*I wild-type fragment. Therefore, it is likely that only one *Ksp*I site exists between RN302 and pA4.2c11, and that it is not deleted by the c^{202G} deletion.

Isolation of Cosmid Clones From the *fit1* Region

Many of the techniques currently used to isolate cDNAs from genomic DNA require cloned DNA segments smaller in size than those found in YAC clones (reviewed in Parrish and Nelson, 1992). Therefore, to facilitate the isolation of cDNAs from the *fit1* region, a subgenomic cosmid library was constructed from both D7E6 and D18H2 DNAs.

Total yeast DNA was prepared from the yeast clones containing D6E7 and D18H2 and was partially digested with the

restriction enzyme *Mbo*I (see Materials and Methods). Size-selected, partially digested DNAs were ligated into the *Bam*HI cloning site of the pCOS2EMBL vector. A total of ~7000 and ~3600 clones were generated for the D6E7 and D18H2 libraries, respectively. Considering that the yeast genome is approximately 1.3×10^7 bp, and that the average cosmid clone size is estimated to be 35-40 kb, then 1500 to 1700 clones would be needed to ensure that all genomic sequences are represented in each library (at 99% probability) (Maniatis et al., 1982). Therefore, it is likely that most sequences representing D6E7 and D18H2 are present in the respective libraries.

To isolate cosmid clones potentially containing mouse DNA inserts, the cosmid libraries were screened with DNA probes representing B1 and B2 repetitive elements. B1 and B2 sequences are short, repetitive elements found throughout the mouse genome at a frequency equal to, on average, either a B1 or B2 element being present in every 10 kb of DNA (about 1×10^5 copies/haploid mouse genome) (Krayev et al., 1982). A total of 10 clones in the D6E7 cosmid library hybridized with the B1/B2 probe, and six of these primary positives hybridized with the B1/B2 probe upon rescreening. These six clones were isolated and designated D6E7.1 through D6E7.6. (Several clones in the D18H2 library hybridized to the B1/B2 probe; however, since at least part of the *fit1* gene must be contained within clone D6E7, only cosmids from the D6E7-cosmid library were isolated initially.)

To isolate additional cosmid clones from the *D7Rn5--D7CwrllD* interval, the D6E7-cosmid library was then screened with the pA4.2c11 and RN302 DNA probes. Three clones hybridized with the pA4.2c11 probe; one of these corresponded to clone D6E7.6, whereas the other two pA4.2c11-positive clones did not rescreen. A total of ten clones hybridized with the RN302 probe, of which one corresponded to the isolated D6E7.4 clone. Since the RN302 DNA probe is known to be deleted by the c^{202G} deletion (Fig. 4, Section V), and therefore, not within the interval containing the *fit1* gene, none of the remaining RN302-positive cosmids were purified. In summary, screening of the D6E7-cosmid library with B1/B2 DNA probes, and with RN302 and pA4.2c11, has yielded six cosmid clones in the *D7Rn5--D7Cwr11D* interval.

Mapping D6E7-Derived Cosmid Clones Within the *D7Rn5–D7Cwr11D* Interval

Complex DNA probes, such as cosmid clones or phage clones, have been successfully used to screen DNAs for rearrangements (*e.g.*, Annemieke et al., 1991), and to screen RNA blots and cDNA libraries for coding sequences (reviewed in Parrish and Nelson, 1993). In an effort to map rapidly the D6E7-derived cosmids within the *D7Rn5--D7Cwr11D* interval, each of the six cosmid clones were individually hybridized to Southern blots of DNA from wild-type mice,

and mice carrying the c^{202G}, c^{AL}, $c^{24R145L}$, and c^{11DSD} deletions [*i.e.*, mice of the genotype c^{ch}/ Df(*c*)]. If an individual cosmid clone detects a size-altered fragment (presumably the deletion breakpoint-fusion fragment) in DNA from an animal carrying a deletion, then that cosmid spans the deletion breakpoint, or maps near it. Any cosmid detecting a deletion breakpoint-fusion fragment would have to map a distance equal to, or less than, the size of the rearranged fragment away from the deletion breakpoint. By screening each of the D6E7-derived cosmid clones in this manner, some or all of the clones may be rapidly placed on the physical map. Map positions for each of the cosmid clones would facilitate any search in the region for transcripts, since clones deleted by the c^{202G} deletion can be excluded from further analyses.

Representative hybridizations of some of the D6E7-derived cosmids are shown in Fig. 20. As shown in Fig 20A, cosmid D6E7.4 detects several wild-type *Kpn*I fragments, in addition to a size-altered 7.5-kb *Kpn*I fragment in c^{ch}/c^{AL} DNA. This result suggests that, as expected (since RN302 hybridizes to D6E7.4), cosmid D6E7.4 spans, or maps near (within 7.5 kb), the c^{AL} distal deletion breakpoint. Since no rearranged fragments were detected in c^{202G} DNAs with any of the enyzmes tested, it is presumed that D6E7.4 maps within the interval between the distal breakpioints of the c^{AL} and c^{202G} deletions and it does not cross the c^{202G}-distal deletion breakpoint. Therefore, D6E7.4 does not map within the interval defining the *fit1* locus and can be excluded from further analyses.

Fig 20B shows that cosmid clone D6E7.5 detects wild-type *BstE*II fragments of 24.2 kb and 4.0 kb in size in all DNAs. Additionally, D6E7.5 detects a size-altered fragment of 15.1 kb, presumbly representing a deletion-breakpoint fusion fragment, in *BstE*II-digested $c^{ch/c^{24R145L}}$ DNA, and a size-altered 9.5-kb *BstE*II fragment in $c^{ch/c^{11DSD}}$ DNA (Fig. 20B; note that the 9.5-kb *BstE*II fragment detected in $c^{ch/c^{11DSD}}$ DNA is not evident in this figure). D6E7.5 also detects size-altered fragments in $c^{ch/c^{24R145L}}$ and $c^{ch/c^{11DSD}}$ DNAs digested with *Kpn*I (data not shown). Thus, cosmid D6E7.5 maps near, or spans, the distal breakpoints of the c^{11DSD} and $c^{24R145L}$ deletions. These results also suggest that, since D6E7.5 detects the c^{11DSD} deletion breakpoint, D6E7.5 may contain pA4.2c11 [which was derived from the distal end of c^{11DSD} (Sharan et al., 1991)]. Although not originally detected in the cosmid library screen with pA4.2c11, subsequent gel electrophoresis of restriction enzyme digests revealed that D6E7.5 and D6E7.6 overlap significantly (~16 kb), and, therefore, D6E7.5 may contain pA4.2c11.

Each of the remaining D6E7-derived cosmids were screened in a similar manner on Southern blots of wild-type and deletion DNAs digested with six different restriction enzymes (*Bam*HI, *Sac*I, *Kpn*I, *Sal*I, *Xho*I, and *BstE*II). Cosmids D6E7.1 and D6E7.3 hybridized to the Southern blots, indicating that these clones did indeed contain mouse-DNA inserts, but no size-altered fragments were detected in any of the deletion DNAs (data not shown). Therefore, these two clones could not be placed on the physical map by this method;

however, it was assumed that these clones mapped into either the interval between the distal breakpoints of the c^{AL} and c^{202G} deletions or between the c^{202G} and $c^{24R145L}$ deletions, but did not map close enough to a deletion breakpoint to detect the breakpoint-fusion fragment. Subsequent gel electrophoresis of restriction-enzyme digests of D6E7.3 and D6E7.4 revealed that these two cosmids apparently overlap by approximately 15 kb (data not shown). Therefore, since RN302 is known to hybridize to D6E7.4, D6E7.3 must either map proximal to RN302 and proximal to the distal breakpoint of the c^{AL} deletion, or distal to RN302 and the distal breakpoint of the c^{AL} deletion. If D6E7.3 does map distal to the c^{AL} breakpoint, then restriction enzyme sites for each of the enzymes screened must exist between D6E7.3 and the c^{AL} distal deletion breakpoint, since no size-altered fragments were detected by D6E7.3 in c^{ch}/c^{AL} DNAs digested with each of these enzymes. However, since D6E7.3 is apparently deleted by the c^{202G} deletion, it may also be excluded from further analyses. Comparison of restriction enzyme digests of D6E7.1 and other D6E7-derived cosmids did not reveal any overlapping fragments; therefore, cosmid D6E7.1 remained inconclusively mapped.

Hybridizations of cosmids D6E7.2 and D6E7.6 showed identical patterns (data not shown). Subsequent restriction enzyme digests of these two clones indicated that the cosmids were identical and must have been duplicated during isolation. As noted above, pA4.2c11 hybridizes to D6E7.6, and, as expected, cosmid clone D6E7.6 does

detect size-altered fragments in c^{ch}/c^{11DSD} and $c^{ch}/c^{24R145L}$ DNAs digested with at least two different enzymes (*Kpn*I and *Bst*EII) (data not shown). Therefore, these results confirm that D6E7.6 maps within the *fit1* interval, at the *D7Cwr11D* locus (defined by pA4.2c11).

Concurrent with attempts to map the D6E7-derived cosmids by whole-cosmid hybridization, random DNA probes were generated from each cosmid and mapped on Southern blots of genomic DNA from *Mus musculus-Mus spretus* F_1 hybrids carrying *c* deletions from this region (Johnson et al., 1989). Fig. 21 shows representative mapping blots for two DNA probes, one derived from cosmid D6E7.6 (Fig. 21A), and a second derived from D6E7.4 (Fig. 21B.). A 4.0-kb *Eco*RI fragment derived from D6E7.6 (designated D6E7.6 R4.0) hybridizes to 8.1-kb and 5.3-kb fragments in *Xba*I-digested *Mus musculus* DNA, and to 8.1-kb and 3.6-kb fragments in *Xba*I-digested *Mus spretus* DNA. Fig. 21A shows that the 5.3-kb *Mus musculus*-specific fragment is absent in Spt/c^{26DVT} DNA, but is present in Spt/c^{AL}, $Spt/c^{24R145L}$, Spt/c^{202G}, and Spt/c^{11DSD} DNA. Additionally, D6E7.6 R4.0 detects a size-altered fragment (~17.3 kb) in c^{ch}/c^{11DSD} and Spt/c^{11DSD} DNAs (Fig 21A.). These data further confirm the map position of D6E7.6 at the *D7Cwr11D* locus.

A 3.0-kb *Bam*HI fragment derived from D6E7.4 (designated D6E7.4 B3.0) hybridizes to three fragments (~22.5 kb, 8.0 kb, and 2.3 kb) in *Eco*RI-digested *Mus musculus* DNA (Fig. 21B). In *Eco*RI-digested *Mus spretus* DNA, D6E7.4 B3.0 detects a 12.4-kb and a 8.9-kb fragment, in addition to the 22.5-kb and 2.3-kb fragments (Fig. 21B).

Fig. 21B shows that D6E7.4 B3.0 is deleted by the c^{26DVT}, c^{202G}, $c^{24R145L}$, and c^{11DSD} deletions, but is not deleted by the c^{AL} deletion. Therefore, D6E7.4 B3.0 maps in the interval between the distal breakpoints of the c^{AL} and c^{202G} deletions. These results confirm that the D6E7.4 cosmid maps at the *D7Rn5* locus.

Mapping of a DNA probe from cosmid D6E7.5 confirmed the previously assigned map position at the *D7Cwr11D* locus (data not shown). DNA probes from the D6E7.3 cosmid could not be mapped in this manner because of repetitive elements being present in all probes tested. Additionally, no DNA probe derived from cosmid D6E7.1 detected restriction fragment variants between *Mus musculus* and *Mus spretus* DNAs with any of the enzymes tested, and, therefore, could not be mapped by the panels of *Mus musculus-Mus spretus* F_1 hybrids. Thus, by combining the results of whole cosmid hybridization and mapping with the *Mus musculus-Mus spretus* F_1 hybrid panels, with the exception of cosmid D6E7.1, all of the cosmids derived from D6E7 have been placed on the physical map, and a summary of the approximate map positions of these clones is shown in Fig. 22.

Attempts to Identify Transcripts in the *fit1* Region

A number of methods are currently available for isolating transcribed sequences from cloned genomic DNA (reviewed in

Parrish and Nelson, 1993). Since two large segments of cloned DNA exist in the *fit1* region (D6E7 and D18H2), and cosmid clones have been isolated from the region as well, several cloned-DNA-based methods for identifying transcripts were utilized in an effort to identify a candidate *fit1* transcript.

Most of the methods currently used to identify coding sequences in genomic DNA can be divided into two groups: those that are "expression-dependent" or "expression-independent". Expression-dependent methods include using DNA probes to screen directly cDNA libraries and Northern blots. A major disadvantage to this technique is that the gene of interest may be detected only if it is expressed in the tissue(s) represented in the cDNA library or Northern blot. Importantly, complex DNA probes, such as YAC clones, cosmids, and phage clones, have been successfully used to detect transcripts in cDNA libraries and on Northern blots (*e.g.*, Elvin et al., 1990; Rommens et al., 1989). However, the use of complex probes further complicates this technique, since the probes may contain large numbers of repetitive sequences, which can result in poor signals, increased background, and false positives.

In an attempt to identify candidate transcripts in the *fit1* region, cosmids D6E7.5, D6E7.6, and D6E7.1 were used as probes in screens of both cDNA libraries and Northern blots. Also, to possibly isolate additional DNA probes within the *D7Rn5--D7Cwr11D* interval, cosmids D6E7.3 and D6E7.4 were used as probes on the cDNA libraries and Northern blots. YAC clone D18H2 was also isolated by

PFGE and used as a probe on cDNA libraries; however, YAC clone D6E7 was not used directly to screen cDNA libraries because it comigrates with a yeast chromosome of similar size and could not be completely isolated from yeast genomic sequences. Since the *fit1* phenotype is known to be present at least as early as E14.5 of gestation (Figs. 7 and 8), implying that the *fit1* gene is expressed early in development, cDNA libraries prepared from E8.5 embryos and E14.5 fetuses were screened. Since the *fit1* gene presumably plays a role in hematopoiesis (see Section III), in addition to screening Northern blots of RNA prepared from E14.5 fetuses, Northern blots of RNA from adult hematopoietic tissues (liver and spleen) were also screened.

Cosmids D6E7.3, D6E7.5, and D6E7.6 did not detect positively hybridizing clones in any of the cDNA libraries screened, and failed to detect transcripts in any tissue (adult spleen, liver, and skin poly-(A+) RNA; whole E14.5 fetal poly-(A+) RNA; see Materials and Methods) represented on Northern blots. YAC clone D18H2 also failed to detect positively hybridizing clones in the cDNA libraries screened. However, cosmid D6E7.1, and DNA probes subsequently isolated from this cosmid, did detect a strongly hybridizing transcript in all tissues represented on Northern blots, and hybridized to several cDNA clones in both the E8.5 and E14.5 cDNA libraries (data not shown). Subsequent isolation and partial sequence analysis of a subset of these cDNA clones, however, revealed that the clones were of ribosomal DNA origin. Direct sequence analysis of a subclone

from D6E7.1 confirmed that this cosmid contained yeast ribosomal DNA (data not shown), and, therefore, the cosmid was most likely detecting mouse ribosomal DNA contaminants in the cDNA libraries. Cosmid D6E7.1 was, therefore, eliminated from further analyses. Cosmid D6E7.4 also detected several positive clones in the E8.5 cDNA library. However, Southern blot analysis of isolated clones revealed that these cDNAs contained highly repetitive sequences (data not shown). Indeed, a significant proportion of cDNAs contain interspersed repetitive elements, primarily in 3' untranslated sequences (Taylor and Piko, 1987; Parimoo et al., 1993). Therefore, the cDNAs isolated with cosmid D6E7.4 most likely represent artifactual clones that do not map within the *D7Rn5--D7Cwr11D* region. Additionally, since cDNAs isolated with D6E7.4 could not represent the *fit1* gene, these cDNAs were excluded from further analyses. In summary, therefore, no candidate transcripts were identified by screening cDNA libraries or Northern blots with the isolated cosmids within the *D7Rn5--D7Cwr11D* interval or with YAC clone D18H2.

Expression-independent methods, which include cross-species sequence homology screening ("zoo blots") and exon amplification, may be used to identify coding sequences without initially requiring expression of the gene of interest. Coding sequences are generally much more highly conserved between species than are noncoding sequences. Cross-species sequence-homology screening (*i.e.*, "zoo-blot" screening) involves hybridizing candidate DNA probes, at

reduced stringency, to panels of DNAs from a variety of species. A DNA probe that detects fragments in other species often contains coding sequences. However, there are disadvantages to this method, including the restrictions that usually very small DNA fragments must be screened, not all fragments containing conserved sequences contain coding sequences, and once sequence conservation is detected Northern blots and/or cDNA libraries representing the appropriate tissue must be screened to detect a transcript. Thus, if large regions of DNA are to be screened, this method can be very tedious and time-consuming. However, cross-species sequence homology has been successfully used to identify a number of genes (reviewed in Parrish and Nelson, 1993).

A second "expression-independent" method allows the isolation of exons from genomic DNA after selective removal of intronic sequences by eukaryotic splicing mechanisms (Buckler et al., 1991). Briefly, genomic DNA fragments are cloned into a mammalian expression vector (pSPL1), in which the cloning site is within HIV-1 *tat* intron sequences, flanked by 5' and 3' splice sites and rabbit β globin sequences (Buckler et al., 1991). Recombinant clones are then transfected into COS-7 cells (an African Green monkey fibroblast cell line), where transcription of the expression vector is driven by the SV40 early promoter (pSPL1 also contains the SV40 poly(A) addition recognition sequence). The vector-derived RNA is processed *in vivo*, and the splice sites of any exon contained within an inserted genomic fragment, if in the correct orientation,

will be paired with the *tat* splice sites and retained in the mature RNA. Cytoplasmic RNA is then prepared, reverse transcribed, and amplified by PCR with oligonucleotide primers specific to rabbit β globin sequences. If the genomic fragment does not contain an exon in the correct orientation, then a vector-specific control-sized fragment will be amplified. If, however, an exon has been cloned in the correct orientation, then this "trapped" exon will be amplified with the flanking vector sequences, and a larger amplified fragment will be recovered. Any identified exons would then need to be confirmed through Northern blot analysis and cDNA library screening. Despite some inherent technical problems [noted in Church et al., (1993, 1994)], exon amplification has been used to identify a number of genes (*e.g.*, Vulpe et al., 1993; Trofatter et al., 1993; reviewed in Parrish and Nelson, 1993).

DNA fragments from cosmids D6E7.3, D6E7.4, D6E7.5, and D6E7.6 were screened for coding sequences by both cross-species sequence homology screening and by exon amplification. DNA fragments, ~0.5-kb to ~9.0-kb in size, were hybridized at reduced stringency to Southern blots containing DNA from mouse, human, dog, trout, chicken, and oppossum. No cross-hybridizing fragments were detected for any probe (data not shown). Additionally, DNA fragments from each cosmid, as well as from YAC clone D18H2, were digested with *Bam*HI, *Bgl*II, and doubly digested with *Bam*HI + *Bgl*II, and subcloned into the *Bam*HI cloning site of the pSPL1 vector. These clones were then assayed for the presence of coding sequences

by the exon amplification method (described above). A number of PCR products generated from these experiments were subsequently screened on Northern blots and on Southern blots (to determine if the product hybridized to mouse DNA; *i.e.*, if the product was mouse-DNA derived). However, since none of these fragments hybridized to mouse genomic DNA, all were presumed to be vector derived artifacts (data not shown). Since YAC clone D6E7 can not be completely separated from yeast genomic DNA, it was not screened by these methods. Therefore, and unfortunately, no candidate transcripts were identified in the *D7Rn5--D7Cwr11D* region through the expression-independent methods of zoo-blot analyses or exon amplification.

A DNA Probe Maps Between The Distal Breakpoint of The c^{202G} Deletion and The *D7Cwr11D* Locus

A 900-kb YAC contig of the region from the *eed* locus to the *exed* locus, which includes the YACs D6E7 and D18H2, has been constructed (Holdener et al., in preparation). One of the YACs within this contig, designated FEID4, was isolated with the proximal end-probe of YAC clone D6E7, and is approximately ~750 kb in size. Mapping of the end-clones of FEID4 with respect to other YAC clones in the region revealed that, although the clone is chimeric (the proximal end-clone does not map to mouse Chr 7), the distal end-

clone does hybridize to YAC clone D6E7 (Holdener et al., in prep.). Thus, since FEID4 is ~750 kb in size, it may extend distally, beyond the distal breakpoint of the c^{202G} deletion, into the *fit1* interval. Indeed, Holdener et al., (in prep.) report that, based upon hybridization to D6E7, the FEID4 distal end-clone maps 85-120 kb proximal to *D7Cwr11D*. Since the c^{202G} distal breakpoint is estimated to be at least 245 kb proximal to *D7Cwr11D* (Fig. 18), FEID4 should map within the *fit1* interval. To determine the map position of the distal end of YAC FEID4 with respect to the deletions defining the *fit1* border, Southern blots of genomic DNA from *Mus musculus-Mus spretus* F_1 hybrids carrying various *c* deletions were screened with the distal end-probe of FEID4 (kindly provided by B. Holdener). The FEID4 distal end-probe hybridizes to a 22.8-kb *Bam*HI fragment in *Mus spretus* DNA, but to a 7.1-kb *Mus musculus*-specific *Bam*HI fragment (Fig. 23). Fig. 23 shows that the *Mus musculus*-specific fragment is absent in Spt/c^{26DVT}, Spt/c^{11DSD}, and $Spt/c^{24R145L}$ DNAs, but is present in Spt/c^{202G} and Spt/c^{AL} DNAs. Because the FEID4 distal end-probe is not deleted by the c^{202G} deletion, but is deleted by the $c^{24R145L}$ deletion, it maps within the *fit1* interval.

Isolation of A Cosmid Clone With The FEID4 Distal End-Probe

The FEID4 distal end-clone represents the only DNA probe that maps completely within the *fit1* interval (*i.e.*, it is deleted by the

$c^{24R145L}$ deletion, but not by the c^{202G} deletion). Screens of zoo blots and Northern blots with the FEID4 distal end-clone, however, were negative (data not shown). Despite these results, the FEID4 distal end-clone represents a potentially important DNA probe for continued molecular analysis of the *fit1* locus. Therefore, it was of interest to isolate cosmid clones positive for the FEID4 distal end-clone, which could then be screened for coding sequences in the same manner as described above for other cosmid clones.

Because the FEID4 distal end-clone maps within the interval spanned by YAC clone D6E7, initially, the D6E7-derived cosmid library was screened; however, no positive clones were identified. Subsequently, a cosmid library of ~1.2 X 10^5 clones, made from a mixture of 129/Rl and C3Hf/Rl splenic DNA, was screened. However, once again, no positive clones were identified. Approximately 1.6 X 10^5 cosmid clones constructed from 129/Sv splenic DNA was then screened with the FEID4 distal end-clone, and one positive clone was identified and purified. This cosmid clone, designated $FEID4_{dist.1}$, is currently being screened for coding sequences by the various techniques described above for other cosmids in the *fit1* region. Additionally, $FEID4_{dist.1}$ represents an important DNA clone that should prove to be an important reagent for continued molecular analysis of the *fit1* region. A map of the *D7Rn5-D7Cwr11D* interval, including the approximate map positions of YAC clones D6E7, D18H2, and FEID4, $FEID4_{dist}$, and the D6E7-derived cosmid clones is shown in Fig. 24.

VII. DISCUSSION

Physical Analysis of the *fit1* Interval

Despite phenotypic analyses of mice expressing mutations of the *fit1* gene, which indicate that this gene is crucial for normal hematopoietic differentiation as well as for normal pre- and postnatal growth and viability, the precise function of the *fit1* gene and its role in development remain unclear (see Section III). Thus, in addition to further phenotypic analyses, a greater understanding of the role of *fit1* in normal development and hematopoietic differentiation will be gained by molecular characterization of the gene. The *fit1* gene, identified by five ENU-induced mutations (Rinchik et al., 1990), has been mapped through complementation analyses to a specific subregion of the *c* deletion complex, defined by the distal breakpoints of the c^{3DENb}, c^{AL}, and c^{202G} deletions (proximally) and the $c^{24R145L}$ and c^{11DSD} deletions (distally) (Potter et al., submitted; Section V). Subsequent cloning of the c^{AL} deletion breakpoint fusion fragment, and isolation and mapping of a DNA probe from the distal end of c^{AL} (RN302), in addition to mapping of a DNA probe derived from the distal end of the c^{11DSD} deletion (pA4.2c11), established that at least part of the *fit1* gene must map between the distal breakpoints of the c^{202G} and $c^{24R145L}$ deletions (Potter et al., submitted; Section V.). Long-range physical-mapping data with DNA probes RN302 and pA4.2c11 were used to determine that the *fit1* interval is ~530 kb or

less (Potter et al., submitted; Section V). Therefore, the definition of a physical interval containing at least part of the gene, the availability of flanking DNA markers, and the existence of deletion breakpoints that delimit the *fit1* region all suggest that a positional-cloning strategy could be used to isolate the *fit1* gene.

Since these results suggest that the region to be analysed for a candidate *fit1* transcript is potentially 530 kb, and since most techniques currently available for isolating cDNAs from genomic DNA require large segments of cloned DNA, the next step necessary for isolation of the *fit1* gene is to obtain additional DNA probes from the region and to narrow the interval in which at least part of the gene must map. To this end, two YAC clones selected with the pA4.2c11 probe (*D7Cwr11D*) were obtained (Holdener et al., in prep). The proximal end of YAC clone D6E7 was shown to be deleted by the c^{AL} deletion; therefore, since the c^{202G} deletion is known to extend further distally than the c^{AL} deletion, D6E7 presumably spans the entire *fit1* interval from pA4.2c11 to the c^{202G} distal breakpoint. Thus, molecular analysis of D6E7 could facilitate efforts to identify the *fit1* gene. Additionally, YAC D18H2 has been shown to overlap YAC D6E7 by only 19 kb surrounding the pA4.2c11 probe, and therefore extends at least 320 kb distal to pA4.2c11 (Holdener et al., in prep.). Since the complementation analyses used to map *fit1* cannot rule out the possibility that part of the *fit1* gene may map distal to the c^{11DSD} deletion distal breakpoint (pA4.2c11), then characterization of D18H2 may also facilitate isolating the *fit1* gene.

To characterize further the physical map of the *fit1* region, and to map RN302 and pA4.2c11 on D6E7 more precisely, rare-cutting restriction enzyme maps were constructed for D6E7 and D18H2 (Fig. 18). Hybridization of RN302 to blots of partially digested YAC DNAs revealed that it maps within the proximal 70 kb of D6E7 (Fig. 18; data not shown). The map position of pA4.2c11 was determined to be very near the distal end of D6E7 and at the extreme proximal end of D18H2 (Fig. 18; data not shown). This map position is consistent with the results of Holdener et al. (in prep.), which place pA4.2c11 within 19 kb of the overlapping ends of D6E7 and D18H2. Thus, since RN302 may map anywhere within the 70-kb *Eag*I fragment at the proximal end of D6E7, and pA4.2c11 maps within 19 kb of the distal end of D6E7, the minimum distance between these two probes is 295-315-kb. Since the c^{202G} deletion is known to remove RN302 (*D7Rn5*) (Fig. 4, Section V), the interval from pA4.2c11 to the distal breakpoint of the c^{202G} deletion is presumably less than 295-315 kb.

The restriction maps of D6E7 and D18H2 also established that clusters of rare-cutter sites are located within the *fit1* region (Fig. 18). Many genes are associated with a high density of unmethylated CpG dinucleotides near their 5' or 3' ends, which are identified by sensitivity to digestion with restriction enzymes that contain one or more CpG dinucleotides in their recognition sequence (Bird, 1986, 1987). Indeed, the number of genes in the human genome is estimated to be 50,000 to 100,000, and the estimated number of CpG islands is approximately 30,000 (Elvin et al., 1992); thus, it is likely

that a significant proportion of genes will be associated with CpG islands. Additionally, recent characterization of the MHC Class II locus demonstrated the utility of CpG-island identification, where 18 of 20 new transcripts identified in the region were identified based on CpG-island association (Sargent et al., 1989; Kendall et al., 1990). Therefore, scanning YACs for potential CpG islands may provide an estimate of gene density within particular regions, and may facilitate attempts to isolate a particular gene of interest.

The rare-cutter restriction map of D6E7 identified at least one potential CpG island, ~240-245 kb from the distal end of D6E7, that contains at least four rare-cutting sites (*Bss*HII, *Ksp*I, *Mlu*I, and *Nar*I) (Fig. 18). This cluster contains sites for two restriction enzymes frequently found in CpG islands (*Bss*HII and *Ksp*I) (Bird, 1989), and is, therefore, considered a moderate candidate for a true CpG island. Only one other cluster within D6E7 contained more than one of the rare-cutting sites frequently found in true CpG islands (Fig. 18). A 20-30-kb interval located ~65-kb from the distal end of D6E7 contains three rare-cutting sites, including *Bss*HII and *Eag*I, which qualifies this cluster as a moderate candidate island. Thus, one of these island sites may, although not necessarily, be associated with the *fit1* gene. Additionally, the restriction map of D18H2 shows at least two potential CpG-island sites distal to pA4.2c11 (Fig. 18). One of these sites, located approximately 130 kb from the proximal end of D18H2, is a cluster of at least 4 to 5 restriction sites, including three of the four restriction enzyme sites frequently found in true

CpG islands (*Not*I, *Bss*HII, and *Eag*I), and, therefore, is considered a strong CpG-island candidate. Since the complementation mapping data do not exclude the possibility that part of the *fit1* gene maps distal to the $c^{24R145L}$ deletion (Table 1, Section V), and since the 5' to 3' orientation of the *fit1* gene is unknown, either of these two potential islands could also be associated with the *fit1* gene.

It should be noted, however, that YAC clones will likely contain more rare cutting sites than are typically observed in genomic DNA, due to methylation of some of these sites in genomic DNA. In mammalian DNA, the deoxycytidine nucleotide found in CpG dinucleotides is often methylated. These methylated sequences are usually not associated with the 5' end of a gene that is actively transcribed (Bird, 1987); thus, if clusters of restriction enzyme sites found in cloned DNA contain methylated sequences in genomic DNA, and, therefore, are not functional cutting sites, then the cluster of rare-cutting sites may not represent a true CpG island. Recent analysis of 22 YAC clones from human chromosome 21 showed that 90-95% of most rare-cutting enzyme sites found in the YAC DNA were methylated in genomic DNA (Tassone et al., 1992). However, for enzyme sites more frequently found in true CpG islands [*Not*I, *Bss*HII, *Eag*I, and *Sst*II (or *Ksp*I)] (Bird, 1989), only 65-80% of the sites were apparently methylated in genomic DNA (Tassone et al., 1992). More DNA probes would have to be obtained from the *fit1* region for PFG analyses to determine the methylation status of most of the rare-cutter sites in the region. However, my results do show

that RN302 and pA4.2c11 hybridize to a common 530-kb *Eag*I fragment in genomic DNA (Fig 5; Section V.); therefore, the three *Eag*I sites between RN302 and pA4.2c11, known to be present in D6E7 (Fig. 18), are likely to be methylated in genomic DNA. *Eag*I sites were included in two of the three proposed candidate CpG islands between RN302 and pA4.2c11, and, therefore, these proposed islands may not be associated with transcribed sequences. However, the strongest candidate island identified in D6E7 does not contain an *Eag*I site, but does contain four other rare-cutter sites, two of which (*Bss*HII and *Ksp*I) are frequently found in CpG islands (Fig. 18) (Bird, 1989). Thus, of at least five potential CpG-island sites identified in D6E7 and D18H2, evidence exists that perhaps two of them are not good candidates.

In addition to allowing the identification of several potential CpG-island sites, the physical mapping of D6E7 and D18H2 has provided insight into a means of determining the map position of the distal breakpoint of the c^{202G} deletion with respect to the strongest candidate CpG-island site within D6E7. Complementation analyses determined that the c^{202G} deletion defines the proximal border of the *fit1* region (*i.e.*, the c^{202G} deletion is the most distally extending deletion that does not delete any part of the *fit1* gene) (Table 1; Section V). Therefore, any transcript deleted or disrupted by the c^{202G} deletion can be excluded as a candidate for *fit1*. Based on the restriction map, the strongest candidate CpG island within D6E7 is located ~240-245 kb proximal to pA4.2c11, and, furthermore, three of

the four enzymes sites in this cluster cut only once in the interval between RN302 and pA4.2c11 (Fig. 18). However, PFGE analyses demonstrated that the c^{202G} deletion does not remove the *Ksp*I site within the cluster of rare-cutter sites. Thus, the c^{202G} deletion presumably does not delete this putative CpG-island site either (Fig. 19). Consequently, if a transcript is associated with this island site, the c^{202G} deletion probably does not delete it, and it may, therefore, be considered a candidate for the *fit1* gene. However, it should also be noted that some CpG-island sites are found at the 3' end of, or within, transcribed sequences (Elvin et al., 1992), and thus, a gene associated with this D6E7-CpG island could conceivably be disrupted by the c^{202G} deletion. Also, the orientation of any transcript that might be associated with this island site is unknown; thus, even if the island were associated with the 5' end of a gene, the 5' end of the gene may be centromere-distal to its 3' end, and extend proximally beyond the c^{202G} deletion distal breakpoint. Nonetheless, these results place the c^{202G} deletion distal breakpoint within a 140-kb interval, between the D6E7-*Ksp*I site and the proximal end of D6E7, which sets the maximum size of the interval containing at least part of the *fit1* gene as being 245 kb.

Although some methods for isolating cDNAs directly from genomic DNA have been developed, most current methods do require large segments of cloned DNA (reviewed in Parrish and Nelson, 1993). Additionally, many techniques used to identify transcribed sequences require assaying relatively small segments of DNA at a

time. For example, a human gene (designated *FMR-1*) implicated in Fragile-X syndrome has been recently cloned by constructing a subgenomic cosmid library from a YAC clone known to span the region of interest (Annemieke et al., 1991). Cosmid clones were isolated from the YAC-derived library by hybridization with human-specific Alu-repetitive elements. The *FMR-1* gene was subsequently identified by screening cosmid clones on cDNA libraries constructed from tissues expected to express the fragile-X syndrome gene (Annemieke et al., 1991). Therefore, a subgenomic cosmid library from YACs D6E7 and D18H2 was constructed to provide additional DNA probes within the *fit1* interval.

Since at least part of the *fit1* gene must map within the interval spanned by YAC D6E7, effort was focused on obtaining cosmid clones from the D6E7-derived cosmid library. A total of five cosmid clones were isolated from the D6E7-derived cosmid library, all of which were selected by hybridization to B1/B2 mouse repetitive elements. Two of these clones (D6E7.3 and D6E7.4) mapped near the *D7Rn5* locus and were deleted by the c^{202G} deletion (Fig. 20 and Fig. 22). Therefore, these cosmids could not contain any part of the *fit1* gene. Of the three remaining cosmids, D6E7.5 and D6E7.6 were mapped to the *D7Cwr11D* locus, whereas D6E7.1 could not be conclusively mapped (Fig. 22). Subsequent analyses of D6E7.1 indicated that this cosmid contained at least some yeast ribososmal DNA and it was excluded from further analyses (see below).

Although approximately four times the number of cosmid clones necessary to ensure complete representation of D6E7 sequences in the library were screened, only clones representing the proximal and distal ends of the YAC were recovered (Fig. 22). Therefore, the D6E7-derived cosmid library may not be representative of D6E7 sequences located in the middle of the YAC. This suggestion is supported by the fact that no cosmid clones in the D6E7-derived cosmid library hybridized to a DNA probe ($FEID4_{dist}$) shown to map to the middle of the *fit1* region (thus, to the middle of D6E7) (Fig. 23). However, two cosmid libraries constructed from wild-type genomic DNA were subsequently screened with $FEID4_{dist}$, and only one positive clone was identified. Therefore, the genomic sequences located within the *fit1* interval may be intrinsically difficult to clone in cosmid vectors. An estimated 8.9% of the human genome has sequence characteristics that render them difficult to clone (Wyman et al., 1985).

Alternatively, since the cosmids recovered were selected with B1/B2 repetitive elements, perhaps these elements are not dispersed evenly in this region and none of the cosmids representing internal D6E7 sequences contained them. B1/B2 repetitive elements are short repeats found throughout the mouse genome. On average, based upon the estimated number of these elements in the mouse genome, B1/B2 repeats would be found approximately in every 10 kb of DNA (Krayev et al., 1982). Therefore, every cosmid clone of 35-45-kb might be expected to contain at least one copy of a B1/B2 repetitive element.

However, these sequences are most likely not evenly distributed, and, thus, large segments of DNA may exist that do not contain these elements.

Attempts to Isolate a Candidate *fit1* Transcript(s)

All attempts, with a variety of methods, to isolate the *fit1* gene failed to identify a candidate transcript. A wide variety of techniques exist for identifying coding sequences, and each has certain advantages and disadvantages (reviewed in Parrish and Nelson, 1993). Certain techniques, termed "expression-dependent", require expression of the gene of interest initially to identify the transcript. These methods include direct-screening of cDNA libraries (Parimoo et al., 1991; Lovett et al., 1991; reviewed in Parrish and Nelson, 1993) and more standard Northern-blot analysis. These methods have the common disadvantage that the transcript of interest must be expressed in the tissue that is represented in the cDNA library or Northern blot to be screened. However, complex DNA probes, such as YAC, cosmid, and phage clones, have been successfully used to identify transcripts by these methods, and, therefore, large segments of DNA can be rapidly screened (Parrish and Nelson, 1993). However, an added disadvantage of using complex DNA probes is that repetitive sequences within a probe can lead to poor signals, increased background signal, and false positives. Thus, negative

results from screening complex probes on cDNA libraries and Northern blots does not necessarily mean that transcribed sequences do not exist within the probe.

D6E7-derived cosmid clones D6E7.1, D6E7.3, D6E7.4, D6E7.5, and D6E7.6 were all screened on cDNA libraries constructed from 8.5-day and 14.5-day total embryos, and on Northern blots containing polyA+ RNA from 14.5-day embryos, and adult spleen and liver. Several positive cDNA clones were obtained with cosmid D6E7.1, and an abundant transcript was detected on all Northern blots screened with this cosmid. However, subsequent sequence analysis of a subset of the isolated cDNAs and from genomic subclones of D6E7.1 revealed that they were of yeast ribosomal DNA origin. Additionally, cosmid D6E7.4 hybridized to several positive cDNA clones; subsequent analyses of a subset of these cDNAs indicated that they were highly repetitive. A significant proportion of transcribed sequences contain B1/B2 repetitive elements in 3' untranslated sequences (Taylor and Piko, 1987; Parimoo et al., 1993). Thus, these cDNAs were concluded to be artifactual. All other cosmids did not detect any positive cDNAs or transcripts on any of the libraries of Northern blots screened.

These negative results may suggest that no coding sequences are contained within the screened cosmids. Indeed, only a limited region of the entire *fit1* interval is represented in these cosmid clones, and, therefore, it is certainly possible that the *fit1* gene may not map within the region spanned by them. Alternatively, if the *fit1* transcript is expressed at only very low levels, or if the gene is

expressed at a very specific time of development, or is expressed in a tissue-specific manner, then the gene could easily be missed in such screens of cDNA libraries or Northern blots. Additionally, as mentioned above, the use of complex DNA probes has certain disadvantages. Indeed, since YAC D18H2 is easily isolated from yeast genomic sequences on preparative PFGs, it was also used to screen cDNA libraries. YAC clones have been successfully used to isolate cDNAs (*e.g.*, Elvin et al., 1990). However, although it is likely that transcribed sequences are contained within the 340-kb spanned by D18H2, no positive clones were obtained. Although, this could be due to the reasons cited above (*e.g.*, the wrong tissues assayed), high levels of background signals also obscured analysis of these hybridizations. Since YAC D6E7 cannot be sufficiently isolated from yeast genomic sequences, no attempt was made to use it directly as a probe on libraries or Northern blots.

Other methods utilized to isolate coding sequences do not require the expression of the gene of interest, at least not initially, and these are termed "expression-independent". Expression-independent methods include screening sequences for cross-species sequence homology (or "zoo-blotting") and exon-trapping methods. Screening DNA probes for cross-species sequence conservation has been used quite successfully in a number of cases (*e.g.*, Monaco et al., 1986; Rommens et al., 1989; Rose et al., 1990). Transcribed sequences are more highly conserved among species than are non-transcribed sequences. Therefore, candidate DNA fragments may be hybridized

to panels of DNAs from a number of different species; those fragments detecting sequences in different species are likely to contain coding sequences. This method allows screening DNA sequences without relying on expression of the gene, thus circumventing the problems of screening the appropriate tissues. However, ultimately Northern blots and cDNA libraries have to be screened with any conserved sequences in order to isolate the gene. One major disadvantage to this method is that relatively small fragments must be screened in order to detect the cross-species homology. When large regions must be screened, this necessitates a tremendous amount of effort. Additionally, any genes that have diverged significantly from other species through evolution may not be detected by this method.

None of the DNA probes isolated from D6E7-derived cosmid clones (with the exception of D6E7.1, which is known to contain yeast ribosomal DNA sequences) gave signals on zoo blots. The DNA probes were generated by restriction enzyme digestions with enzymes that cut frequently, and fragments ranging in size from ~0.5 kb to 9.0 kb were screened, although most fragments were 1-4-kb in size (data not shown). These results support the negative results above and suggest that perhaps no transcribed sequences are contained within these cosmids. However, often cross-species homology is only detected when very small fragments are used as probes. Thus, some cross-species homology may have been undetected if it were contained within a large fragment screened.

Another "expresssion-independent" method for identifying transcribed sequences is exon amplification (Buckler et al., 1991). This method, which screens 1 to 4-kb fragments cloned into a mammalian expression vector for an intact exon, has been used successfully to screen large genomic regions for transcriptional units (*e.g.*, Trofatter et al., 1993; The Huntington's Collaborative Group, 1993). However, cloning YAC DNA fragments is reportedly not as efficient as screening cosmid or phage clones (Church et al., 1994). Thus, efficient screening of large regions with the exon amplification technique probably requires that the region be subcloned into either phage or cosmid clones.

All of the D6E7-derived cosmid clones, as well as isolated YAC D18H2 DNA, were assayed for exons with the exon amplification method. Although a number of potential positive PCR products were initially identified, none hybridized to mouse DNA and were, therefore, concluded to be vector-derived artifacts. Recently, it has been reported that a cryptic splice site within the vector-derived HIV-1 *tat* intronic sequences can result in a large percentage of the generated PCR products being artifactual (Church et al., 1993). Another potential difficulty that reduces the efficiency of this system is that the predominant PCR product will be vector derived, due to the presence of genomic fragments that do not contain exons. As a result, competition among the PCR templates will favor the smaller, more abundant template. Although modifications to the exon-amplification vector have recently been described (Church et al.,

1994), all of the analyses performed in this study were carried out with the original exon-amplification vector (Buckler et al., 1991).

Because no exons were identified with the exon-amplification method, this may also support the possible conclusion that no coding sequences are contained within the region spanned by the isolated D6E7-derived cosmids. However, since the original exon-amplification vector accepts only inserts with *Bam*HI compatible ends, it is possible that an exon contained in these cosmids is not intact within a *Bam*HI, *Bgl*II, or *Bam*HI + *Bgl*II fragment. Additionally, the *fit1* gene could conceivably contain only one exon, and, therefore, it would lack functional splice sites. Another possibility is that the reported disadvantages associated with the original exon amplification vector (noted above) decreased the efficiency of this method, leading to nondetection of an exon actually present.

Future Analyses

The results of the initial molecular analysis of the *fit1* region, described here, will facilitate the eventual isolation of the gene, and, therefore, contribute to an increased understanding of its role in hematopoietic differentiation and in normal pre- and postnatal growth and viability. This work has narrowed the interval in which at least part of the *fit1* gene must map, and has identified several

CpG islands that might mark the 5' end of the *fit1* gene. Additionally, the $FEID4_{dist}$ probe, which was mapped to the c^{202G}-$c^{24R145L}$ interval (Fig. 23), represents an important anchor point for future analyses of the *fit1* region. Indeed, a cosmid clone was recently isolated with $FEID4_{dist}$; continued analysis of this clone, and others that may be isolated with DNA probes from this cosmid, may facilitate identification of the *fit1* gene. Also, physical-mapping results, which contributed to localization of a number of deletion breakpoints, should facilitate molecular characterization of loci mapping at the proximal ends of those deletions. For example, the $c^{24R145L}$ deletion, whose distal breakpoint was found to be within 15 kb of the pA4.2c11 DNA probe at the *D7Cwr11D* locus (Fig. 2, Section V), breaks distal to a locus necessary for mesoderm formation (*msd*) (Holdener et al., in press). Additionally, the cosmid libraries generated from D6E7 and D18H2 could be extremely useful reagents for continued chromosome walking within the region, and for any further attempts to isolate candidate *fit1* transcripts. Therefore, the work presented here should contribute to further characterization of the *fit1* locus, as well as to other loci within the *c*-deletion complex.

One approach to continuing a search for a candidate *fit1* gene is to continue to isolate DNA probes from the region, and to screen them by the same techniques described in this study. For this approach, the $FEID4_{dist}$ DNA probe represents an important reagent, since it is the only DNA probe analyzed to date that maps within the interval that must contain at least part of the *fit1* gene.

The cosmid clone isolated with the $FEID4_{dist}$ probe could be screened by zoo-blot analysis, by Northern and cDNA library screening, and by exon amplification, as described above. Also, additional overlapping cosmids may be isolated by subcloning the end fragments of the $FEID4_{dist}$-positive cosmid and screening either the D6E7-derived cosmid library or other genomic DNA cosmid libraries. This approach could be continued until the entire interval from the c^{202G} distal deletion breakpoint to the distal breakpoint of the $c^{24R145L}$ deletion is spanned, which would result in the cloning of the *fit1* gene in cosmids. However, screening the above mentioned cosmid libraries with the $FEID4_{dist}$ clone yielded only one positive cosmid clone; therefore, if the DNA sequences in this region are not amenable to cloning, then this approach may prove to be more difficult than normally experienced.

Another technique that might be applicable to isolating the *fit1* gene is preferential cloning of fragments near CpG-island sites within YAC clones (Elvin et al., 1992). Since several potential CpG-island sites were identified in the *fit1* region in this study (Fig. 18), this technique could potentially be used to identify a candidate *fit1* transcript. However, YAC DNA must be purified from all yeast chromosomal DNA by preparative PFGE in order to eliminate cloning of yeast genomic sequences. Once completely separated, the YAC DNA is then removed from the agarose block and digested with the rare-cutter of choice (chosen from an identified CpG-island site), as well as with an enzyme that cuts more frequently. The doubly

digested YAC DNA is then cloned into a plasmid vector with compatible termini. One disadvantage of this technique is that, if a fragment is successfully cloned, then a transcript must still be identified by screening on zoo blots and/or Northerns and cDNA libraries. Additionally, a potentially major disadvantage of this technique is that a number of false-positives may be obtained if all yeast genomic DNA was not removed during PFGE. Since any fragment cloned must be screened by hybridization(s), the addition of a large number of false-positives may increase the labor intensity and time involved in this technique to such an extent that it is prohibitive. The two CpG-island sites in the *fit1* region located 90 kb and 130 kb distal to pA4.2c11 (Fig. 18), however, may be amenable to this strategy, since YAC clone D18H2 can be easily separated from yeast chromosomal DNA by PFGE. However, YAC clone D6E7 cannot be easily separated from yeast genomic DNA, and, therefore, this technique may not be easily applied to this YAC. It is important to note, also, that the *fit1* gene need not necessarily be associated with any of the CpG islands identified in this study.

A third approach, recently developed, which provides a means of potentially identifying all of the transcripts located within a YAC clone, is cDNA direct selection (reviewed in Parrish and Nelson, 1993). Although different variations have been described (Parimoo et al., 1991; Lovett et al., 1991), basically YAC (or cosmid) DNA is annealed with a complete cDNA library. Repetitive sequences and other contaminants must be quenched by prehybridization with a

mixture of blocking reagents (yeast DNA, mouse DNA repetitive elements, etc.). Nonspecifically hybridizing sequences are then removed, and specific cDNAs that remain annealed to the target DNA are amplified by PCR with primers specific to the cDNA vector. This method offers several advantages over other screening methods. For example, this method is insensitive to the presence of introns or cryptic splice sites, which can hinder exon-trapping techniques. Additionally, this technique is equally sensitive to YAC or cosmid DNA used as the target DNA, and, therefore, can be used to quickly screen several YACs in a relatively short period of time without having to subclone the YAC. Once again, however, the major disadvantage is that this method is "expression-dependent", in that, any gene(s) present in a particular YAC clone will only be detected if it is expressed in the cDNA library selected for screening. This problem may be avoided if pooled cDNA libraries from different sources are screened. Additionally, yeast contamination in cDNA libraries can lead to the selection of a number of artifactual clones, particularly if total yeast DNA (including the YAC of interest) is used as target DNA. Also, all isolated cDNAs will have to be screened by some method to determine which, if any, are actually located on the targeted YAC. Nonetheless, this technique represents a potentially useful method for isolating the *fit1* gene. Since separation of the target YAC from yeast genomic DNA is not required, then this technique could be used on YAC D6E7 (which must contain at least part of the *fit1* gene). Additionally, the phenotype analyses performed

in this study suggest that cDNA libraries constructed from hematopoietic tissues (spleen, liver, bone marrow, etc.), as well as E14.5 fetal cDNA might be logically screened for the *fit1* gene. Therefore, since at least part of the *fit1* gene must be located on the D6E7 YAC clone, this method represents one of the most promising techniques available that might be used to isolate *fit1*.

Given the increasing density of transcripts mapped in both human and mouse chromosomes, two related, and increasingly successful, approaches to identifying genes, which avoid exhaustive cloning exercises, are based upon the map position of the gene of interest. The "candidate gene" approach utilizes the map position of the locus of interest (defined as a mutation or disease locus), and then the genes already known to map within that region are considered as possible candidates. Those genes that are expressed in the "appropriate" tissues and at the correct time of development are then examined for mutations or alterations of expression in individuals displaying the mutant phenotype. As the transcriptional map continues to become more dense, this approach should become the method of choice, since the work intensity required in positional-cloning strategies can be eliminated. Indeed, this approach has recently been used successfully in several cases (reviewed in Ballabio, 1993; Collins, 1993). For example, X-linked spinal and bulbar muscular atrophy (SBMA) is an adult-onset form of motorneuron disease that is thought to be associated with signs of androgen insensitivity (La Spada et al., 1991). Linkage analyses

mapped (SBMA) to the long arm of the human X chromosome, in the same region as the androgen receptor gene. Given the associated androgen insensitivity, the androgen receptor gene seemed to be a likely candidate for SBMA. Subsequent sequence analysis of PCR-amplified exons of the androgen receptor gene from SBMA patients revealed mutations that segregated with the disease (La Spada et al., 1991).

The "candidate gene" approach may not be applicable to cloning the *fit1* gene at this time, since no other mouse genes have currently been mapped to the *fit1* interval, as defined as the region between the c^{202G} and $c^{24R145L}$ distal deletion breakpoints. However, a similar approach, that also relies upon the map position of the gene of interest, may prove to be useful in identifying the *fit1* gene. Extensive regions of conserved synteny have been established between mouse and human chromosomes (Nadeau, 1989). Thus, the human homologs of a group of linked mouse genes may, in some cases, also be found linked in a region of conserved synteny of the human genome. For example, the human homologs of several loci mapping within an extensive region of mouse Chr 7, extending from the *p* locus to the *Fah* locus, map to the long arm of human Chr 15 (Peters, 1994). Therefore, when a locus of interest is mapped to a specific region in either the mouse or in humans, if no candidate gene maps in that region, the conserved region may be examined for a suitable candidate.

Unfortunately, the conservation of synteny map within *Fes-Hbb* region in mouse Chr 7 is not conclusively defined. The *Fes* locus and the *Fah* locus, both of which map proximal to *c* in the mouse (see Fig. 25), map to the long arm of human chromosome 15. The human homolog of the *c* locus (tyrosinase), however, maps to the long arm of human Chr 11. The *Mod2* locus, which maps distal to *c* in the mouse (Fig. 25), maps to human chromosome 6p. The *Omp* locus maps near the *sh1* locus in the mouse, distal to *c* and *Mod2*, and the human homolog maps to the long arm of human Chr 11, as does tyrosinase (*c*). Finally, the *Hbb* locus maps distal to *c*, *Mod2*, and *Omp*; the human homolog of *Hbb* maps to the short arm of Chr 11. Therefore, based on the current homology map, and assuming that it has a human homolog, it would be difficult to assign the *fit1* locus to a particular region of conserved synteny. However, if the syntenic regions surrounding both the *tyr* and *Hbb* loci are considered, then at least two or three possible candidate genes may be suggested.

Since the phenotype analyses performed in this study suggest that the *fit1* locus is necessary for normal hematopoiesis, the *fit1* gene might be expected to be expressed in hematopoietic tissues. The expression patterns of two loci mapping near the *Hbb* locus in human Chr 11 suggest them as possible *fit1* candidates. A surprisingly large number of cell-surface antigens associated with hematopoietic cells are encoded by genes located on human Chr 11 (Grzeschik and Kazazian, 1985). Although the function of most of these cell-surface antigens is unknown, most are thought to play a

role in cell-cell communications and/or in signal transduction pathways. A cell-surface marker, designated *Mer-2*, which is associated with the red blood cell membrane, was cloned and mapped to human Chr 11, near the *Hbb* locus (Bill et al., 1987). The function of the *Mer-2* gene remains undetermined; however, it is intriguing that it is expressed on red blood cells, since the red blood cells in *fit1* mutants are abnormal.

A second gene that maps near the *HBB* locus in human Chr 11 is the *hemopexin* (*HPX*) gene (Cai and Law, 1986). Hemopexin is a plasma glycoprotein with the highest affinity for heme of any characterized heme-binding protein. It is believed to function as a heme scavenger essential in reutilization of heme-bound iron and/or in prevention of heme-catalyzed oxidative damage (Muller-Eberhard et al., 1968; Morgan et al., 1993). Indeed, red blood cells incubated with toxic levels of heme rapidly undergo membrane distortion due to disruption of the lipid bylayer by free heme, which has a high affinity for lipids (Solar et al., 1991). Additionally, hemopexin is expressed almost exclusively in hematopoietic tissues (Nikkila et al., 1991). Therefore, the *HPX* gene is an attractive candidate for the *fit1* gene. The red blood cells found in *fit1* mutants are characterized by hypochromia, anisocytosis and poikilocytosis, which can be indicative of an iron-deficient anemia (Wintrobe et al., 1974). If the *HPX* gene product is necessary for iron reutilization, a defective *HPX* gene product might lead to an apparent iron deficiency. Also, if the

HPX gene product is unable to bind free heme, this could result in the unusually shaped RBCs present in *fit1* mutants.

The myeloid α-3-fucosyltransferase gene (*FUT4*) has recently been mapped, by somatic cell hybrid analyses, near the tyrosinase locus on the long arm of human Chr 11 (Reguigne et al., 1994). The synthesis of the Lewis^X antigen, which is thought to play a role in cell-cell communication, requires the addition of fucose onto a precursor polysaccharide, a reaction catalyzed by different α-3-fucosyltransferases (Mollicone et al., 1990). Each of the fucosyltransferases differ by their acceptor-specificity requirements, their tissue distribution, and their expression during embryonic and fetal development. A great deal of interest has recently been focused on the fucosyltransferases since their oligosaccharide products are potential ligands for the selectin adhesion molecules (Reguine et al., 1994). The myeloid α-3-fucosyltransferase gene is expressed at early stages of embryonic development, but is replaced during organogenesis in all tissues except certain myeloid and lymphoid cell types (Mollicone et al., 1990). Certain types of congenital dyserythropoietic anemias (CDAs), characterized by unusually shaped RBCs and erythroblastic multinuclearity (Wintrobe et al., 1974), have been shown to result from defects in genes responsible for catalyzing the attachment of carbohydrate moities to glycoproteins in hematopoietic cells (Fukuda et al., 1990). Additionally, mammalian carbohydrates associated with glycoconjugates have many biological functions (Ioffe and Stanley, 1994). Thus, although mutations in the

FUT4 gene have not been reported, they could conceivably produce a range of phenotypic consequences; therefore, based upon its map position and possible biological functions, the *FUT4* gene may also be considered a candidate *fit1* gene.

Based upon the examples listed above, a comparative gene approach and/or a candidate gene approach may be a viable method for identifying the *fit1* gene. The next step necessary for each of the candidates listed above, or any candidate gene identified, is to gather proof that the candidate gene is indeed *fit1*. Initially, any candidate cDNA should be mapped with respect to the c^{202G} deletion. Any candidate gene that is deleted or disrupted by the c^{202G} deletion can be eliminated, since the complementation data show that the c^{202G} deletion does not disrupt the *fit1* gene (Table 1, Section V). Additionally, any candidate cDNA should hybridize to the D6E7 YAC clone. These initial screens would then be followed by screening on Southern blots and Northern blots prepared from mice carrying the various *fit1* mutations, to detect any possible alterations at the DNA or RNA level, respectively. However, since the *fit1* mutations were induced by ENU, they are presumably point mutations and no gross alterations may be expected, particularly at the DNA level. Characterization of a number of ENU-induced mutations at the *rosy* locus in *Drosophila*, however, has revealed a large number of point mutations that resulted in an altered transcript size, due to frameshift mutations, aberrant splicing, or premature termination of the transcript (Gray et al., 1991). Therefore, because there are five

independent *fit1* mutations, it is possible that at least one detectable alteration of the transcript may be detectable.

If no gross rearrangements are detected, other methods would have to be used to screen the candidate gene sequences in *fit1* DNA for possible mutations (Dianzani et al., 1993). One approach would be to clone the candidate gene from *fit1* mutant DNA, sequence the *fit1*-derived cDNA, and compare the *fit1* sequence to the wild-type sequence. However, this represents a potentially difficult and time-consuming process, particularly if the candidate cDNA is large. Alternative methods for rapidly screening genomic sequences, based upon the sequence-dependent migration of short DNA fragments in polyacrylamide gels, have been developed [single-stranded conformation polymorphism (SSCP), reviewed in Dianzani et al., 1993; denaturing gradient gel electrophoresis (DGGE), Fisher and Lerman, 1983]. These techniques have been frequently used to detect single-base pair changes in a number of genes (*e.g.*, Gray et al., 1991; Hogg et al., 1992; Attree et al., 1989; Blanquet et al., 1993). Additionally, fragments representing exon sequences may be quickly generated with the use of the PCR, and large genes containing many exons can be quickly screened (Blanquet et al., 1993).

Assuming that mutations can be detected in a candidate *fit1* gene, the strongest evidence that a particular candidate is indeed the gene will come from correction-of-phenotype experiments utilizing transgenic mice. Additionally, definitive proof could be provided by using homologous recombination to disrupt the candidate *fit1* gene,

and then demonstrate that mice homozygous for the disrupted candidate gene display the *fit1* phenotype.

In any case, this work presented in this study has provided the initial characterization necessary for identification of the *fit1* gene by any one of a number of techniques. Molecular identification and characterization of the *fit1* gene will lead to an increased understanding of its role in pre- and postnatal development, and continued characterization of will contribute to the continuing physical and functional characterization of the mammalian genome.

LIST OF REFERENCES

Adler, S. S. and Trobaugh, F.E.: Hemopoietic support capacity of adult mouse liver. Studies in ^{89}Sr marrow-ablated mice. *Blood 52*: 293-300, 1978.

Aisen, P.: Some physicochemical aspects of iron metabolism. *In* R. Porter (ed.); *Iron Metabolism*, Elsevier, New York, pp. 1-17, 1977.

Annemieke, J.M., Verkerk, H., Pieritt, M., Sutcliffe, J., Fu, Y.H., Kuhl, D., Pizzuti, A., Reiner, O., Richards, S., Victoria, M., Zhang, F., Eussen, B., van Ommen, G., Blonden, L., Riggins, G., Chastain, J., Kunst, C., Galjaard, H., Caskey, T., Nelson, D., Oostra, B., and Warren, S.: Identification of a gene (*FMR-1*) containing a CGG repeat coincident with a breakpoint cluster region exhibiting length variation in Fragile X syndrome. *Cell 65*: 905-914, 1991.

Attree, O., Vidaud, D., Vidaud, M., Amselem, S., Lavergne, J., and Goossens, M.: Mutations in the catalytic domain of human coagulation factor IX: rapid characterization by direct genomic sequencing of DNA fragments displaying an altered melting behavior. *Genomics 4*: 266-272, 1989.

Ausubel, F.M., Brent, R., Kingston, R.E., Moore, D.D., Seidman, J.G., Smith, J.A., and Struhl, K. (eds.): *Current Protocols in Molecular Biology: Volume 1*, John Wiley and Sons, New York, 1989.

Aviv, H. and Leder, P.: Purification of biologically active globin messenger RNA by chromotography on oligothymidylic acid-cellulose. *PNAS 69*: 1408-1412, 1972.

Ballabio, A.: The rise and fall of positional cloning? *Nature Genetics 3*: 277-279, 1993.

Bannerman, R.M., Edwards, J.A., and Pinkerton, P.H.: Hereditary disorders of the red cells in animals. *Prog. Hematol. 8*: 131-179, 1973.

Basch, R.S. and Berman, J.W.: Thy-1 determinants are present on many murine hematopoietic cells other than T cells. *Eur. J. Immunol. 12*: 359-364, 1982.

Bass, B. and Beckner, S.: Role of lymphokines and cytokines in bone marrow stem cell differentiation. *Focus 12*: 90-95, 1992.

Bates, P.F. and Swift, R.A.: Double cos site vectors: simplified cosmid cloning. *Gene 26*: 137-146, 1983.

Batzer, M.A., Tedeschi, B., Fossett, N.G., Tucker, A., Kilroy, G., Arbour, P., and Lee, W.R.: Spectra of molecular changes induced in DNA of *Drosophila* spermatozoa by 1-ethyl-1-nitrosourea and X-rays. *Mut. Res. 199*: 255-268, 1988.

Beamer, W.G. and Cresswell, L.A.: Defective thyroid ontogenesis in fetal hypothyroid (*hyt/hyt*) mice. *Anat. Rec. 202*: 387-393, 1982.

Beamer, W.G., Eicher, E.M., Malthais, L.J., and Southard, J.L.: Inherited primary hypothyroidism in mice. *Science 212*: 61-62, 1981.

Berstein, S.E.: Bone marrow implantation therapy in Hertwig's anemic mice. *Jackson Lab. Ann. Rep. 47*: 59, 1975.

Biljanovic-Paunovic, L., Stojanovic, N., Mostarica-Stojkovic, M., Ramic, Z., Ivanovic, Z., Basara, N., Clemons, G.K., and Pavlovic-

Kentera, V.: Hematopoietic growth factors in anemia of Belgrade laboratory (*b/b*) rats. *Exp. Hematol. 20*: 1257-1262, 1992.

Bill, J., Palmer, E., and Jones, C.: Molecular cloning of MER-2, a human chromosome-11-encoded red blood cell antigen, using linkage of cotransfected markers. *Somat. Cell Mol. Genet. 13*: 553-561, 1987.

Bird, A.P.: CpG-rich islands and the function of DNA methylation. *Nature 321*: 209-213, 1986.

Bird, A.P.: CpG islands as gene markers in the vertebrate nucleus. *Trends in Genetics 3*: 342-347, 1987.

Bird, A.P.: Two classes of observed frequency for rare-cutter sites in CpG islands. *Nucleic Acids Res 17*: 9485-9494, 1989.

Blanquet, V., Turleau, C., Gross, M., Goossens, M., and Besmond, C.: Identification of germline mutations in the RB1 gene by denaturant gradient gel electrophoresis and polymerase chain reaction direct sequencing. *Hum. Mol. Genet. 2*: 975-979, 1993.

Bradley, T.R. and Metcalf, D.: The growth of mouse bone marrow cells *in vitro*. *Austr. J. Exp. Biol. Med. Sci. 44*: 287-300, 1966.

Brennan, M.J., Oldberg, A., Ruoslahti, E., Brown, K., and Schwartz, N.: Immunological evidence for two distinct chondroitin sulfate proteoglycan core proteins: differential expression in cartilage matrix deficiency mice. *Dev. Biol. 98*: 139-147, 1983.

Buckler, A.J., Chang, D.D., Graw, S.L., Brook, J.D., Haber, D.A., Sharp, P.A., and Housman, D.E.: Exon amplification: a strategy to

isolate mammalian genes based on RNA splicing. *PNAS 88*: 4005-4009, 1991.

Burke, D.T., Carle, G.F., and Olson, M.V.: Cloning of large segments of exogenous DNA into yeast by means of artificial chromosome vectors. *Science 236*: 806-812, 1987.

Burke, D.T., Rossi, J.M., Leung, J., Koos, D.S., and Tilghman, S.M.: A mouse genomic library of yeast artificial chromosome clones. *Mammalian Genome 1*: 65, 1991.

Cai, G.-Y. and Law, M.L.: Cloning and characterization of a human gene coding for hemopexin. (Abstract) *Am. J. Hum. Genet. 39*: A191, 1986.

Camper, S.A., Saunders, T.L., Katz, R.W., and Reeves, R.H.: The *pit-1* transcription factor gene is a candidate for the murine Snell dwarf mutation. *Genomics 8*: 586-590, 1990.

Chandra, R.K., Au, B., Woodford, G., and Hyam, P.: Iron status, immune response and susceptibility to infection. *In* R. Porter (ed.); *Iron Metabolism*, Elsevier, New York, pp. 249-268, 1977.

Cheng, T.C., Beamer, W.G., Phillips III, S., Bartke, A., mallonee, R.L., and Dowling, C.: Etiology of growth hormone deficiency in little, Ames, and Snell dwarf mice. *Endocrinology 113*: 1669-1678, 1983.

Church, D.M., Banks, L.T., Rogers, A.C., Graw, S.L., Housman, D.E., Gusella, J.F., and Buckler, A.J.: Identification of human chromosome 9 specific genes using exon amplification. *Hum. Mol. Gen. 2*: 1915-1920, 1993.

Church, D.M., Stotler, C.J., Rutter, R.L., Murrell, J.R., Troffatter, J.A., and Buckler, A.J.: Isolation of genes from complex sources of mammalian genomic DNA using exon amplification. *Nature Genetics 6*: 98-105, 1994.

Coffman, R.L. and Weissman, I.L.: A monoclonal antibody that recognizes B cells and pre B cell precursors in mice. *J. Exp. Med. 153*: 169-179, 1981.

Collins, F.S.: Positional Cloning: Let's not call it reverse anymore. *Nature Genetics 1*: 3-6, 1992.

Darling, S.M. and Abbott, C.M.: Mouse models of human single gene disorders I: Non-transgenic mice. *Bioessays 14*: 359-366, 1992.

Davies, K.A. and Lux, S.E.: Hereditary disorders of the red cell membrane skeletion. *Trends in Genetics 5*: 222-227, 1989.

Demetri, G.D.: Hematopoietic growth factors: current knowledge, future prospects. *In* R.F. Ozols (ed.), *Current Problems in Cancer*, Mosby-Year Book, Inc., St. Louis, pp. 179-259, 1992.

Dianzani, I., Camaschella, C., Ponzone, A., and Cotton, R.G.H.: Dilemmas and progress in mutation detection. *Trends in Genetics 9*: 403-405, 1993.

Dick, J.E.: Immune deficient mice as models for human hematopoietic disease. In *Molecular Genetic Medicine, Volume 1*, pp. 77-115, 1991.

Edwards, J., Huebers, H., Kunzler, C., and Finch, C.: Iron metabolism in the Belgrade rat. *Blood 67*: 623-628, 1986.

Ehrich, E., Craig, A., Poutska, A., Frischauf, A.M., and Lehrach, H.: A family of cosmid vectors with the multi-copy R6K replication origin. *Gene 57*: 229-237, 1987.

Elvin, P., Slynn, G., Black, D., Graham, A., Butler, R., Riley, J., Anand, R., and Markham, A.F.: Isolation of cDNA probes using yeast artificial chromosome probes. *Nucleic Acids Res. 18*: 3913-3917, 1990.

Elvin, P., Butler, R., and Hedge, P.J.: Transcribed sequences within YACs: HTF island cloning and cDNA library screening. *In* R. Anand (ed.); *Techniques for the Analysis of Complex Genomes*, Academic Press, New York, pp. 155-172, 1992.

Eppig, J.T. and Barker, J.E.: Chromosome abnormalities in mice with Hertwig's anemia. *Blood 64*: 727-732, 1984.

Erickson, R.P., Gluecksohn-Waelsch, S., and Cori, C.F.: Glucose-6-phophatase deficiency caused by radiation-induced alleles at the albino locus in the mouse. *PNAS 59*: 437-444, 1968.

Evans, M.I., Mukherjee, A.B., and Schulman, J.D.: Animal models of intrauterine growth retardation. *Obstet. Gyn. Surv. 38*: 183-192, 1983.

Fahrner, K., Hogan, B.L.M., and Flavell, R.A.: Transcripts of H:2 and Qa genes in embryonic and adult mice. *EMBO J. 6*: 1265-1271, 1987.

Fischer, S.G. and Lerman, L.S.: DNA fragments differing by single base-pair substitutions are separated in denaturing gradient gels: correspondence with melting theory. *PNAS 80*: 1579-1583, 1983.

Fulop, G.M. and Phillips, R.A.: Use of *scid* mice to identify and quantitate lymphoid-restricted stem cells in long-term bone marrow cultures. *Blood 74*: 1537-1544, 1989.

Fulop, G.M. and Phillips, R.A.: The *scid* mutation in mice causes a general defect in radiation repair. *Nature 347*: 479-482, 1990.

Fukuda, M.N., Masri, K.A., Dell, A., Luzzatto, L., and Moremen, K.W.: Incomplete synthesis of N-glycans in congenital dyserythropoietic anemia type II caused by a defect in the gene encoding α-mannosidase II. *PNAS 87*: 7443-7447, 1990.

Gardener-Garden, M. and Frommer, M.: CpG islands in vertebrate genomes. *J. Mol. Biol. 196*: 261-282, 1987.

Garrick, L.M., Gniecko, K., Liu, Y., Cohan, D.S., Grasso, J.A., and Garrick, M.D.: Iron distribution in Belgrade rat reticulocytes after inhibition of heme synthesis with succinylacetone. *Blood 81*: 3414-3421, 1993.

Gaylor, M.S., Chervenick, P.A., and Boggs, D.R.: Neutrophil kinetics after acute hemorrhage. *Am. J. Physiol. 131*: 1332-1336, 1969.

Gluecksohn-Waelsch, S.: Genetic control of morphogenetic and biochemical differentiation: lethal albino deletions in the mouse. *Cell 16*: 225-237, 1979.

Gray, M., Charpentier, A., Walsh, K., Wu, P., and Bender, W.: Mapping point mutations in the *Drosophila* rosy locus using denaturing gradient gel blots. *Genetics 127*: 139-149, 1991.

Green, M.C.: Catalog of mutant genes and polymorphic loci. *In* M.F. Lyon and A.G. Searle (eds.); *Genetic Variants and Strains of the*

Laboratory Mouse: 2nd. edition, pp. 12-403, Oxford University Press, Oxford, England, 1989.

Groden, J., Thliveris, A., Samowitz, W., Carlson, M., Gelbert, L., Albertsen, H., Joslyn, G., Stevens, J., Spirio, L., Robertson, M., Sargeant, L., Krapcho, K., Wolff, E., Burt, R., Hughes, J.P., Warrington, J., McPherson, J., Wasmuth, J., Le Paslier, D., Abderrahim, H., Cohen, D., Leppert, M., and White, R.: Identification and characterization of the familial adenomatous polyposis coli gene. *Cell 66*: 589-600, 1991.

Grzeschik, K.-H. and Kazazian, H.H.: Report of the committee on the genetic constitution of chromosomes 10, 11, and 12. *Cyto. Cell Genet. 40*: 179-205, 1985.

Hayhoe, F.G.J. and Flemans, R.J. (eds.): *An atlas of haematological cytology*, John Wiley and Sons, New York, 1970.

Hellman, S. and Grate, H.E.: Enhanced erythropoiesis with concomitant diminished granulopoiesis in preirradiated recipient mice. *Blood 31*: 605-612, 1968.

Herr, W., Sturm, R.A., Clerc, R.G., Corcoran, L.M., Baltimore, D., Sharp, P.A., Ingraham, H.A., Rosenfeld, M.G., Finney, M., Ruvkun, G., and Horvitz, H.R.: The POU domain: a large conserved region in the mammalian *Pit-1*, *Oct-1*, *Oct-2*, and *Caenorhabditis elegans unc-86* gene products. *Genes Dev. 2*: 1513-1516, 1988.

Herrmann, B.G., Labeit, S., Poustka, A., King, T.R., and Lehrach, H.: Cloning of the T gene required in mesoderm formation in the mouse. *Nature 343*: 617-622, 1990.

Hogg, A., Onadim, Z., Baird, P.N., Cowell, J.K.: Detection of heterozygous mutations in the RB1 gene in retinoblastoma patients using single-stranded conformation polymorphism analysis and polymerase chain reaction sequencing. *Oncogene 7*: 1445-1451, 1992.

Holdener, B.C., Brown, S.D.M., Angel, J.M., Nicholls, R.D., Kelsey, G., and Magnuson, T.: Mouse chromosome 7. *Mammalian Genome 4*, S110-S120, 1993.

Holdener, B.C., Thomas, J.W., Potter, M.D., Rinchik, E.M., Sharan, S.K., Schumacher, A., and Magnuson, T.: Localization of eed: Evidence for a single gene required for axial organization of the mouse embryo. In preparation.

Holdener, B.C., Faust, C., Rosenthal, N.S., and Magnuson, T.: msd is required for mesoderm induction in mice. *Development 120*, in press, 1994.

Hughes, P.C.R. and Tanner, J.M.: A longitudinal study of the growth of the black-hooded rat: methods of measurement and rates of growth for skull, limbs, pelvis, nose-rump and tail lengths. *J. Anat. 106*: 349-370, 1970.

Humphries, R.K., Eaves, A.C., and Eaves, C.J.: Self-renewal of hemopoietic stem cells during mixed colony formation in vitro. *PNAS 78*: 3629-3633, 1981.

Huntington's Disease Collaborative Research Group.: A novel gene containing a trinucleotide repeat that is expanded and unstable on Huntington's disease chromosomes. *Cell 72*: 971-983, 1993.

Ioffe, E., and Stanley, P.: Mice lacking *N*-acetylglucosaminyltransferase I activity die at mid-gestation, revealing and essential role for complex or hybrid N-linked carbohydrates. *PNAS 91*: 728-732, 1994.

Jacob, F.: *The Logic of Life*, (English translation by B.E. Spillman), Pantheon Press, New York, 1920.

Johnson, D.R. and Wise, J.M.: Cartilage anomaly (*can*); a new mutant gene in the mouse. *J. Embryol. Exp. Morphol. 25*: 21-31, 1971.

Johnson, D.K., Hand, R.E., Jr., and Rinchik, E.M.: Molecular mapping within the mouse albino-deletion complex. *PNAS 86*: 8862-8866, 1989.

Jones, R.J., Wagner, J.E., Celano, P., Zicha, M.S., Sharkis, S.J.: Separation of pluripotent hematopoietic stem cells from spleen colony-forming cells. *Nature 347*: 188-189, 1990.

Kelsey, G., Ruppert, S., Beerman, F., Grund, C., Tanguay, R.M., and Schutz, G.: Rescue of mice homozygous for lethal albino deletions: implications for an animal model for the human liver disease tyrosinemia type 1. *Genes Dev. 7*: 2285-2297, 1993.

Kendall, E., Sargent, C.A., and Campbell, R.D.: Human major histocompatibility complex contains a new cluster of genes between

the HLA-D and complement C4 loci. *Nucleic Acids Res. 18*: 7251-7257, 1990.

Kimata, K., Barrach, H.J., Brown, K.S., and Pennypacker, J.P.: Absence of proteoglycan core protein in cartilage from *cmd/cmd* (cartilage matrix deficiency) mice. *J. Biol. Chem. 256*: 6961-6968, 1981.

Kishimoto, T., Akira, S., and Taga, T.: Interleukin-6 and its receptor: a paradigm for cytokines. *Science 258*: 593-597, 1992.

Klebig, M.L., Kwon, B.S., and Rinchik, E.M.: Physical analysis of murine albino deletions that disrupt liver-specific gene regulation or mesoderm development. *Mammalian Genome 2*: 51-63, 1992a

Klebig, M.L., Russell, L.B., and Rinchik, E.M.: Murine fumarylacetoacetate hydrolase (*Fah*) gene is disrupted by a neonatally lethal albino deletion that defines the hepatocyte-specific developmental regulation 1 (*hsdr-1*) locus. *PNAS 89*: 1363-1367, 1992b.

Krammer, M.S., Olivier, M., McLean, F.H., Willis, D.M., and Usher, R.H.: Impact of intrauterine growth retardation and body proportionality on fetal and neonatal outcome. *Pediatrics 86*: 707-713, 1990.

Krayev, A.S., Markusheva, T.V., Kramerov, D.A., Ryskov, A.P., Skryabin, K.G., Bayev, A.A., and Georgiev, G.P.: Ubiquitous transposonlike repeats B1 and B2 of the mouse genome. *Nucleic Acids Res. 10*: 7461-7465, 1982.

La Spada, A.R., Wilson, E.M., Lubahn, D.B., Harding, A.E., and Fischbeck, K.H.: Anrdrogen receptor gene mutations in X-linked spinal and bulbar muscular atrophy. *Nature 352*: 77-79, 1991.

Leeson, T.S. and Leeson, C.R. (eds.): *Histology*, W.B. Saunders Company, Philadelphia, 1981.

Leiter, E.H., Beamer, W.G., Shultz, L.D., Barker, J.E., and Lane, P.W.: Mouse models of genetic diseases. In *Birth Defects: Original Article Series, Volume 23*, pp. 221-257, 1987.

Lewis, S.E., Turchin, H.A., and Wojtowicz, T.E.: Fertility studies of complementing genotypes at the albino locus of the mouse. *J. Reprod. Fertil. 53*: 197-202, 1978.

Li, S., Crenshaw, E., Rawson, E., Simmons, D., Swanson, L., and Rosenfeld, M.G.: Dwarf locus mutants lacking three pituitary cell types result from mutations in the POU-domain gene *pit-1*. *Nature 347*: 528-533, 1990.

Lovett, M., Kere, J., and Hinton, L.M.: Direct selection: a method for the isolation of cDNAs encoded by large genomic regions. *PNAS 88*: 9628-9632, 1991.

Maniatis, T., Fritsch, E.F., and Sambrook, J. (eds.): *Molecular Cloning: A Laboratory Manual*, Cold Spring Harbor Laboratory, New York, 1982.

Meyerowitz, E.M., Smyth, D.R., and Bowman, J.L.: Abnormal flowers and pattern formation in floral development. *Development 106*: 209-217, 1989.

Miale, J.B. and Rywlin, A.M.: The hematopoietic system. *In* W.A.D. Anderson and J.M. Kissane (eds.); *Pathology: Volume 2*, 7th edition, pp. 1483-1574, C.V. Mosby Co., St. Louis, 1977.

Mollicone, R., Gibaud, A., Francois, A., Ratcliffe, M., Oriol, R.: Acceptor specificity and tissue distribution of three human α-3-fucosyltransferases. *Eur. J. Biochem. 191*: 169-176, 1990.

Monaco, A.P., Neve, R.L., Colletti-Feener, C., Bertelson, C.J., Kurnit, D.M., and Kunkel, L.M.: Isolation of candidate cDNAs for portions of the Duchenne muscular dystrophy gene. *Nature 323*: 646-650, 1986.

Morgan, W.T., Muster, P., Tatum, F., Kao, S., Alam, J., and Smith, A.: Identification of the histidine residues of hemopexin that coordinate with heme-iron and of a receptor-binding region. *J. Biol. Chem. 268*: 6256-6262, 1993.

Muller-Eberhard, U., Javid, J., Liem, H., Hanstein, A., and Hanna, M.: Plasma concentrations of hemopexin, haptoglobin and heme in patients with various hemolytic anemias. *Blood 32*: 811-815, 1968.

Nadeau, J.H.: Maps of linkage and synteny homologies between mouse and man. *Trends in Genetics 5*: 82-86, 1989.

Nikkila, H., Gitlin, J.D., and Muller-Eberhard, U.: Rat hemopexin. Molecular cloning, primary structural characterization, and analysis of gene expression. *Biochemistry 30*: 823-829, 1991.

Niswander, L., Yee, D., Rinchik, E.M., Russell, L.B., and Magnuson, T.: The albino deletion complex and early

postimplantation survival in the mouse. *Development 102*: 45-53, 1988.

Niswander, L., Yee, D., Rinchik, E.M., Russell, L.B., and Magnuson, T.: The albino-deletion complex in the mouse defines genes necessary for development of embryonic and extraembryonic ectoderm. *Development 105*: 175-182, 1989.

Ogawa, M., Porter, P.N., and Nakahata, T.: Renewal and commitment to differentiation of hemopoietic stem cells (an interpretive review). *Blood 61*: 823-829, 1983.

Ogawa, M.: Differentiation and proliferation of hematopoietic stem cells. *Blood 81*: 2844-2853, 1993.

Parimoo, S., Patanjali, S., Shukla, H., Chaplin, D.D., and Weissman, S.M.: cDNA selection: Efficient PCR approach for the selection of cDNAs encoded in large chromosomal fragment. *PNAS 88*: 9623-9627, 1991.

Parimoo, S., Patanjali, S., and Weissman, S.M.: Normalization and selection with short-fragment cDNAs. In *Methods in Molecular Genetics, Volume I*, Academic Press, Inc., pp. 23-50, 1993.

Parrish, J.E. and Nelson, D.L.: Methods for finding genes: a major rate-limiting step in positional cloning. *GATA 10*: 29-41, 1993.

Pastink, A., Vreeken, C., Nivard, M.J.M., Searles, L.L., and Vogel, E.W.: Sequence analysis of *N*-ethyl-*N*-nitrosourea *vermilion* mutations in *Drosophila melanogaster*. *Genetics 123*: 123-129, 1989.

Pavlovic-Kentera, V., Basara, N., Biljanovic-Paunovic, L., Vasiljevska, M., and Rolovic, Z.: Erythroid progenitors in anemic Belgrade laboratory (*b/b*) rats. *Exp. Hematol. 17*: 812-815, 1989.

Peters, J. (ed.): New linkage, synteny, allelism, in situ hybridization, and physical mapping data. *Mouse Genome 92*: 19-61, 1994.

Pfrimmer, W., Joyce, R.A., Turner, R., and Boggs, D.R.: Kinetics of the development of methylcellulose-induced hepatic hematopoiesis in adult mice. *Blood 51*: 611-622, 1978.

Ploemacher, R.E. and Brons, R.H.: Separation of CFU-S from primitive cells responsible for reconstitution of the bone marrow hemopoietic stem cell compartment following irradiation: evidence for a pre-CFU-S cell. *Exp. Hematol. 17*: 263-266, 1989.

Pluznik, P.H. and Sachs, L.: The induction of colonies of normal "mast" cells by a substance in conditioned medium. *Exp. Cell Res. 43*: 553-563, 1965.

Pollack, R.N. and Divon, M.Y.: Intrauterine growth retardation: definition, classification, and etiology. *Clinical Obstet. Gyn. 35*: 99-107, 1992.

Popp, R.A., Bailiff, E.G., Skow, L.C., Johnson, F.M., and Lewis, S.E.: Analysis of a mouse α-globin gene mutation induced by ethylnitrosourea. *Genetics 105*: 157-167, 1983.

Popp, D.M., Popp, R.A., Lock, S., Mann, R.C., and Hand, R.E.: Use of multiparameter analysis to quantitate hematological damage from exposure to a chemical (ethylene oxide). *J. Tox. Env. Health 18*: 543-565, 1986.

Potter, M.D., Klebig, M.K., Carpenter, D.A., and Rinchik, E.M.: Genetic and physical mapping of the *fitness 1* (*fit1*) locus within the Fes-Hbb region of mouse chromosome 7. *Mammalian Genome*, submitted.

Poustka, A., Pohl, T.M., Barlow, D.P., Frischauf, A.M., and Lehrach, H.: Construction and use of human chromosome jumping libraries from*Not*I-digested DNA. *Nature 325*: 353-355, 1987.

Reguigne, I., James, M.R., Richard, C.W., Mollicone, R., Seawright, A., Lowe, J.B., Oriol, R., and Couillin, P.: The gene encoding myeloid α-3-fucosyltransferase (*FUT4*) is located between D11S388 and D11S919 on 11q21. *Cytogent. Cell Genet. 66*: 104-106, 1994.

Reif, A.E. and Allen, J.M.: The AKR thymic antigen and its distribution in leukemias and nervous tissues. *J. Exp. Med. 120*: 413-433, 1964.

Ricketts, C. and Cavill, I.: Iron kinetics and erythropoiesis. *In* R. Porter (ed.); *Iron Metabolism*, Elsevier, New York, pp. 145-166, 1977.

Rinchik, E.M., Russell, L.B., Copeland, N.G., and Jenkins, N.A.: Molecular genetic analysis of the dilute-short ear (*d-se*) region of the mouse. *Genetics 112*: 321-342, 1986.

Rinchik, E.M., Machanoff, R., Cummings, C.C., and Johnson, D.K.: Molecular cloning and mapping of the ecotropic leukemia provirus Emv-23 provides molecular access to the albino-deletion complex in mouse chromosome 7. *Genomics 4*: 251-258, 1989.

Rinchik, E.M. and Russell, L.B.: Germ-line deletion mutations in the mouse: tools for intensive functional and physical mapping of regions of the mammalian genome. *In* K.E. Davies and S.M. Tilghman (eds.); *Genome Analysis Volume 1: Genetic and Physical Mapping*, pp. 121-158, Cold Spring Harbor Press, Plainview, NY, 1990

Rinchk, E.M., Carpenter, D.A., and Selby, P.B.: A strategy for fine-structure functional analysis of a 6- to 11- centimorgan region of mouse chromosome 7 by high-efficiency mutagenesis. *PNAS 87*: 896-900, 1990.

Rinchik, E.M. and Carpenter, D.A.: *N*-ethyl-*N*-nitrosourea-induced prenatally lethal mutations define at least two complementation groups within the embryonic ectoderm development (*eed*) locus in mouse chromosome 7. *Mammalian Genome 4*, 349-353, 1993.

Rinchik, E.M., Carpenter, D.A., and Long, C.L.: Deletion mapping of four loci defined by *N*-ethyl-*N*-nitrosourea-induced postimplantation-lethal mutations within the *pid-Hbb* region of mouse chromosome 7. *Genetics 135*: 1117-1123, 1993a.

Rinchik, E.M., Tonjes, R.R., Paul, D., and Potter, M.D.: Molecular analysis of radiation-induced *albino* (*c*) locus mutations that cause death at preimplantation stages of development. *Genetics 135*: 1107-1116, 1993b.

Rittenhouse, E., Dunn, L.C., Cookingham, J., Calo, C., Spiegelman, M., Dooher, G.B., and Bennett, D.: Cartilage matrix deficiency

(*cmd*): a new autosomal recessive mutation in the mouse. *J. Embryol. Exp. Morphol. 43*: 71-84, 1978.

Rolovic, Z., Jovanovic, T., Stankovic, Z., and Marinkovic, N.: Abnormal megakaryocytopoiesis in the Belgrade laboratory rat. *Blood 65*: 60-64, 1985.

Rolovic, Z., Basara, N., Stojanovic, N., Suvajdzic, N., and Pavlovic-Kentera, V.: Abnormal megakaryocytopoiesis in the Belgrade laboratory rat. *Blood 77*: 456-460, 1991.

Rommens, J.M., Iannuzzi, M.C., Bat-sheva, K., Drumm, M.L., Melmer, G., Dean, M., Rozmahel, R., Cole, J.L., Kennedy, D., Hidaka, N., Zsiga, M., Buchwald, M., Riordan, J.R., Tsui, L.C., and Collins, F.S.: Identification of the cystic fibrosis gene: chromosome walking and jumping. *Science 245*: 1059-1065, 1989.

Rose, E.A., Glaser, T., Jones, C., Smith, C.L., Lewis, W.H., Call, K.M., Minden, M., Champagne, E., Bonetta, L., Yeger, H., and Housman, D.E.: Complete physical map of the WAGR region of 11p13 localizes a candidate Wilm's tumor gene. *Cell 60*: 495-508, 1990.

Royer-Pokora, B., Kunkel, L.M., Monaco, A.P., Goff, S.C., Newburger, P.E., Baihner, R.L., Cole, S.F., Curnutte, J.T., and Orkin, S.H.: Cloning the gene for an inherited human disorder-chronic granulomatous disease-on the basis of its chromosomal location. *Nature 322*: 32-38, 1986.

Ruppert, S., Kelsey, G., Schedl, A., Schmid, E., Thies, E., and Schutz, G.: Deficiency of an enzyme of tyrosine metabolism

underlies altered gene expression in newborn liver of lethal albino mice. *Genes Dev. 6*: 1430-1443, 1992.

Russell, E.S.: Hereditary anemias of the mouse: a review for geneticists. *Adv. Gen. 20*: 357-459, 1979.

Russell, E.S., McFarland, E.C., and Peters, H.: Gametic and pleiotropic defects in mouse fetuses with Hertwig's macrocytic anemia. *Dev. Biol. 110*: 331-337, 1985.

Russell, L.B., Montgomery, C.S., and Raymer, G.D.: Analysis of the albino-locus region of the mouse: IV. Characterization of 34 deficiencies. *Genetics 100*: 427-453, 1982.

Russell, W.L.: X-ray-induced mutations in mice. *Cold Spring Harbor Symp. Quant. Biol. XVI*: 327-336, 1951.

Sargent, C.A., Dunham, I., and Campbell, R.D.: Identification of a multiple HTF-island associated genes in the human major histocompatibility complex class III region. *EMBO J. 8*: 2305-2312, 1989.

Searle, A.G., Edwards, J.H., and Hall, J.G.: Mouse homologues of human disease. *J. Med. Genet. 31*: 1-19, 1994.

Sharan, S.K., Holdener-Kenny, B., Ruppert, S., Schedl, A., Kelsey, G., Rinchik, E.M., and Magnuson, T.: The albino-deletion complex of the mouse: Molecular mapping of deletion breakpoints that define regions necessary for development of the embryonic and extraembryonic ectoderm. *Genetics 129*: 825-832, 1991.

Sharan, S.K., Holdener-Kenney, B., Threadgill, D.W., and Magnuson, T.: Genomic mapping within the albino-deletion

complex using individual early postimplantation mouse embryos. *Mammal. Genome 3*: 79-83, 1992.

Sladic-Simic, D., Pavic, N., Zivkovic, N., Martinovic, D., and Martinovitch, P.N.: Changes in the offspring of female rats exposed to 50r of X-rays when eight days old. *Brit. J. Radiology 36*: 542- 543, 1963.

Sladic-Simic, D., Zivkovic, N., Pavic, D., Marinkovic, D., Martinovic, J., and Martinovitch, P.N.: Hereditary hypochromic microcytic anemia in the laboratory rat. *Genetics 53*: 1079-1089, 1966.

Smith, C.L., Kleo, S.R., and Cantor, C.R.: Pulsed-field gel electrophoresis and technology of large DNA molecules. *In* K.E. Davies (ed.); *Genome Analysis: A Practical Approach*, pp. 41-68, Cold Spring Harbor Press, Plainview, NY, 1988.

Solar, I., Muller-Eberhard, U., Shviro, Y., and Shaklai, N.: Long-term intercalation of residual hemin in erythrocyte membranes distorts the cell. *Biochem. Biophys Acta. 1062*: 51-58, 1991..

Spangrude, G.J., Heimfeld, S., and Weissman, I.L.: Purification and characterization of mouse hematopoietic stem cells. *Science 241*: 58-62, 1988.

Stahl, N. and Yancopoulos, G.D.: The alphas, betas, and kinases of cytokine receptor complexes. *Cell 74*: 587-590, 1993.

Stojanovic, N., Jovcic, G., Basara, N., and Pavlovic-Kentera, V.: Granulopoiesis in anemic Belgrade laboratory (*b/b*) rats. *Exp. Hematol. 18*: 379-383, 1990.

Tassone, F., Cheng, S., and Gardiner, K.: Analysis of chromosome 21 yeast artificial chromosome (YAC) clones. *Am. J. Hum. Genet. 51*: 1251-1264, 1992.

Tavassoli, M.: Embryonic and fetal hemopoiesis: an overview. *Blood Cells 1*: 269-281, 1991.

Taylor, K.D. and Piko, L.: Patterns of mRNA prevalence and expression of B1 and B2 transcripts in early mouse enbryos. *Development 101*: 877-892, 1987.

Till, J.E. and McCulloch, E.A.: A direct measurement of the radiation sensitivity of normal mouse bone marrow cells. *Radiat. Res. 14*: 213-222, 1961.

Trofatter, J.A., MacCollin, M., Rutter, J., Murrell, J., Duyao, M., Parry, D., Eldridge, R., Kley, N., Menon, A., Pulaski, K., Haase, V.H., Ambrose, C., Munroe, D., Bove, C., Haines, J., Martuza, R.L., MacDonald, M., Seizinger, B., Short, M., Buckler, A.J., and Gusella, J.F.: A novel moesin-, ezrin-, radizin-like gene is a candidate for the Neurofibromatosis 2 tumor suppressor. *Cell 72*: 791-800, 1993.

Smithies, O.: Animal models of human genetic diseases. *Trends in Genetics 9*: 112-116, 1993.

Vulpe, C., Levinson, B., Whitney, S., Packman, S., and Gitschier, J.: Isolation of a candidate gene for Menkes disease and evidence that it encodes a copper-transporting ATPase. *Nature Genetics 3*: 7-13, 1993.

Wallace, M.R., Marchuk, D.A., Andersen, L.B., Letcher, R., Odeh, H.M., Saulino, A.M., Fountain, J.W., Brereton, A., Nicholson, J., Mitchell, A.L., Brownstein, B.H., and Collins, F.S.: Type 1 Neurofibromatosis gene: identification of a large transcript disrupted in three NF1 patients. *Science 249*: 181-186, 1990.

Weksberg, R., Buchwald, M., Sargent, P., Thompson, M.W., and Siminovitch, L.: Specific cellular defects in patients with Fanconi anemia. *J. Cell Physiol. 101*: 311-324, 1979.

Winter, R.M.: Malformation syndromes: a review of mouse/human homology. *J. Med. Genet. 25*: 480-487, 1988.

Wintrobe, M.M., Lee, G.R., Boggs, D.R., Bithell, T.C., Athens, J.W., and Foerster, J. (eds.): *Clinical Hematology*, Lea and Febiger, Philadelphia, 1974.

Wyman, A.R., Wolfe, L.B., and Botstein, D.: Propagation of some human DNA sequences in bacteriophage λ vectors requires mutant *Escherichia coli* hosts. *PNAS 82*: 2880-2884, 1985.

GENERAL APPENDICES

APPENDIX A

TABLES

TABLE 1. Hybridization Probes[a]

Probe	Locus	Restriction Fragment Used As Probe	Reference[b]
pA4.2c11	*D7Cwr11D*	4.2-kb *Sph*I	Sharan et al. (1991)
RN302	*D7Rn5*	1.8-kb *Bam*HI-*Pst*I	-
94.1	*α*[c]	0.5-kb *Eco*RI-*Hind*III	Rinchik et al. (1986)
RN286	d	1.7-kb *Kpn*I	-
RN254	*D7Rn4*	0.9-kb *Eco*RI-*Hind*III	Klebig et al. (1992b)
RN259	*D7Rn2*	1.45-kb *Xba*I-*Eco*RI	Klebig et al. (1992b)
D6E7.1	d	e	-
D6E7.3	d	e	-
D6E7.4	d	e	-
D6E7.5	d	e	-
D6E7.6	d	e	-

TABLE 1. Continued.

Probe	Locus	Restriction Fragment Used As Probe	Reference[b]
FEID4$_{dist}$	f	0.6-kb *Hha*I	Holdener-Kenny et al. (in preparation)
D6E7.4 B3.0	g	3.0-kb *Bam*HI	-
D6E7.6 R4.0	g	4.0-kb *Eco*RI	-
pYAC4 left	h	2.6-kb *Pvu*II-*Bam*HI	Burke et al., 1987
pYAC4 right	h	1.6-kb *Pvu*II-*Bam*HI	Burke et al., 1987

[a] Several anonymous probes generated from D6E7-derived cosmid clones to be screened on zoo blots are not listed.

[b] Probes with no reference were derived in this study.

[c] No locus designation given. The locus maps proximal to the Chr-9 *dilute* (*d*) locus, within a number of deletions surrounding *d*.

[d] Whole cosmid clone with no locus designation. Each maps within the *D7Rn5-D7Cwr11D* interval.

[e] An accurate size of each of the whole cosmid clones used as probes was not determined.

[f] No locus designation given. The locus maps in the *D7Rn5-D7Cwr11D* interval.

[g] These probes are anonymous probes with no locus designation. Each was derived from a D6E7-derived cosmid clone, and maps in the *D7Rn5-D7Cwr11D* interval.

[h] pBR322 derived-sequences specific to either the left or right arm of the pYAC4 vector.

TABLE 2. Recorded Weight Measurements for Wild-type and *fit 1* Mice[a].

DAY	Control	4397SB	494SB
0	1.60 ± 0.22 (35)	0.978 ± 0.08 (19)[b]	1.20 ± 0.11 (18)[b]
2	2.28 ± 0.53 (23)	1.12 ± 0.17 (6)	1.40 ± 0.31 (8)
4	3.21 ± 0.66 (16)	1.58 ± 0.23 (4)	1.90 ± 0.32 (7)
6	4.84 ± 0.93 (14)	2.40 ± 0.43 (4)	2.60 ± 0.37 (7)
8	6.04 ± 1.14 (15)	2.84 ± 0.54 (5)	3.10 ± 0.47 (6)
10	7.40 ± 1.34 (15)	3.54 ± 0.81 (2)	3.80 ± 0.70 (9)
12	8.23 ± 1.70 (14)	3.90 ± 0.76 (3)	4.20 ± 0.91 (7)
14	8.68 ± 2.16 (13)	3.90 ± 0.71 (3)	4.50 ± 1.10 (10)
16	9.54 ± 2.40 (12)	3.39[c] (1)	4.90 ± 1.40 (10)
18	10.30 ± 2.46 (15)	3.90 ± 0.59 (2)	5.20 ± 1.50 (10)
20	11.32 ± 2.70 (14)	4.20 ± 0.62 (2)	5.00 ± 1.30 (9)
22	12.40 ± 2.80 (13)	3.90 ± 0.66 (2)	5.40 ± 1.30 (11)
24	14.50 ± 2.10 (9)	3.80 ± 0.50 (2)	6.90 ± 0.83 (5)
26	16.00 ± 2.40 (8)	4.10 ± 0.66 (2)	7.10 ± 0.69 (4)
28	18.60 ± 1.90 (9)	3.20[c] (1)	7.40 ± 1.80 (6)
30	19.70 ± 2.60 (7)	4.10 ± 0.33 (2)	8.60 ± 0.96 (4)
32	22.00 ± 2.00 (10)[b]	4.50 ± 0.44 (2)[b]	9.60 ± 1.40 (5)[b]

TABLE 2. Continued.

DAY	764SB	3452SB	4226SB
0	1.06 ± 0.11 (12)[b]	1.15 ± 0.11 (12)[b]	1.20 ± 0.19 (15)[b]
2	1.50 ± 0.17 (12)	1.44 ± 0.33 (13)	1.60 ± 0.44 (16)
4	2.10 ± 0.38 (10)	2.60 ± 1.90 (10)	2.20 ± 0.65 (14)
6	2.90 ± 0.62 (8)	2.80 ± 0.59 (10)	2.90 ± 0.81 (14)
8	3.40 ± 0.69 (8)	4.00 ± 0.63 (8)	3.90 ± 0.90 (12)
10	3.97 ± 0.65 (8)	5.20 ± 0.11 (5)	4.40 ± 0.74 (10)
12	4.04 ± 0.84 (8)	5.50 ± 0.85 (5)	4.97 ± 1.00 (9)
14	4.40 ± 0.60 (12)	6.40 ± 1.40 (6)	5.20 ± 1.60 (6)
16	4.30 ± 0.81 (10)	6.70 ± 1.70 (5)	5.70 ± 1.70 (7)
18	4.11 ± 0.96 (8)	6.20 ± 1.30 (4)	5.60 ± 1.70 (6)
20	5.10 ± 0.94 (7)	6.80 ± 1.10 (9)	6.90 ± 2.00 (11)
22	5.70 ± 1.20 (6)	7.80 ± 1.40 (9)	7.60 ± 1.80 (10)
24	6.00 ± 1.70 (4)	8.90 ± 2.00 (7)	9.30 ± 1.60 (5)
26	5.10 ± 1.40 (3)	9.30 ± 2.10 (5)	10.20 ± 2.40 (4)
28	5.80 ± 2.30 (3)		10.20 ± 2.50 (5)
30	6.80 ± 2.70 (2)	9.50 ± 0.81 (3)	9.20 ± 2.40 (2)
32	7.50 ± 2.00[b] (4)	9.60 ± 1.20[b] (3)	12.40 ± 2.30[b] (7)

[a] Weights were recorded as described in Materials and Methods. Mean weights (in grams) for each time point are shown ± S.D., and the number of mice in each group on a particular day is shown in parentheses (N). The *fit1* mutant allele designation is listed as the column heading (*e.g.*, 494SB). All mutants weighed were hemizygotes, *i.e.*, $c\ fit1^{m}/c^{26DVT}$.

[b] Significantly different from controls ($p < 0.05$). Statistic calculated only for birth weight and one other point near weaning age.

[c] No S.D. is shown because only one weight measurement is available for this point.

TABLE 3. Recorded Body length Measurements of *fit1* and Wild-type Littermates[a].

DAY	Control	4397SB	494SB
0	3.29 ± 0.16 (15)[b]	2.67 ± 0.11 (15)[b]	2.80 ± 0.14 (18)[b]
2	3.65 ± 0.24 (14)	2.96 ± 0.19 (7)	3.00 ± 0.17 (7)
4	4.09 ± 0.25 (14)	3.30 ± 0.24 (7)	3.46 ± 0.21 (7)
6	4.64 ± 0.23 (11)	3.73 ± 0.26 (4)	3.83 ± 0.22 (6)
8	4.99 ± 0.24 (10)	3.97 ± 0.32 (3)	4.10 ± 0.29 (6)
10	5.53 ± 0.36 (11)	4.23 ± 0.38 (4)	4.40 ± 0.29 (8)
12	5.86 ± 0.47 (9)	4.57 ± 0.25 (3)	4.63 ± 0.45 (7)
14	6.27 ± 0.60 (9)	4.40 ± 0.00 (2)	4.98 ± 0.35 (11)
16	6.55 ± 0.70 (8)	5.00 ± 0.14 (2)	5.25 ± 0.56 (10)
18	6.78 ± 0.61 (9)	5.00 ± 0.17 (3)	5.73 ± 0.35 (6)
20	6.88 ± 0.65 (8)	5.00 ± 0.14 (2)	5.48 ± 0.65 (10)
22	7.11 ± 0.73 (8)	5.15 ± 0.07 (2)	5.65 ± 0.60 (11)
24	7.74 ± 0.68 (7)	5.15 ± 0.07 (2)	5.79 ± 0.64 (9)
26	8.11 ± 0.45 (7)[b]	5.15 ± 0.07 (2)[b]	6.34 ± 0.34 (5)[b]
28	8.63 ± 0.55 (3)	4.90[c] (1)	6.35 ± 0.77 (4)
30	8.70 ± 0.66 (4)	4.90[c] (1)	6.80 ± 0.00 (2)
32	8.47 ± 0.42 (3)	5.30[c] (1)	

TABLE 3. Continued.

DAY	764SB	3452SB	4226SB
0	2.82 ± 0.13 (11)[b]	2.83 ± 0.13 (16)[b]	2.99 ± 0.19 (15)[b]
2	3.20 ± 0.18 (12)	3.25 ± 0.21 (14)	3.28 ± 0.32 (15)
4	3.59 ± 0.22 (10)	3.67 ± 0.35 (11)	3.64 ± 0.38 (14)
6	3.90 ± 0.35 (4)	4.07 ± 0.32 (9)	3.84 ± 0.24 (8)
8	4.20 ± 0.34 (4)	4.53 ± 0.33 (6)	4.26 ± 0.28 (7)
10	4.55 ± 0.19 (4)	4.90 ± 0.10 (5)	4.63 ± 0.37 (7)
12	4.73 ± 0.36 (6)	5.28 ± 0.33 (5)	4.99 ± 0.51 (9)
14	5.14 ± 0.26 (8)	5.50 ± 0.28 (2)	5.47 ± 0.64 (9)
16	5.07 ± 0.46 (6)	5.40[c] (1)	5.49 ± 0.52 (8)
18	5.10 ± 0.41 (4)	5.67 ± 0.23 (3)	5.81 ± 0.62 (8)
20	5.64 ± 0.60 (5)	5.80 ± 0.36 (4)	5.98 ± 0.60 (10)
22	5.70 ± 0.20 (4)	5.80[c] (1)	6.17 ± 0.50 (9)
24	5.95 ± 0.44 (4)	6.05 ± 0.24 (4)	6.54 ± 0.22 (5)
26	6.00 ± 0.50 (7)[b]	6.03 ± 0.25 (3)[b]	6.70 ± 0.24 (4)[b]
28	5.50 ± 0.14 (2)	6.10 ± 0.14 (2)	6.95 ± 0.48 (4)
30	5.60[c] (1)	6.70 ± 0.26 (4)	7.10 ± 0.37 (4)
32			

[a] Measurements were made as described in Materials and Methods. Mean body lengths for each time point are shown (in cm) ± S.D., and the number of mice in each group on a particular day is shown in parentheses (N). The *fit1* mutant allele designation is listed as the mutant column heading (*e.g.*, 494SB). All mutants measured were hemizygotes, *i.e.*, $c\ fit1^{m}/c^{26DVT}$.

[b] Significantly different from controls ($p < 0.05$). Statistic calculated only for birth length and one other point near weaning age.

[c] No S.D. is shown because only one measurement is available for this point.

TABLE 4. Recorded Tail Length Measurements for *fit1* Mutants and Wild-Type Littermates[a].

DAY	Control	4397SB	494SB
0	1.27 ± 0.23 (15)[b]	0.95 ± 0.05 (15)[b]	0.98 ± 0.08 (18)[b]
2	1.52 ± 0.23 (14)	1.10 ± 0.12 (7)	1.14 ± 0.13 (7)
4	1.93 ± 0.26 (14)	1.41 ± 0.23 (7)	1.37 ± 0.20 (7)
6	2.46 ± 0.24 (11)	1.68 ± 0.17 (4)	1.80 ± 0.13 (6)
8	3.04 ± 0.21 (10)	2.00 ± 0.17 (3)	2.15 ± 0.23 (6)
10	3.82 ± 0.26 (11)	2.53 ± 0.40 (4)	2.68 ± 0.24 (8)
12	4.18 ± 0.26 (9)	2.83 ± 0.64 (3)	3.11 ± 0.29 (7)
14	4.76 ± 0.37 (9)	3.20 ± 0.42 (2)	3.48 ± 0.34 (11)
16	5.13 ± 0.31 (8)	3.40 ± 0.57 (2)	3.69 ± 0.34 (10)
18	5.46 ± 0.32 (9)	3.57 ± 0.55 (3)	4.22 ± 0.18 (6)
20	5.60 ± 0.38 (8)	3.70 ± 0.42 (2)	4.35 ± 0.37 (10)
22	5.83 ± 0.50 (8)	3.85 ± 0.49 (2)	4.45 ± 0.39 (11)
24	6.36 ± 0.36 (7)	4.00 ± 0.42 (2)	4.50 ± 0.36 (9)
26	6.47 ± 0.21 (7)[b]	4.10 ± 0.42 (2)[b]	5.04 ± 0.55 (5)[b]
28	6.87 ± 0.32 (3)	4.00[c] (1)	6.35 ± 0.77 (4)
30	6.88 ± 0.30 (4)	4.00[c] (1)	5.00 ± 0.00 (2)
32	6.97 ± 0.25 (3)	4.50[c] (1)	

TABLE 4. Continued.

DAY	764SB	3452SB	4226SB
0	0.98 ± 0.08 (11)[b]	0.99 ± 0.04 (16)[b]	1.10 ± 0.19 (15)[b]
2	1.23 ± 0.07 (12)	1.26 ± 0.18 (14)	1.38 ± 0.23 (15)
4	1.58 ± 0.14 (10)	1.60 ± 0.28 (11)	1.68 ± 0.35 (14)
6	1.83 ± 0.10 (4)	1.97 ± 0.24 (9)	1.88 ± 0.20 (8)
8	2.43 ± 0.37 (4)	2.63 ± 0.23 (6)	2.30 ± 0.24 (7)
10	2.85 ± 0.33 (4)	3.36 ± 0.15 (5)	2.83 ± 0.24 (7)
12	3.18 ± 0.17 (6)	3.76 ± 0.29 (5)	3.18 ± 0.37 (9)
14	3.43 ± 0.18 (8)	3.80 ± 0.28 (2)	3.66 ± 0.50 (9)
16	3.63 ± 0.25 (6)	4.20[c] (1)	3.94 ± 0.63 (8)
18	3.73 ± 0.38 (4)	4.40 ± 0.10 (3)	4.23 ± 0.62 (8)
20	4.00 ± 0.21 (5)	4.48 ± 0.55 (4)	4.51 ± 0.56 (10)
22	4.15 ± 0.24 (4)	5.00[c] (1)	4.92 ± 0.58 (9)
24	4.50 ± 0.22 (4)	4.90 ± 0.12 (4)	5.34 ± 0.27 (5)
26	4.71 ± 0.42 (7)[b]	5.10 ± 0.10 (3)[b]	5.40 ± 0.38 (4)[b]
28	4.25 ± 0.07 (2)	5.20 ± 0.00 (2)	5.70 ± 0.42 (4)
30	4.40[c] (1)	5.80 ± 0.36 (4)	5.83 ± 0.26 (4)
32			

[a] Tail lengths were measured as described in Materials and Methods. Mean lengths for each time point are shown (in cm) ± S.D., and the number of mice in each group on a particular day is shown in parentheses (N). The *fit1* mutant allele designation is listed as the column heading (*e.g.*, 494SB). All mutants measured were hemizygotes,*i.e.*, *c fit1^{m}/c^{26DVT}*.

[b] Significantly different from controls ($p < 0.05$). Statistic calculated only for birth measurement and one other point near weaning age.

[c] No S.D. is shown because only one weight measurement is available for this point.

TABLE 5. Spleen Weights of *fit1*^{4397SB} Mutants and Wild-type Littermates[a].

	Body	Spleen	%
fit 1	10.5	0.117	1.11
	10.4	0.250	2.40
	5.8	0.058	1.00
	5.5	0.115	2.10
	11.3	0.308	2.73
Mean ± S.D.	8.70 ± 2.81	0.170 ± 0.10	1.87 ± 0.78[b]

	Body	Spleen	%
wild-type	22.8	0.122	0.54
	17.1	0.059	0.34
	20.7	0.086	0.42
	23.3	0.089	0.38
Mean ± S.D.	21.0 ± 2.82	0.089 ± 0.03	0.42 ± 0.09

[a] Total body weight (in grams), spleen weight (in grams), and spleen weight/body weight ratio are shown for each animal, as well as the mean for each of these measurements. Genotypes of the mice were *c fit1*^{4397SB}/*c*^{26DVT} (designated "*fit1*") and c^{ch} +/c^{ch} + ("wild-type").

[b] Significantly different from the mean of the wild-type control ($p < 0.05$).

TABLE 6. White Blood Cell and Reticulocyte Values in Peripheral Blood of *fit1*^{4397SB} Mutants and Littermate Controls[a].

Group	WBC (X 10 ^{6} per ml)	Reticulocytes (%)
Control (3)	6.2 ± 1.6	4.4 ± 1.1
fit1^{4397SB} (3)	1.5 ± 0.5[b]	15.8 ± 4.2[b]

[a] Peripheral blood was removed from 26-32-day-old *fit1*^{4397SB} mutants (*c fit1*^{4397SB}/*c*^{26DVT}) and wild-type littermates (c^{ch} +/c^{ch} +) and stained as described in Materials and Methods. The values represent the mean ± S.D., and the number of mice analysed in each group is shown in parentheses.

[b] Significantly different from control mean, ($p < 0.05$).

TABLE 7. Total Number of Hematopoietic Progenitors in *fit1* Mice and Wild-Type Littermates[a]

Tissue		Total cells [X 10 ^{6}]	CFU-E [X 10 ^{4}]	BFU-E [X 10 ^{3}]	CFU-GM [X 10 ^{3}]
Spleen	c (7)	180.4 ± 19.2	7.6 ± 1.8	2.9 ± 1.2	21.0 ± 1.5
	m (8)	247.9[b] ± 81.3	1.0 ± 0.4	0.1 ± 0.1	9.4 ± 2.3
Bone Marrow[c]	c (7)	43.7 ± 15.6	26.0 ± 1.5	12.0 ± 1.6	110.0 ± 8.9
	m (8)	17.2 ± 5.6	1.9 ± 0.5	0.8 ± 0.4	19.0 ± 4.0
E14.5 Liver	c (6)	28.3 ± 11.8	27.0 ± 1.3	6.1 ± 1.0	46.0 ± 7.5
	m (5)	14.2 ± 11.6	5.3 ± 2.3	0.4 ± 0.2	12.0 ± 3.0

[a] The mean total number of cells per organ listed, and hematopoietic progenitors listed, are shown for wild-type littermates (c) and for *c fit* $1^{4397SB}/_{c}{}^{26DVT}$ mutants (m). The number of mice in each group is shown in parentheses (N).

[b] The mean of the mutant spleen cellularity is not significantly different from the mean cellularity of control spleens (at $p < 0.05$).

[c] The values for bone marrow reflect the total number of cells and progenitors derived from one tibia and one femur from each animal.

TABLE 8. CFU-S Are Reduced in *fit1*^{4397SB} Bone Marrow[a].

	Cellularity (X 10 ^{6})[b]	Total CFU-S	CFU-S/10^{5} cells
c (6)	63.0	3800	6.8 ± 1.9
m (6)	9.0	220	2.4 ± 0.7

a Spleen colony assays were performed, as described in Materials and Methods, with bone marrow-derived cells from a *c fit1*^{4397SB}/*c*^{26DVT} mutant (m) and a c^{ch} +/c^{ch} + wild-type littermate (c). The number of mice in each group is shown in parentheses (N). A group of five irradiated control mice received an injection of 1X phosphate buffered saline (PBS) only, and, after 14 days, had 0.4 CFU-S/spleen (2 colonies found on a total of five spleens).

b The "Cellularity" represents the total number of cells recovered from 1 femur and 1 tibia from each animal.

TABLE 9. Flow Cytometric Analysis of B Cell and T Cell Populations in Spleen and Bone Marrow of *fit1*^{4397SB} Mutants[a].

Tissue		Percent Positive Cells		Total Number of Positive Cells (X 10 ^{6})	
		B220	Thy-1	B220	Thy-1
Bone Marrow	c (12)	39.7 ± 8.4	n.d.[b]	12.1	n.d.
	m (12)	21.2 ± 13.4[c]	n.d.	3.0	n.d.
Spleen	c (10)	49.5 ± 15.2	14.1 ± 3.5	70.8	20.2
	m (11)	15.3 ± 9.3[c]	11.3 ± 4.1	21.3	15.7

[a] Single-cell suspensions from 26-32-day-old *fit1*^{4397SB} mutants (*c fit1*^{4397SB}/*c*^{26DVT}) and wild-type littermates (*c*^{ch} +/*c*^{ch} +) were stained with the B220 and Thy-1 antibodies as described in Materials and Methods. The values are given ± S.D., and the number of mice analyzed in each group is shown in parentheses (N).

[b] n.d. = not determined.

[c] Significantly different from control mean, ($p < 0.05$).

TABLE 10. Restriction-Fragment Sizes Used to Construct a Rare-Cutter Restriction Map of D6E7[a].

Probe	*Bss*HII	*Mlu*I	*Eag*I	*Nar*I
pYAC4 right	385	385	385	385
	320	140	290	145
	270		195	
	240		70	
	145			
pYAC4 left	385	385	385	385
	245	245	315	240
	150		190	
	120		100	
	70			

TABLE 10. Continued.

Probe	*Not*I	*Nru*I	*Cla*I	*Ksp*I
pYAC4 right	385	385	385	385
	b	*b*	310	140
			240	
			170	
			75	
pYAC4 left	385	385	385	385
	b	*b*	315	240
			220	
			145	
			75	

a The restriction fragment sizes (in kb) were obtained from partial- and complete-digests of D6E7 (as described in Materials and Methods). Each fragment size listed under a particular restriction enzyme represents an average size derived from sizes obtained from two to four different partial-digestion experiments. Fragment sizes for a given enzyme, as determined with either the right or left end-probe, may differ slightly ($\leq$ 5 kb). The first size listed under each enzyme represents the total size of D6E7 (~385 kb).

b Only the fragment representing the nondigested YAC was detected. Therefore, it is presumed that this enzyme has no recognition sites within D6E7.

TABLE 11. Restriction-Fragment Sizes Used to Construct a Rare-Cutter Restriction Map of D18H2[a].

Probe	*Bss*HII	*Mlu*I	*Eag*I	*Not*I
pYAC4 right	340	340	340	340
	240	220	130	130
	150	190	90	
	125			
	90			
	60			
pYAC4 left	340	340	340	340
	290	155	250	210
	270	120	220	
	240			
	215			
	110			

TABLE 11. Continued.

Probe	*Nru*I	*Nar*I	*Cla*I	*Ksp*I
pYAC4 right	340	340	N.D.[b]	N.D.
	130	120		
	110	80		
pYAC4 left	340	340	N.D.	N.D.
	230	260		
	210	220		

[a] The restriction fragment sizes (in kb) were obtained as described in TABLE 10 and in Materials and Methods. The first fragment size listed under each enzyme represents the total size of D18H2 (~340 kb).

[b] N.D. = not determined.

APPENDIX B

FIGURES

FIGURE 1. A Genetic Map of the *Fes-Hbb* Region of Mouse Chromosome 7 Showing a Subset of the Albino Deletion Mutations.

The map is a representation of some of the genetic loci in the *Fes-Hbb* region, along with a subset of the deletions surrounding and including the *c* locus. No correlation with physical distance is implied. Loci shown above the chromosome are: *Fes*, feline sarcoma virus protooncogene; *tp*, taupe; *Fah*, fumarlyacetoacetate hydrolase; *c* (*Tyr*), tyrosinase; *Emv23*, integration site of the endogenous ecotropic murine leukemia provirus 23; *Mod2*, mitochondrial malic enzyme; *sh1*, shaker 1; and *Hbb*, globin (β chain) (Green, 1989). The recombination frequencies [in centimorgans (cM)] between marker loci on the genetic map are as follows: *tp*-(3)-*c*-(2)-*Mod2*-(4)-*sh1*-(2)-*Hbb*. The loci indicated below the chromosome are defined by complementation analysis of overlapping *c* deletions (see Rinchik and Russell, 1990 for review). These loci are: *msd*, mesoderm deficient; *hsdr1*, hepatocyte-specific developmental regulation-1; *jdf*, juvenile development and fertility; *eed*, embryonic-ectoderm development; *exed*, extraembryonic-ectoderm development; and *pid*, preimplantation development.

The horizontal lines beneath the chromosome represent a subset of the deletions surrounding the *c* locus and their presumed extents with respect to the functional map. The names of the specific deletions shown are abbreviated, e.g. 26DVT = c^{26DVT}, and are listed above each horozontal line. Deletions with breakpoints that cannot yet be distinguished molecularly are shown with their breakpoints in the same position.

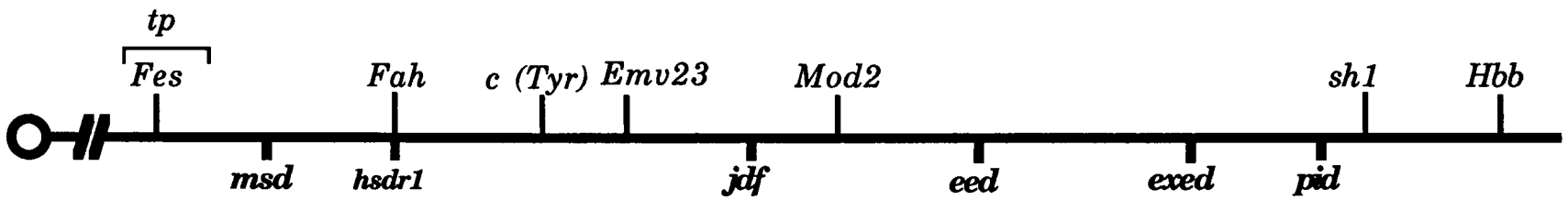

14CoS

20FATw

112K, 3H

11DSD

2YPSj, 5FR60Hg

4FR60Hd, 6H

202G, AL, 24R145L

3DENb

26DVT

FIGURE 2. All *fit1* Mutants are Growth Retarded.

A representative mutant carrying each of the five *fit1* alleles is shown with one wild-type littermate (far right). The genotypes of the mice, beginning at the left, are: *c fit1*^{4397SB}/*c*^{26DVT}, *c fit1*^{494SB}/*c*^{26DVT}, *c fit1*^{764SB}/*c*^{26DVT}, *c fit1*^{3452SB}/*c*^{26DVT}, *c fit1*^{4226SB}/*c*^{26DVT}, and *c*^{ch} +/*c fit1*^{494SB} or *c*^{ch} +/*c*^{26DVT}. All mice shown are 26 days old, and each mouse was generated from the following general mating: *c*^{ch} +/*c fit1*^{m} X *c*^{ch} +/*c*^{26DVT}, where *m* can designate any one of the *fit1* mutations. The wild-type littermate is from the mating that generated the 494SB mutant shown.

FIGURE 3. Weight Measurements for *fit1* Mutants and Wild-type Littermates.

Growth curves were constructed for mice expressing each of the *fit1* mutations and for their wild-type littermates (c^{ch} +/c^{ch} +). The graph shows the mean weight of each group of mice (mutants or control) plotted versus the day of weight measurement (the date of birth was designated day 0). The genotypes (see Materials and Methods) and the weights of mice in each litter studied were recorded at birth and every other day thereafter until either weaning age (30-32 days of age) or until death of the *fit1* mutants in a particular litter (which usually occurs before weaning age). The mean weight values, with S.D., are given in Table 2.

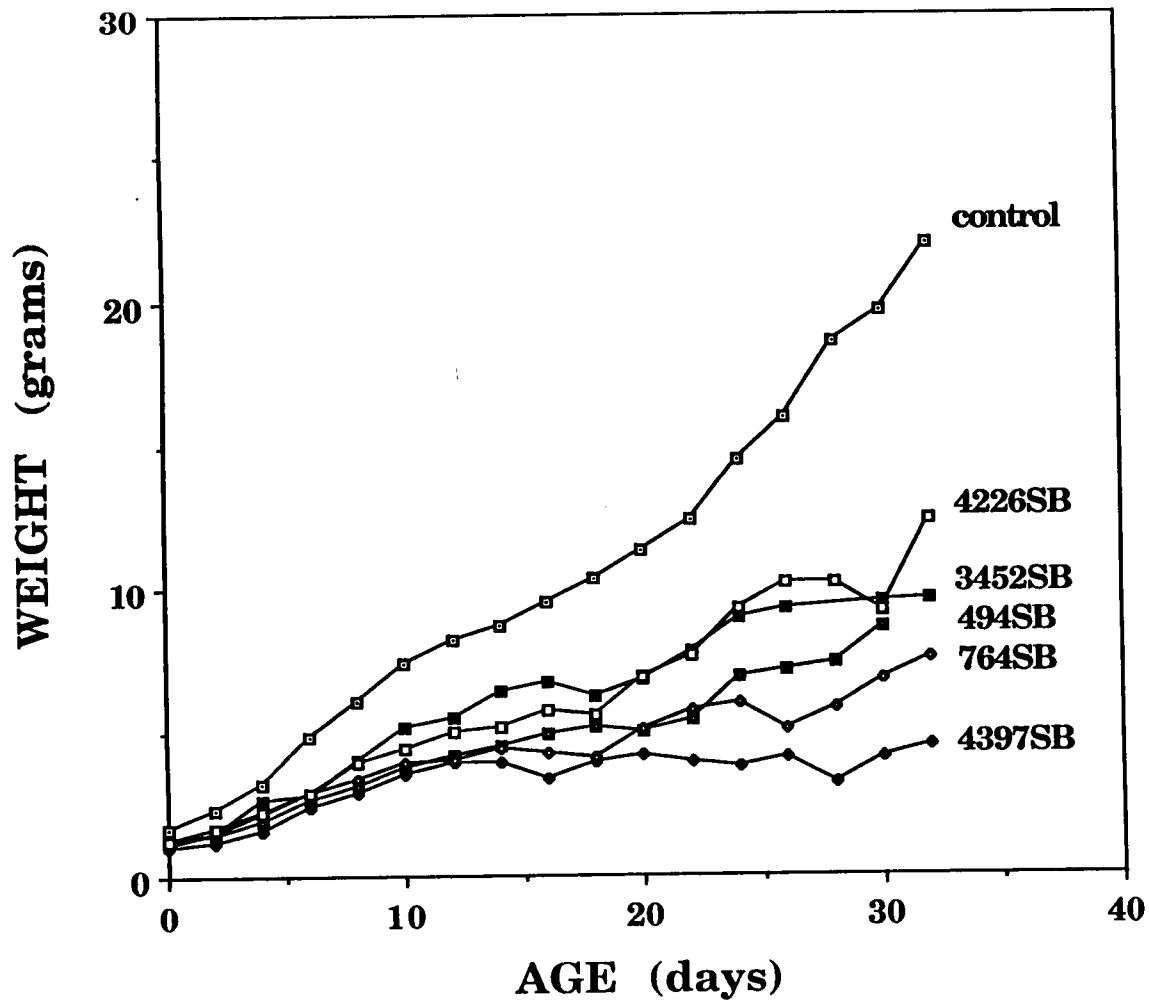
30
20
10
0
WEIGHT (grams)
0
10
20
30
40
AGE (days)
control
4226SB
3452SB
494SB
764SB
4397SB

FIGURE 4. Body Length (Nose-to-Rump) Measurements of *fit1* Mutants and Wild-Type Littermates.

The body lengths of *fit1* mutants ($c\ fit1^{m}/c^{26DVT}$) and wild-type littermates (c^{ch} +/c^{ch} +) were measured at birth and every other day thereafter. Only the mean lengths for the wild-type littermates, 4226SB mutants, and 4397SB mutants plotted versus time are shown; however, measurements were made on mutants from each of the five *fit1* alleles, and all of the means ± S.D., and the number of mice in each group, are presented in Table 3.

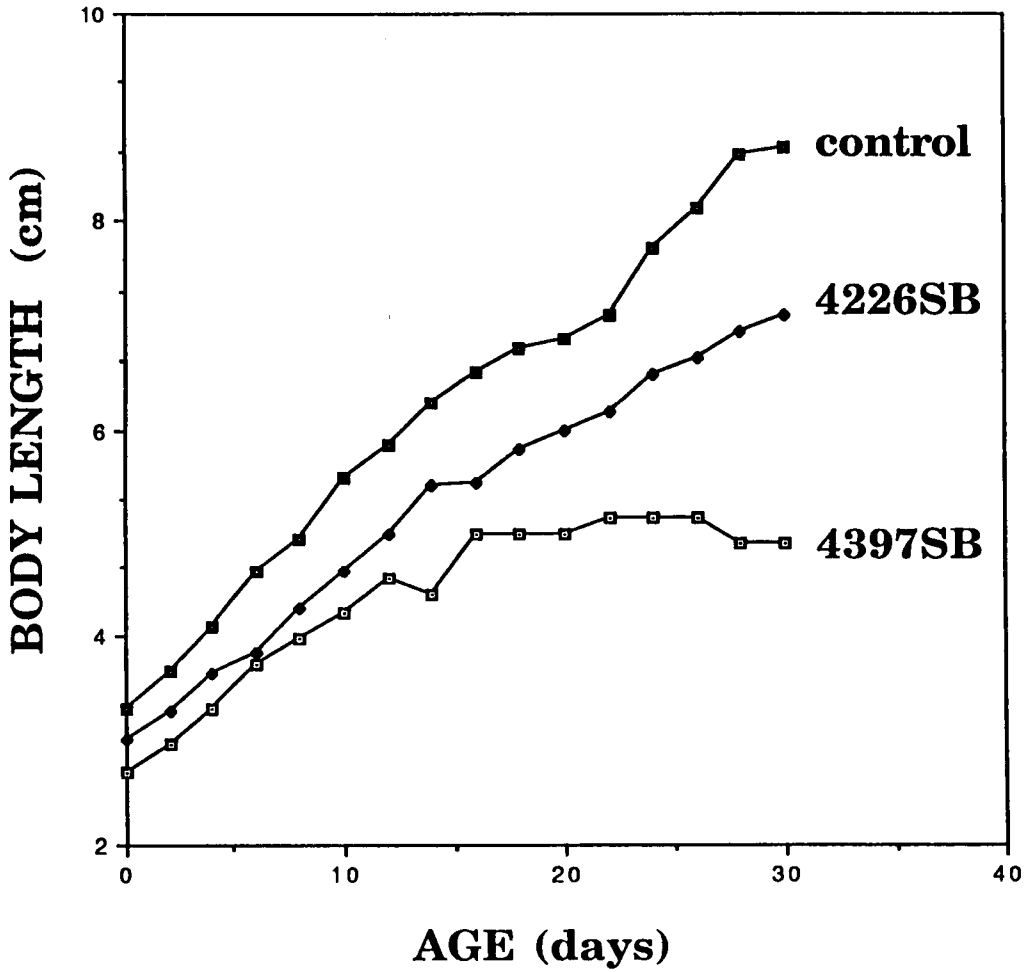
BODY LENGTH (cm)
10
8
6
4
2
0
10
20
30
40
AGE (days)
control
4226SB
4397SB

FIGURE 5. Tail Length (Rump-to-Tip of Tail) Measurements for *fit1* Mutants and Wild-Type Littermates.

The tail lengths of *fit1* mutants (c $fit1^m/c^{26DVT}$) and wild-type littermates (c^{ch} $+/c^{ch}$ $+$) were measured at birth and every other day thereafter. Only the mean lengths for wild-type littermates, 4226SB mutants, and 4397SB mutants plotted versus time are shown; however, measurements were made on mutants from each of the five *fit1* alleles, and all of the means ± S.D., and the number of mice in each group, are presented in Table 4.

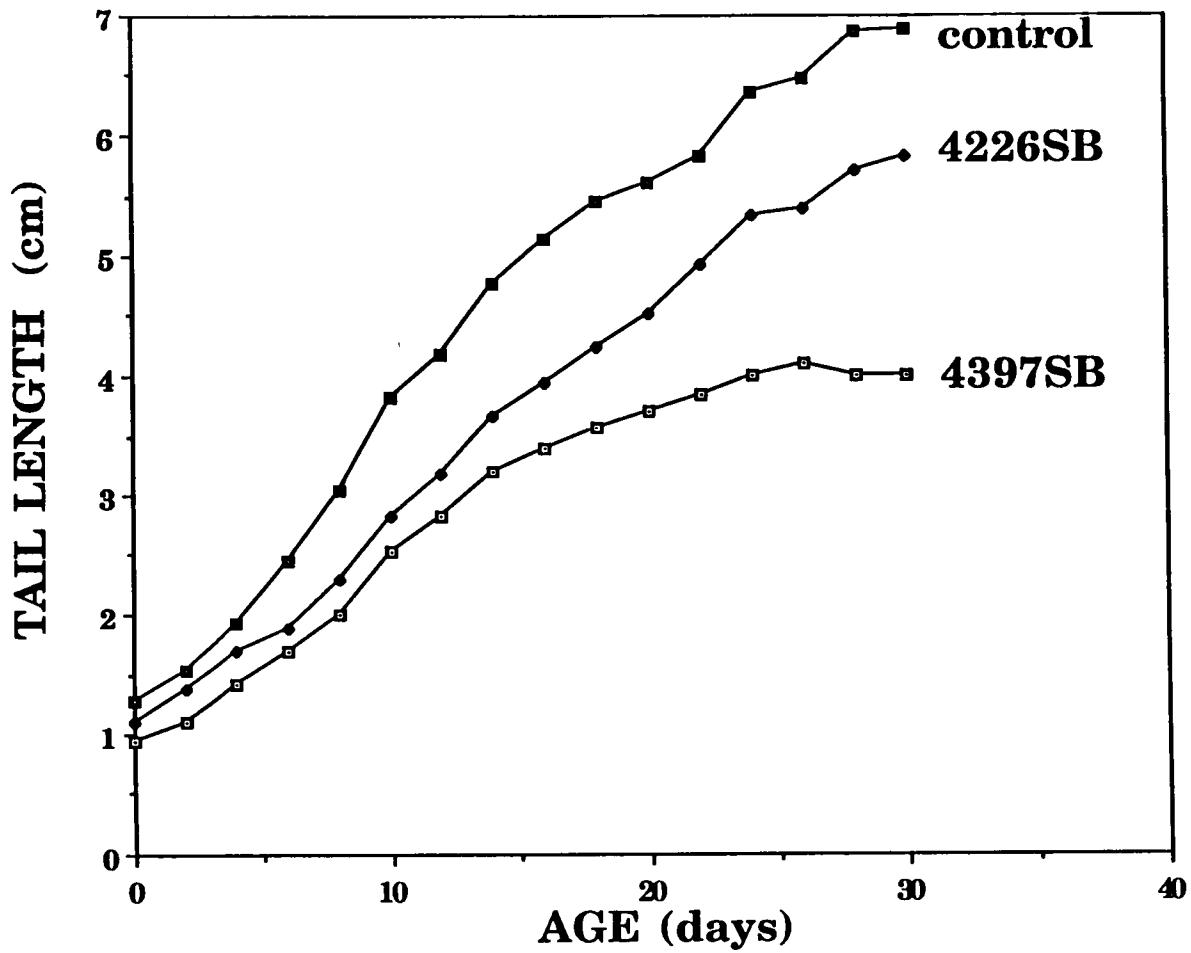
TAIL LENGTH (cm)
AGE (days)
control
4226SB
4397SB
0
1
2
3
4
5
6
7
0
10
20
30
40

FIGURE 6. Proportionality of *fit1* Mutants.

A plot of body length versus tail length, as a measure of shape and proportionality, for $fit1^{4397SB}$ ($c\ fit1^{4397SB}/c^{26DVT}$), $fit1^{4226SB}$ ($c\ fit1^{4226SB}/c^{26DVT}$), and wild-type littermate controls ($c^{ch}+/c^{ch}+$) is shown. The plotted values are based upon the body and tail length values shown in Tables 3 and 4, respectively.

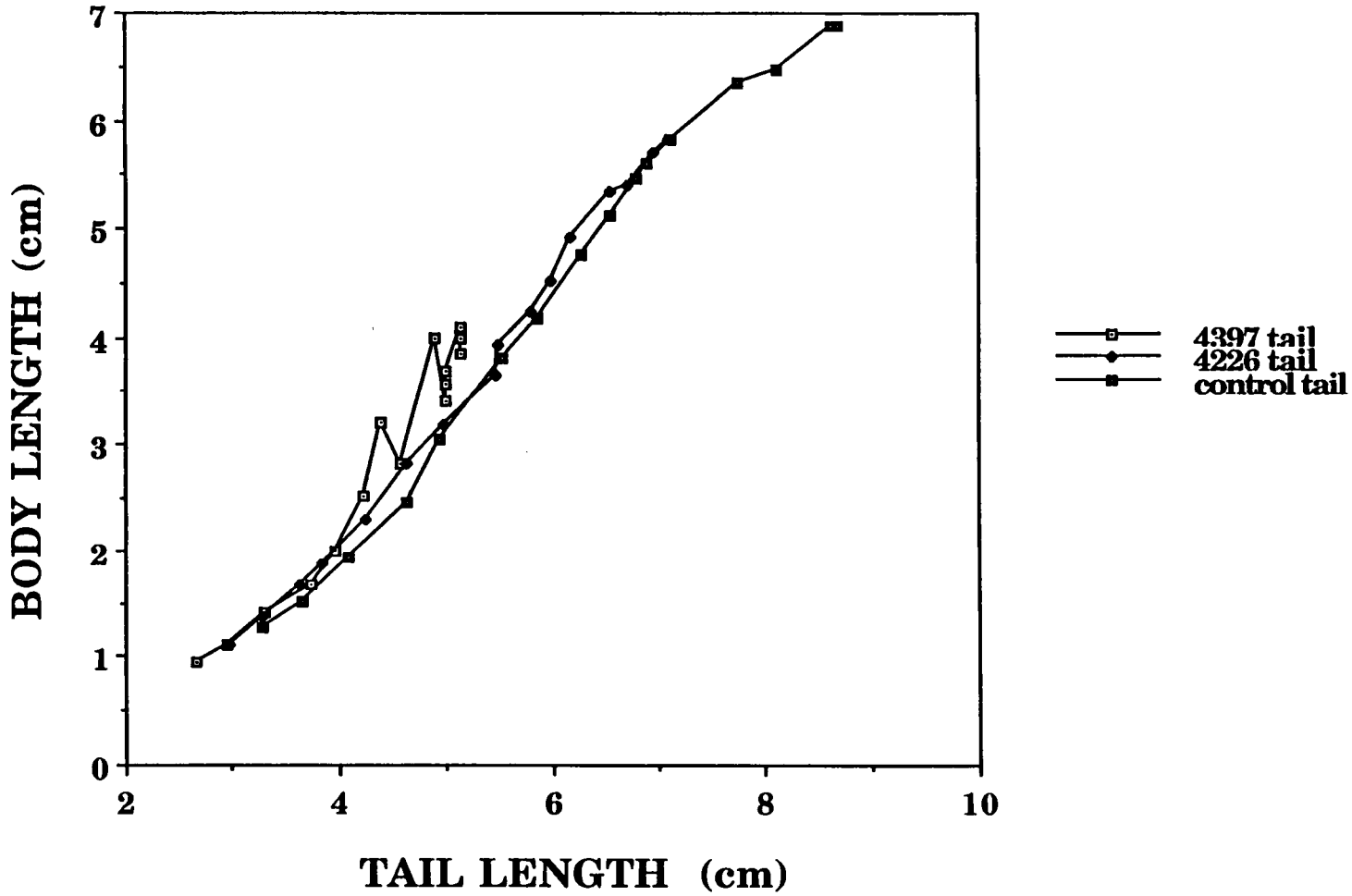
BODY LENGTH (cm)
0
1
2
3
4
5
6
7
2
4
6
8
10
TAIL LENGTH (cm)
4397 tail
4226 tail
control tail

FIGURE 7. *fit1* E14.5 Fetuses are Growth Retarded.

c^{ch} +/c^{26DVT} females were mated to c^{ch} +/c $fit1^{4397SB}$ males and were sacrificed at E14.5 days. The mean weights of eighty-one wild-type embryos and nineteen $fit1^{4397SB}$ mutant embryos are shown, and the difference between the means is significant ($p \leq 0.01$).

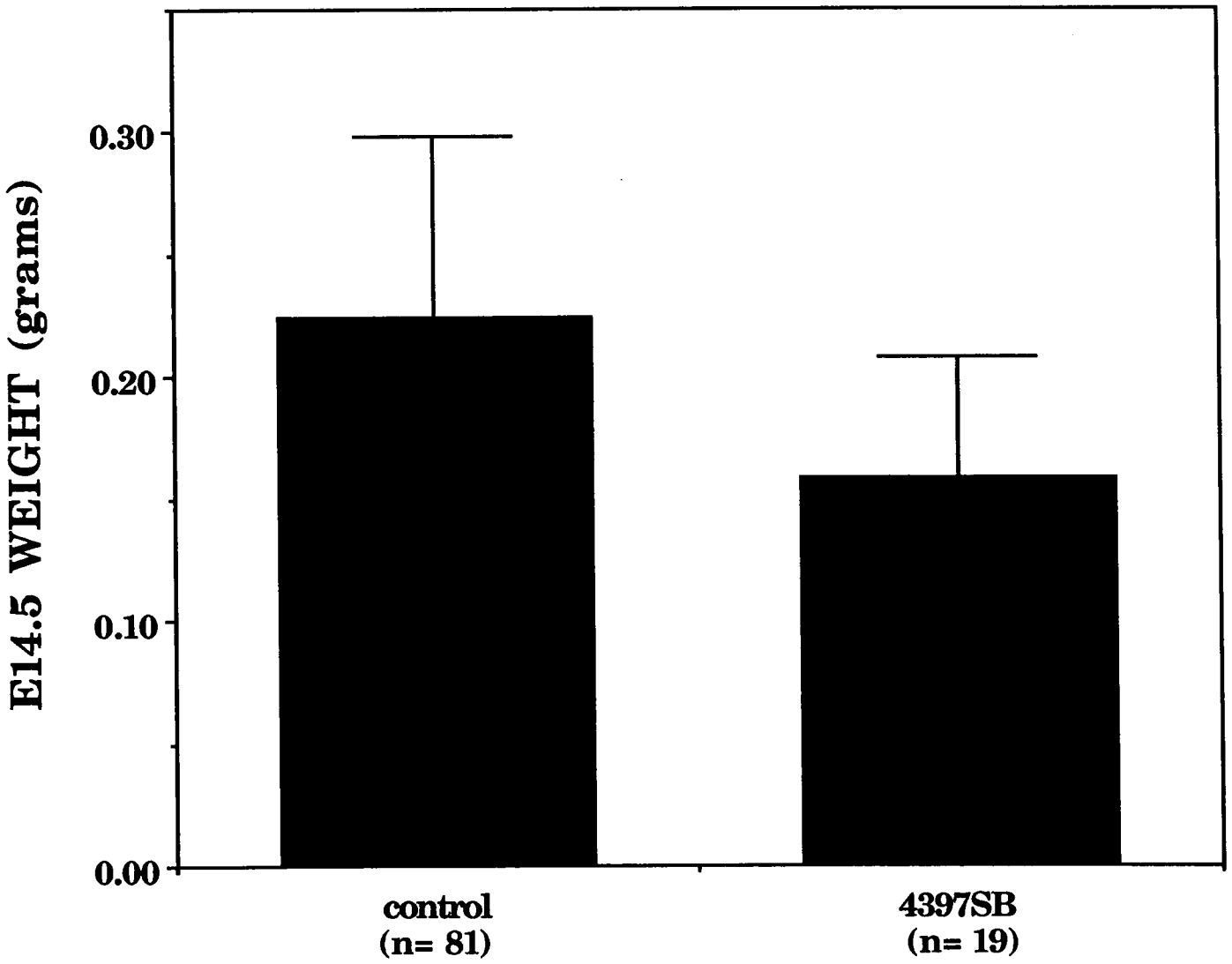
E14.5 WEIGHT (grams)
0.30
0.20
0.10
0.00
control
(n= 81)
4397SB
(n= 19)

FIGURE 8. Comparison of *fit1*^{494SB} and Wild-Type E14.5 Fetuses.

A *fit1*^{494SB} mutant (*c fit1*^{494SB}/*c*^{26DVT}) E14.5 fetus (right) and a wild-type littermate (*c*^{ch} +/*c*^{ch} +; *c*^{ch} +/*c fit1*^{494SB}; or *c*^{ch} +/*c*^{26DVT}) (left) are shown. The fetuses resulted from mating a female carrying the *c*^{26DVT} deletion (*c*^{ch} +/*c*^{26DVT}) to a male *fit1*^{494SB} carrier (*c*^{ch} +/*c fit1*^{494SB}).

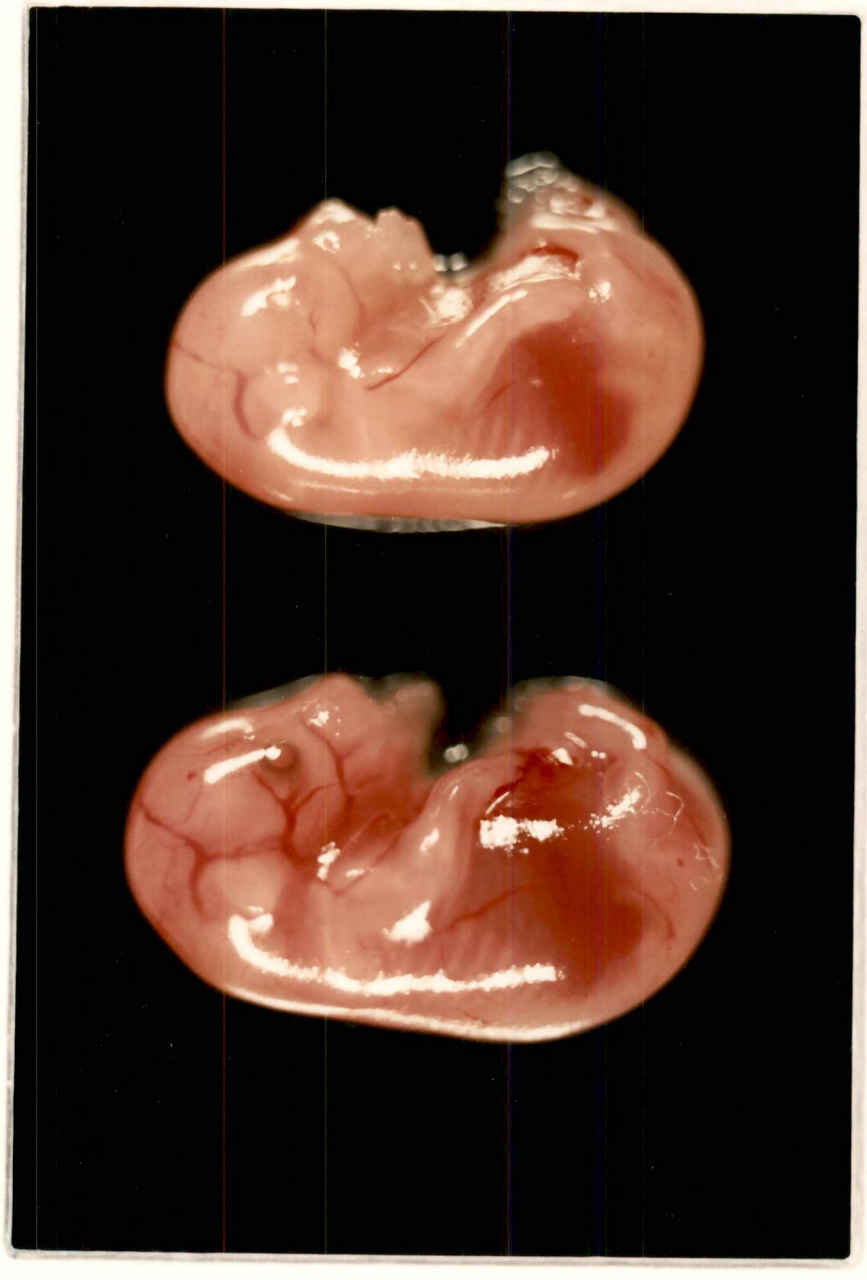

FIGURE 9. Peripheral Blood of a *fit1*^{4397SB} Mutant and a Wild-Type Littermate.

Photomicrographs of smears from (A) wild-type littermate (c^{ch} +/c^{ch} +) and (B) *fit1*^{4397SB} mutant (*c fit1*^{4397SB}/c^{26DVT}) peripheral blood stained with methylene blue, and counterstained with Wrights stain. Both smears were photographed at 60X magnification. RBCs found in the wild-type littermate control (A) are characteristically of uniform size and shape, and are stained evenly. Also, only a small percentage of reticulocytes (immature RBCs, which characteristically stain stippled-blue) are usually seen in normal peripheral blood. RBCs found in *fit1*^{4397SB} peripheral blood are pale and vary in size (anisocytosis) and shape (poikilocytosis). Most are smaller and appear as hollow rings. Also, a high percentage of reticulocytes are seen [blue staining cell dispersed throughout (B)].

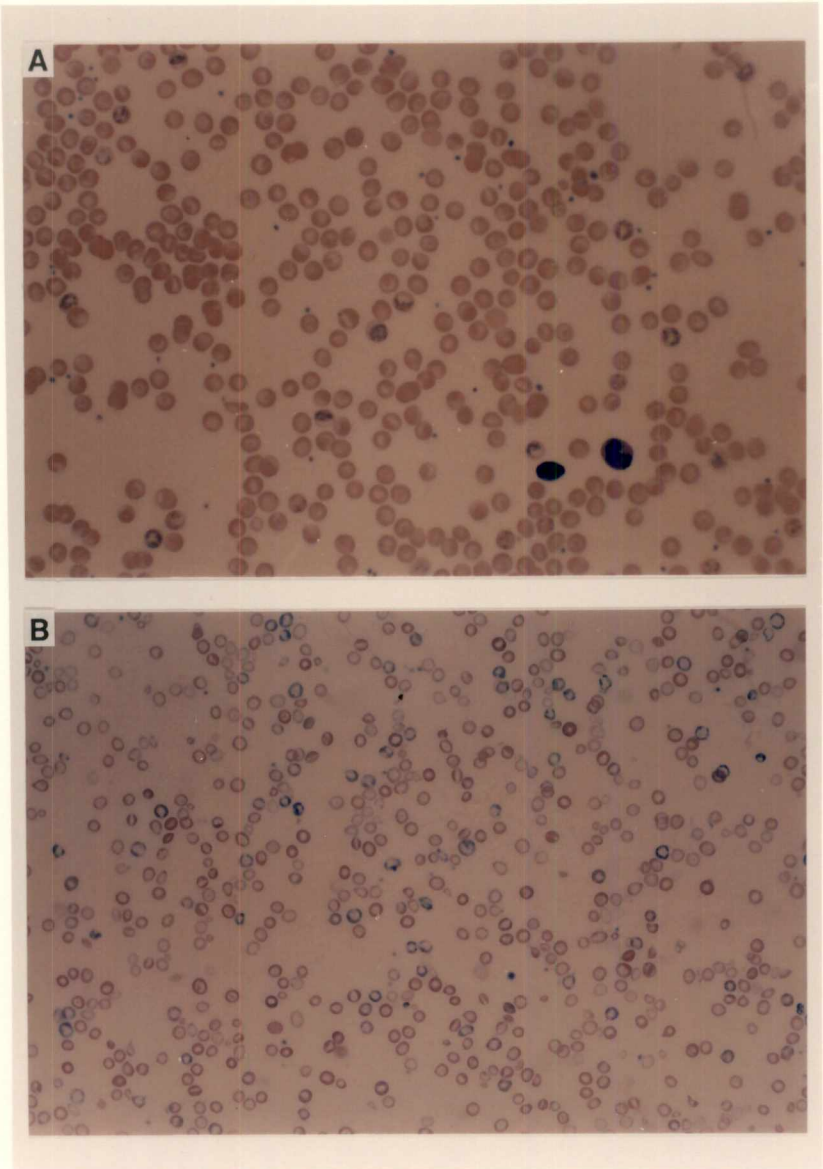
A
B

FIGURE 10. Histological Sections of *fit1*^{4397SB} Mutant and Littermate Control Spleen Tissue.

Photomicrographs of hematoxylin and eosin-stained sections of (A) wild-type littermate (c^{ch} +/c^{ch} +) and (B) *fit1*^{4397SB} (*c fit1*^{4397SB}/c^{26DVT}) spleen. The white pulp is typical lymphoid tissue and is characteristically seen as circular or oval shaped regions of basophilic (blue) staining lymphoid cells rimmed by a pale-staining marginal zone of macrophages [as in (A)]. Surrounding the white pulp are areas of eosinophilic (red) and basophilic hematpoietic cells that comprise the red pulp. In the *fit1*^{4397SB} mutant (B), the white-pulp areas appear smaller, fewer in number, and there is an apparent hyperplasia of the surrounding red pulp. Both the wild-type and *fit1* sections were photographed at the same magnification (X 10).

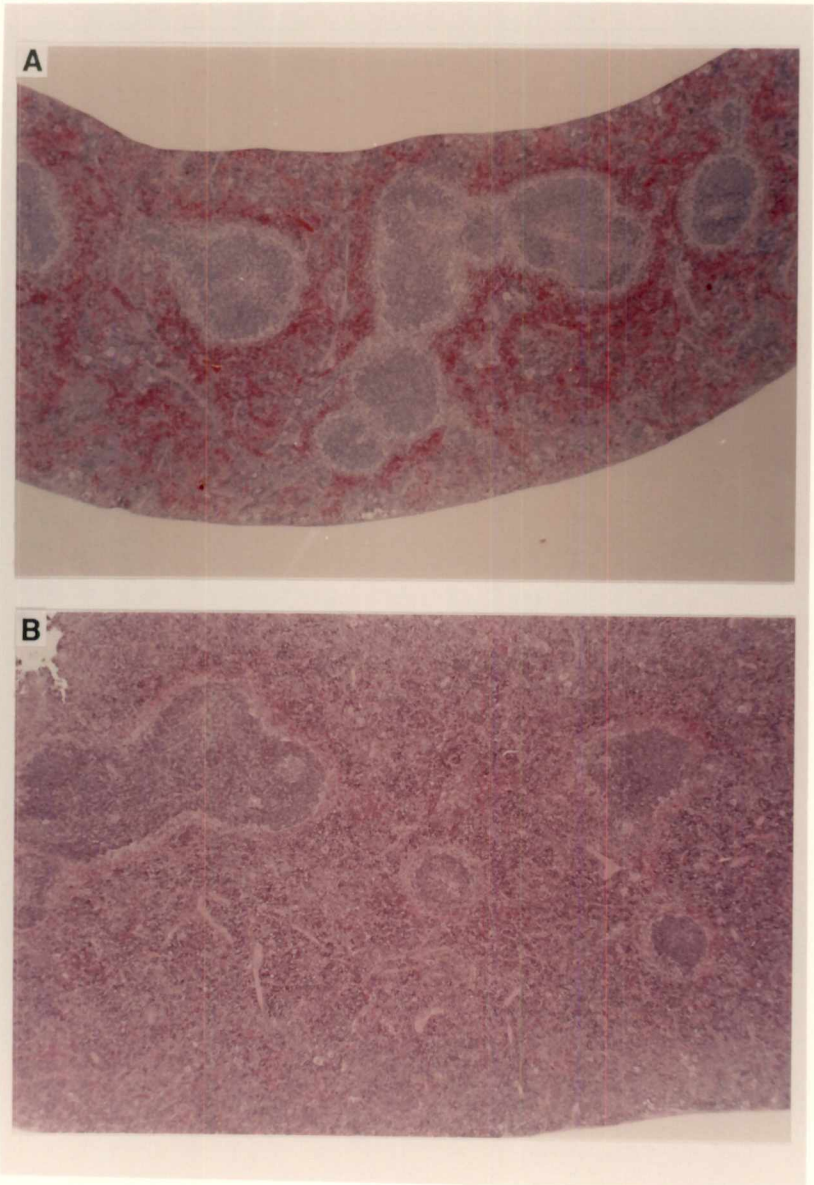
A
B

FIGURE 11. Histological Sections of *fit1*^{4397SB} Mutant and Littermate Control Bone Marrow.

Photomicrographs of hematoxylin and eosin-stained sections of (A) wild-type littermate (c^{ch} +/c^{ch} +) and (B) *fit1*^{4397SB} mutant (*c fit1*^{4397SB}/c^{26DVT}) bone marrow. In normal bone marrow, erythroid cells are seen as collections of cells with darkly staining nuclei [as in (A)]. Surrounding granulocyte-producing cells have a characteristic multi-lobed nucleus [polymorphonuclear cell (PMNs)]. The *fit1*^{4397SB} bone marrow has fewer detectable erythroid cells, and many PMNs. Both sections were photographed at 40X magnification.

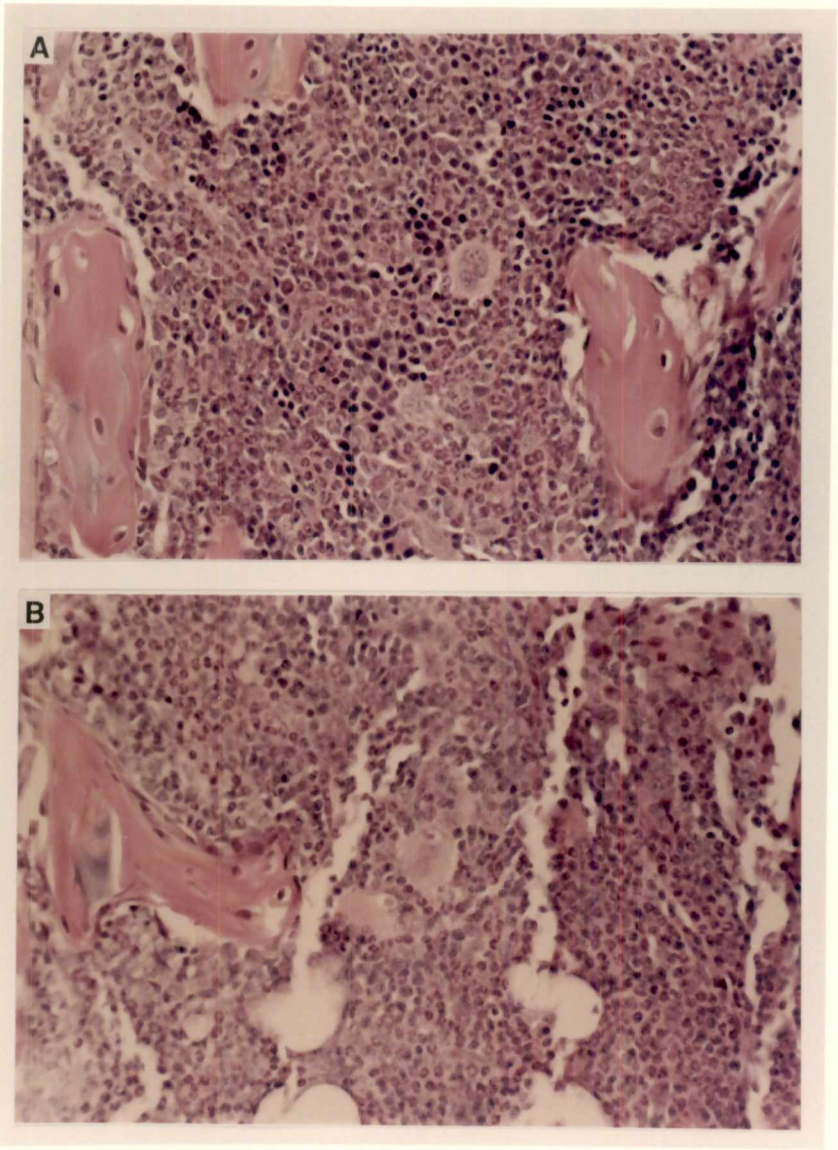
A
B

FIGURE 12. Hematocrit Values and Hemoglobin Concentrations for *fit1* Mutants and Wild-Type Littermates.

Hematocrit values and hemoglobin concentrations were determined for *fit1* mutants (*c fit1*^{m}/*c*^{26DVT}, where *m* = any one of the *fit1* alleles) and for wild-type littermates (*c*^{ch} +/*c*^{ch} +). Hematocrits (A) and hemoglobin concentrations (B) were determined as described in Materials and Methods. The number of mice in each group is shown beneath each column.

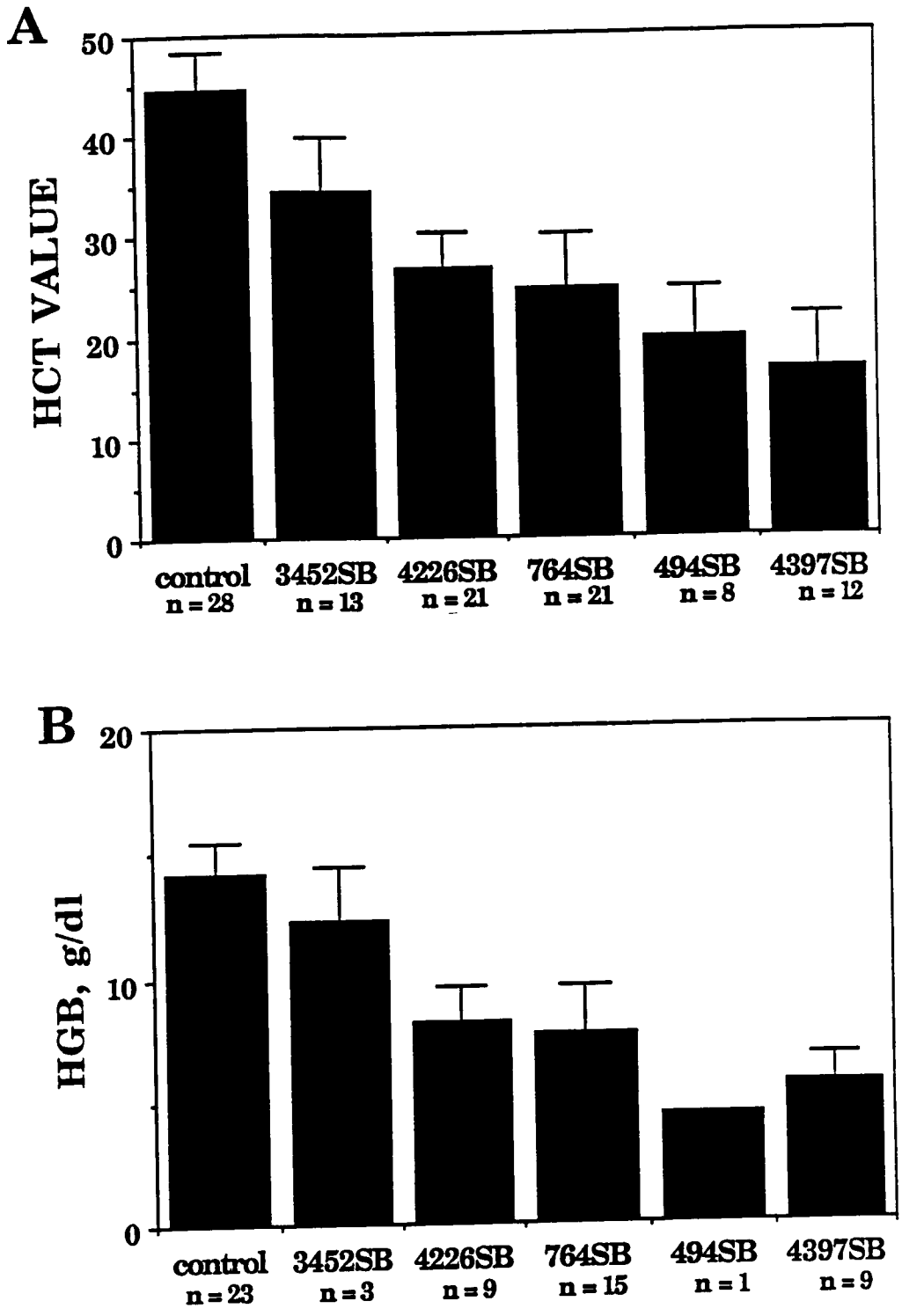
A
HCT VALUE
50
40
30
20
10
0
control
n = 28
3452SB
n = 13
4226SB
n = 21
764SB
n = 21
494SB
n = 8
4397SB
n = 12
B
HGB, g/dl
20
10
0
control
n = 23
3452SB
n = 3
4226SB
n = 9
764SB
n = 15
494SB
n = 1
4397SB
n = 9

FIGURE 13. Hematopoietic Progenitors in Weaning-Age *fit1*^{4397SB} Mutants and Wild-Type Littermates.

The number of hematopoietic progenitors per 10^5 cells was determined for *c fit1*^{4397SB}/*c*^{26DVT} (m) and c^{ch} +/c^{ch} + (+/+) bone marrow (A), and spleen (B), in methylcellulose cultures. The values shown for mutants represent the percent of the control value (mean of mutants/mean of controls), with control values set to 100% (see Table 7 for control values). These data represent the compiled results of 3 experiments, and in individual experiments each value was determined by averaging the number of progenitor colonies in three separate wells.

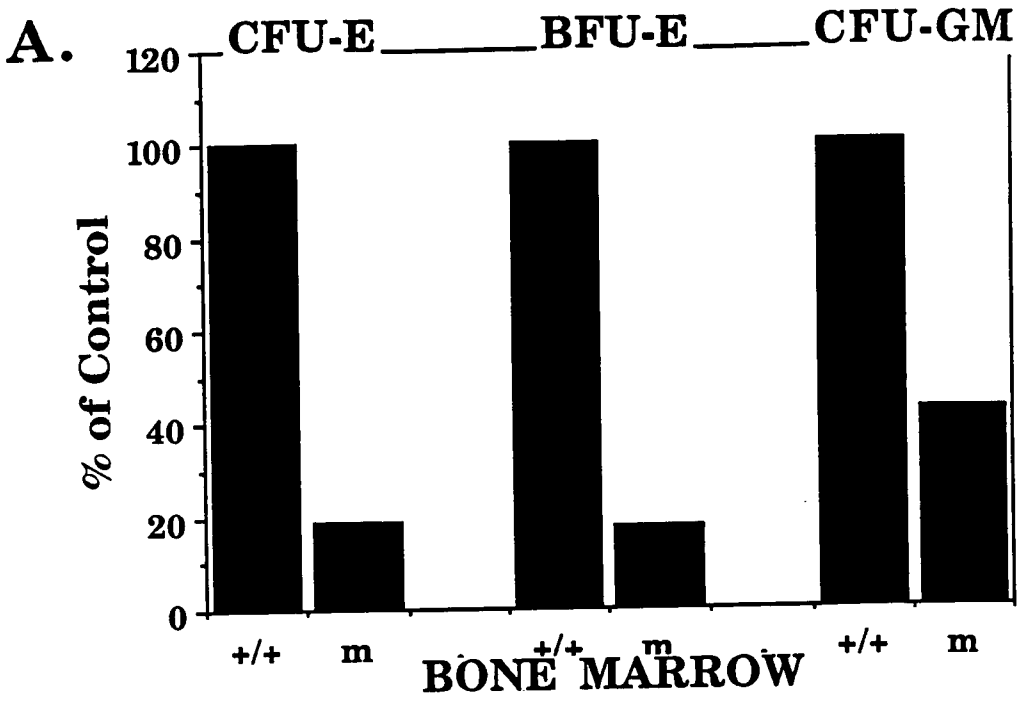
A.
CFU-E
BFU-E
CFU-GM
120
100
80
60
40
20
0
% of Control
+/+
m
+/+
m
+/+
m
BONE MARROW

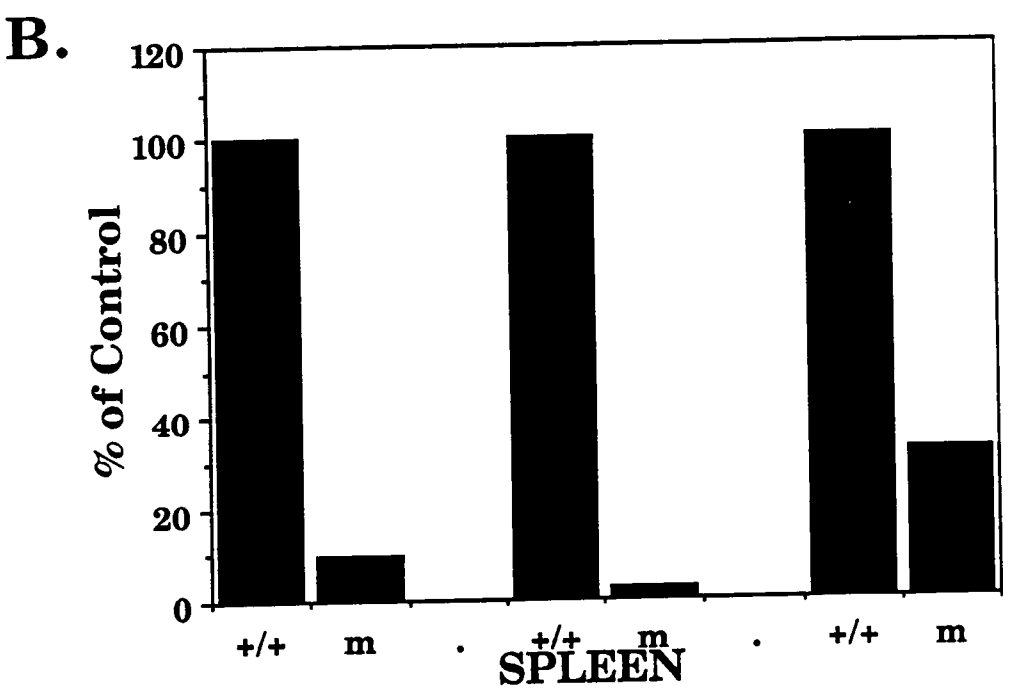
B.
120
100
80
60
40
20
0
% of Control
+/+
m
+/+
m
+/+
m
SPLEEN

FIGURE 14. Hematopoietic Progenitors in *fit1*^{4397SB} and Wild-Type Littermate E14.5 Liver.

The number of hematopoietic progenitors per 10^5 cells in E14.5 fetal liver from *c fit1*^{4397SB}/*c*^{26DVT} and c^{ch} +/c^{ch} + embryos was determined by methylcellulose assays. The values shown represent the cumulative results of three separate experiments and are shown as percent of the mean number of control colonies/10^5 cells, with the control value set to 100%.

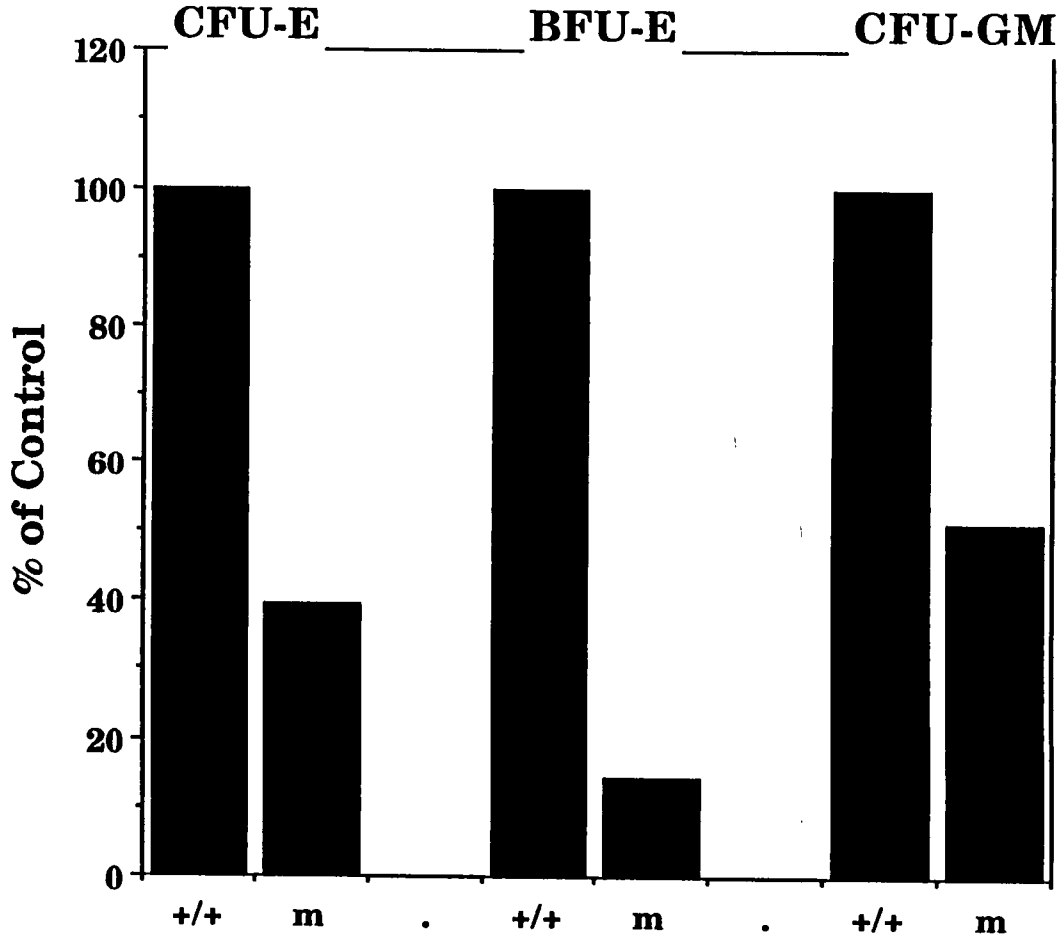

E14.5 FETAL LIVER

FIGURE 15. Histological Sections of *fit1*^{4397SB} Mutant- and Wild-Type Littermate-Derived CFU-S.

Photomicrographs of hematoxylin and eosin-stained sections of (A) wild-type littermate- (c^{ch} +/c^{ch} +) and (B) *fit1*^{43976SB} mutant-derived CFU-S. CFU-S are seen as the large lobed areas in each representative spleen [for example, two CFU-S are evident in the top spleen in (A)]. Both wild-type and mutant sections were photographed at 2X magnification. Fewer colonies are present in the spleen that received *fit1*^{4397SB} bone marrow cells (B), as compared to the number of colonies seen in a spleen receiving wild-type littermate bone marrow cells (A). Additionally, the *fit1*^{4397SB}-derived colonies are smaller in size [only one CFU-S (lower right of bottom spleen) is evident in the spleens shown in (B)], as compared to colonies originating from wild-type cells.

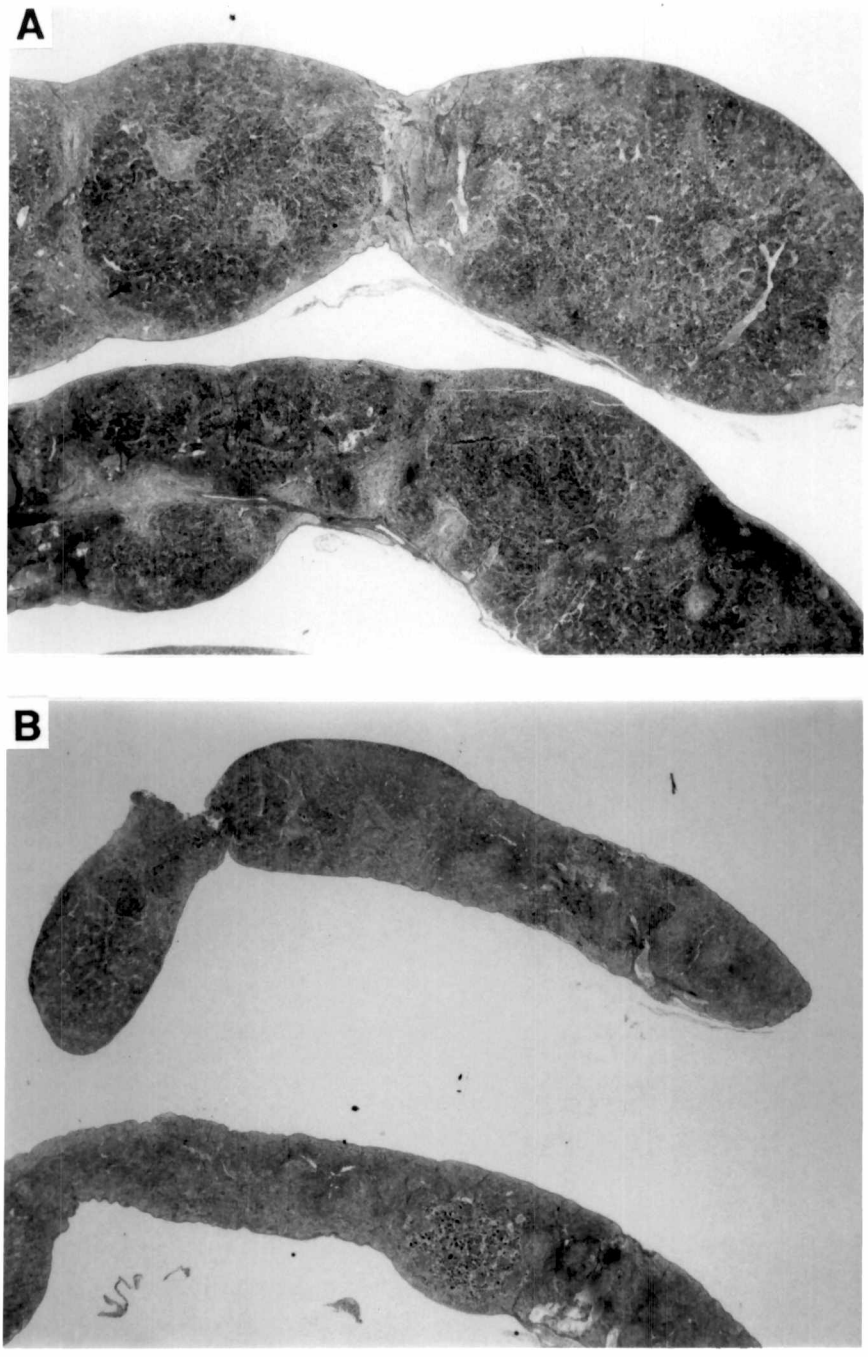
A
B

FIGURE 16. Schematic of the Hierarchical Pathway of Murine Hematopoietic Differentiation

A model of hematopoietic differentiation in the mouse (adapted from Dick, 1991; Demetri, 1992). CFU-S = colony forming unit, spleen; BFU-E = burst forming unit, erythroid; CFU-E = colony forming unit, erythroid; CFU-GM = colony forming unit, granulocyte, macrophage; CFU-MEG = colony forming unit, megakaryocyte; CFU-Eo = colony forming unit, eosinophil; CFU-MIX = colony forming unit, mixed lineage.

MURINE HEMATOPOIETIC DIFFERENTIATION

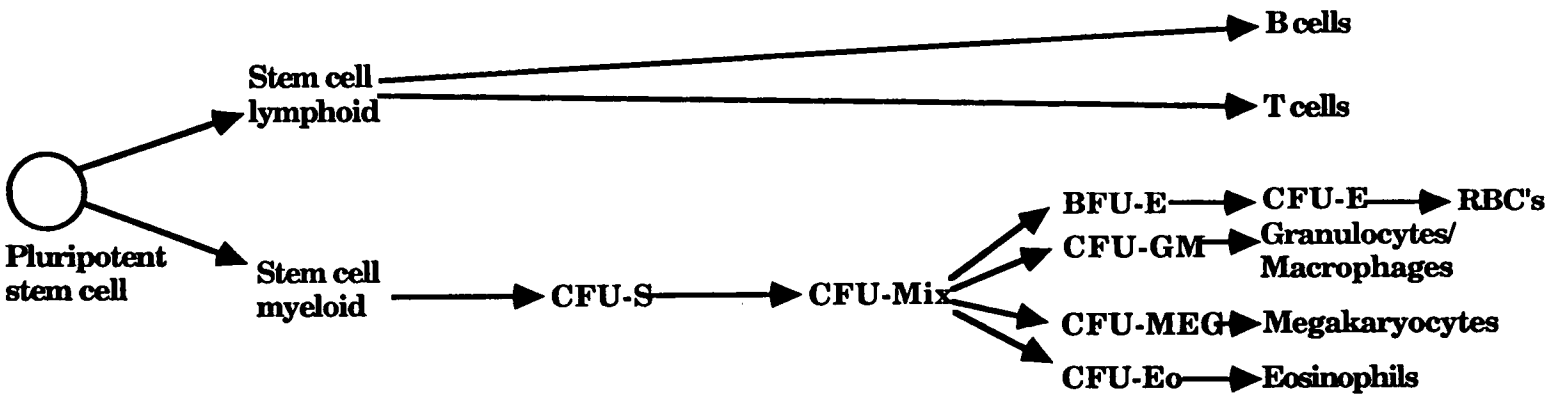

-Ability to self-renew
-Large differentiation capacity

-Little or no self-renewal
-Restricted differentiation capacity

FIGURE 17. Hybridizations of D6E7 and D18H2 Partial Digests With pYAC4 End-Probes.

Representative hybridizations of PFGE blots of partially digested D6E7 DNA (A) and D18H2 DNA (B) with the pYAC4 end probes. Each panel is labeled with the end-specific probe used. The partial digests were performed as described in Materials and Methods, and the enzymes used were *Bss*HII (B), *Mlu*I (M), *Nru*I (Nr), and *Eag*I (E), and are listed above each set of lanes. The DNA molecular weight standards shown are lambda DNA concatamers (concatamers of 48.5 kb). Partially digested DNAs were separated under the following conditions: 10- to 40- second pulse ramp, 180 volts, for 32 hours.

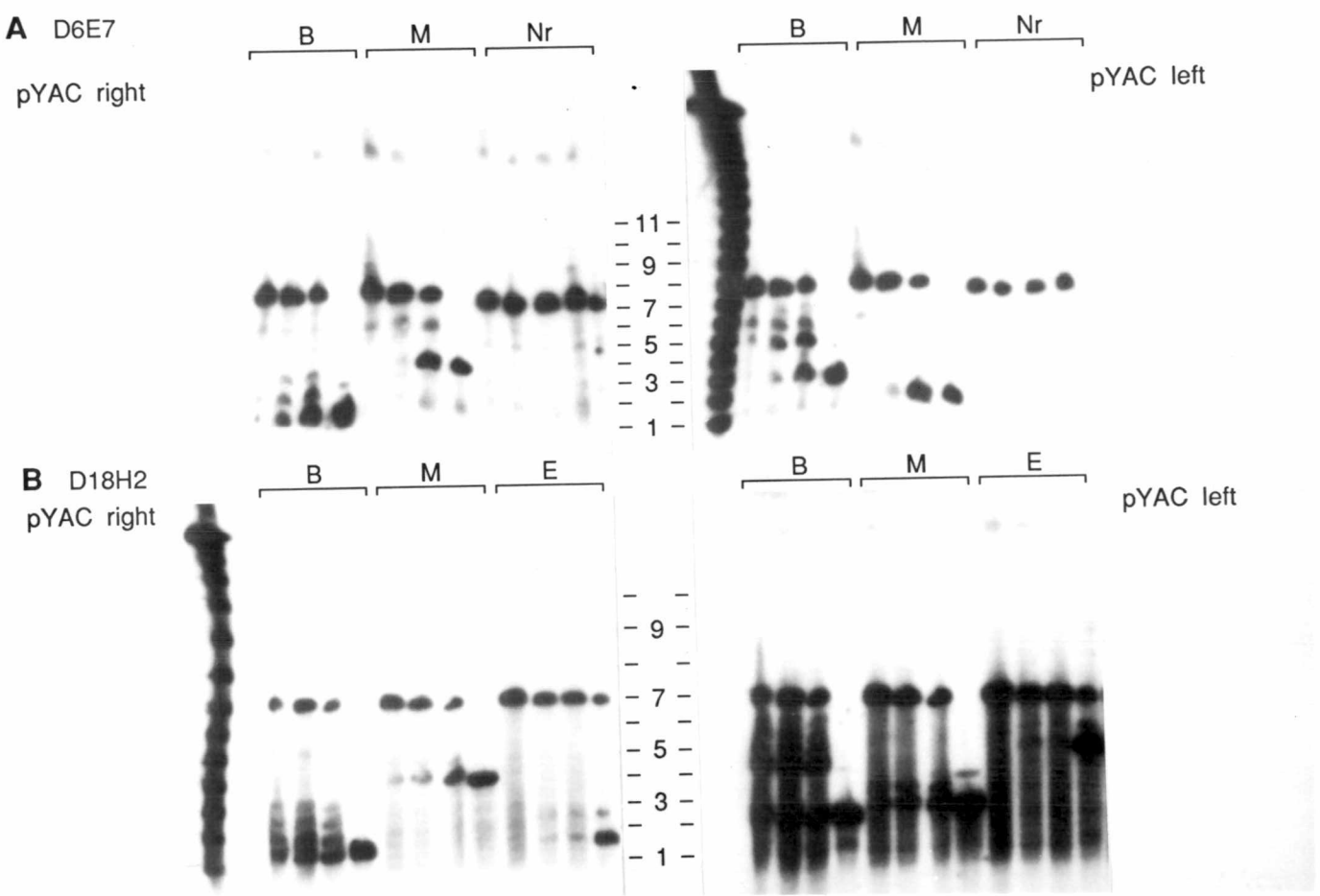
A D6E7
pYAC right
B
M
Nr
B
M
Nr
pYAC left
11
9
7
5
3
1
B D18H2
pYAC right
B
M
E
B
M
E
pYAC left
9
7
5
3
1

FIGURE 18. Rare-Cutter Restriction Map of YACs D6E7 and D18H2.

A long-range restriction map of D6E7 and D18H2 constructed from the data obtained from pulsed-field gel blots of partially digested YAC DNAs (as found in TABLEs 10 and 11, and Fig. 17). Restriction enzyme sites are: B = *Bss*HII, C = *Cla*I, E = *Eag*I, K = *Ksp*I, M = *Mlu*I, N = *Not*I, Na = *Nar*I, and Nr = *Nru*I. The shaded box denotes the *Eag*I fragment within which DNA probe RN302 (*D7Rn5* locus) must map, and the open box represents the approximate map position of pA4.2c11 (*D7CwrllD* locus) within both D6E7 and D18H2.

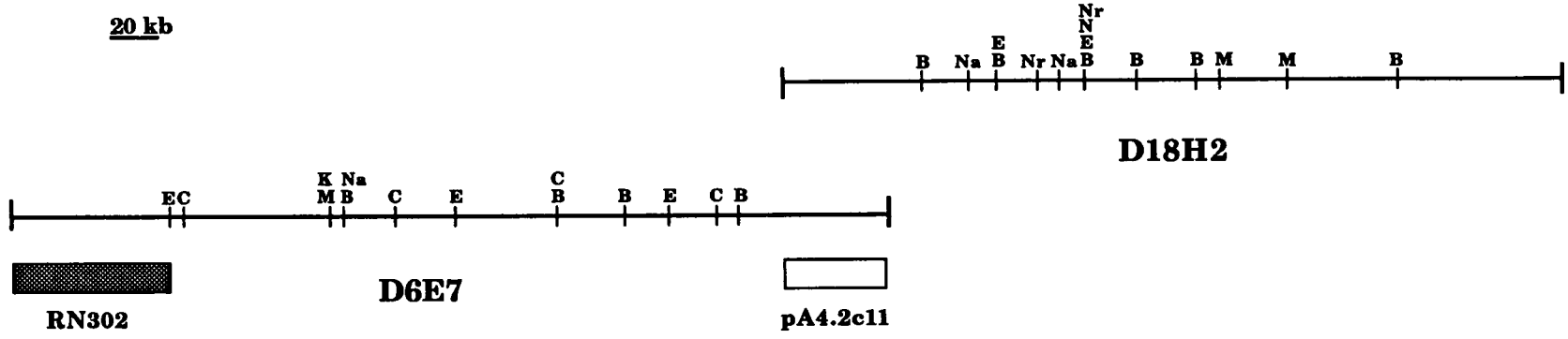
20 kb
B Na E B Nr Na Nr N E B B B M M B
D18H2
E C K M Na B C E C B B E C B
D6E7
RN302
pA4.2c11

FIGURE 19. Localization of The c^{202G} Distal Deletion Breakpoint.

A PFGE blot of stock 2A (c^{ch}/c^{ch}) and (C3H/Rl X 101/Rl)F_1 control DNAs, as well as c^{ch}/c^{202G} and c^{ch}/c^{AL} deletion-heterozygote DNAs, doubly digested with *Eag*I + *Ksp*I and hybridized consecutively with the pA4.2c11 and RN302 probes. The molecular weight standards are lambda DNA concatamers (48.5 kb each step). Digested DNAs were separated under the following conditions: 30- to 80- second pulse ramp, 180 volts, for 32 hrs.

pA4.2c11
St2A (c^{ch}/c^{ch})
(C3Hf/RI x 101/RI) F_1 (+/+)
c^{ch}/202G
c^{ch}/AL
St2A (c^{ch}/c^{ch})
(C3Hf/RI x 101/RI) F_1 (+/+)
c^{ch}/202G
c^{ch}/AL
RN302
13
11
9
7
5
3
1
13
11
9
7
5
3
1

FIGURE 20. Mapping D6E7-Derived Cosmid Clones By Whole-Cosmid Hybridization.

Whole cosmids were hybridized to panels of stock 2A (c^{ch}/c^{ch}) and (C3Hf/Rl X 101/Rl)F1 (+/+) DNAs, as well as to c^{ch}/c^{202G}, $c^{ch}/c^{24R145L}$, c^{ch}/c^{AL}, and c^{ch}/c^{11DSD} deletion-heterozygote DNAs, digested with the indicated enzymes. (A) Cosmid D6E7.4 detects *Kpn*I fragments of 20.1 kb, 6.4 kb, and 3.7 kb, in all DNAs, in addition to a 7.5-kb size-altered fragment in c^{ch}/c^{AL} DNA. (B) Cosmid D6E7.5 detects wild-type *Bst*EII fragments of 24.2 kb and 4.0 kb in all DNAs, in addition to a 15.1-kb size-altered fragment in $c^{ch}/c^{24R145L}$ DNA, and a size-altered 9.5-kb fragment in c^{ch}/c^{11DSD} DNA (not visible in this figure). Marker sizes are lambda + *Hin*dIII.

A
KpnI
St2A (c^{ch}/c^{ch})
(C3Hf/Rl x 101/Rl) F_1 (+/+)
c^{ch}/202G
c^{ch}/24R145L
c^{ch}/AL
c^{ch}/11DSD
23.1
9.4
6.6
4.4
2.3
2.0
B
BstEII
St2A (c^{ch}/c^{ch})
(C3Hf/Rl x 101/Rl) F_1 (+/+)
c^{ch}/202G
c^{ch}/24R145L
c^{ch}/AL
c^{ch}/11DSD
23.1
9.4
6.6
4.4
2.3
2.0

FIGURE 21. Mapping Fragments From D6E7-Derived Cosmids To Specific Subregions of The *c* Deletion Complex.

Random fragments from the D6E7-derived cosmids were mapped by Southern blot analysis of *Mus musculus/Mus spretus* F_1 hybrids. DNAs from *Mus musculus/Mus spretus* F_1 deletion heterozygotes, *M. musculus* deletion-heterozygote dams [c^{ch}/Df(*c*)], and *M. spretus* sires (*Spt*) are shown. (A) DNA probe D6E7.6 R4.0 detects *Xba*I fragments of 8.1 kb and 5.3 kb in *M. musculus* DNA, and detects fragments of 8.1 kb and 3.6 kb in *Xba*I-digested *M. spretus* DNA. The 5.3-kb *M. musculus* specific fragment is absent only in the *Spt*/c^{26DVT} DNA, but is present in all other *M. spretus* deletion heterozygotes. This probe also detects a 17.3-kb size-altered fragment in c^{ch}/c^{11DSD} and *Spt*/c^{11DSD} DNAs (due to the c^{11DSD} deletion breakpoint); therefore, this fragment maps near the *D7Cwr11D* locus. (B) DNA probe D6E7.4 B3.0 hybridizes to three fragments (22.5 kb, 8.0 kb, and 2.3 kb in size) in *Eco*RI-digested *M. musculus* DNA, and to fragments (12.4 kb and 8.9 kb) in *M. spretus* *Eco*RI-digested DNA, in addition to the 22.5-kb and 2.3-kb fragments. The 8.0-kb *M. musculus*-specific fragment is absent in all *M. spretus* deletion heterozygotes, except *Spt*/c^{AL} DNA. Thus, D6E7.4 B3.0 maps to the interval between the distal breakpoints of the c^{AL} and c^{202G} deletions. Note that: the DNAs shown in (B) were hybridized on three separate Southern blots run under different conditions, and, therefore, the fragments detected by D6E7.4 B3.0 are at different positions in each panel.

A
D6E7.6 R4.0
c^ch/26DVT
Spt /26DVT
c^ch/AL
Spt /AL
c^ch/24R145L
Spt /24R145L
c^ch/202G
Spt /202G
c^ch/11DSD
Spt /11DSD
Spt
23.1
9.4
6.6
4.4
2.3
2.0
B
D6E7.4 B3.0
c^ch/AL
Spt /AL
c^ch/26DVT
Spt /26DVT
Spt
c^ch/202G
Spt /202G
c^ch/24R145L
Spt /24R145L
c^ch/11DSD
Spt /11DSD
23.1
9.4
6.6
4.4
2.3
2.0

FIGURE 22. Approximate Map Positions of The D6E7-Derived Cosmids

The approximate map positions of the D6E7-derived cosmids are shown, with the exception of cosmid D6E7.1, whose map position could not be determined. Loci shown are as defined in Fig. 1. No physical distance is implied by the lengths of the lines.

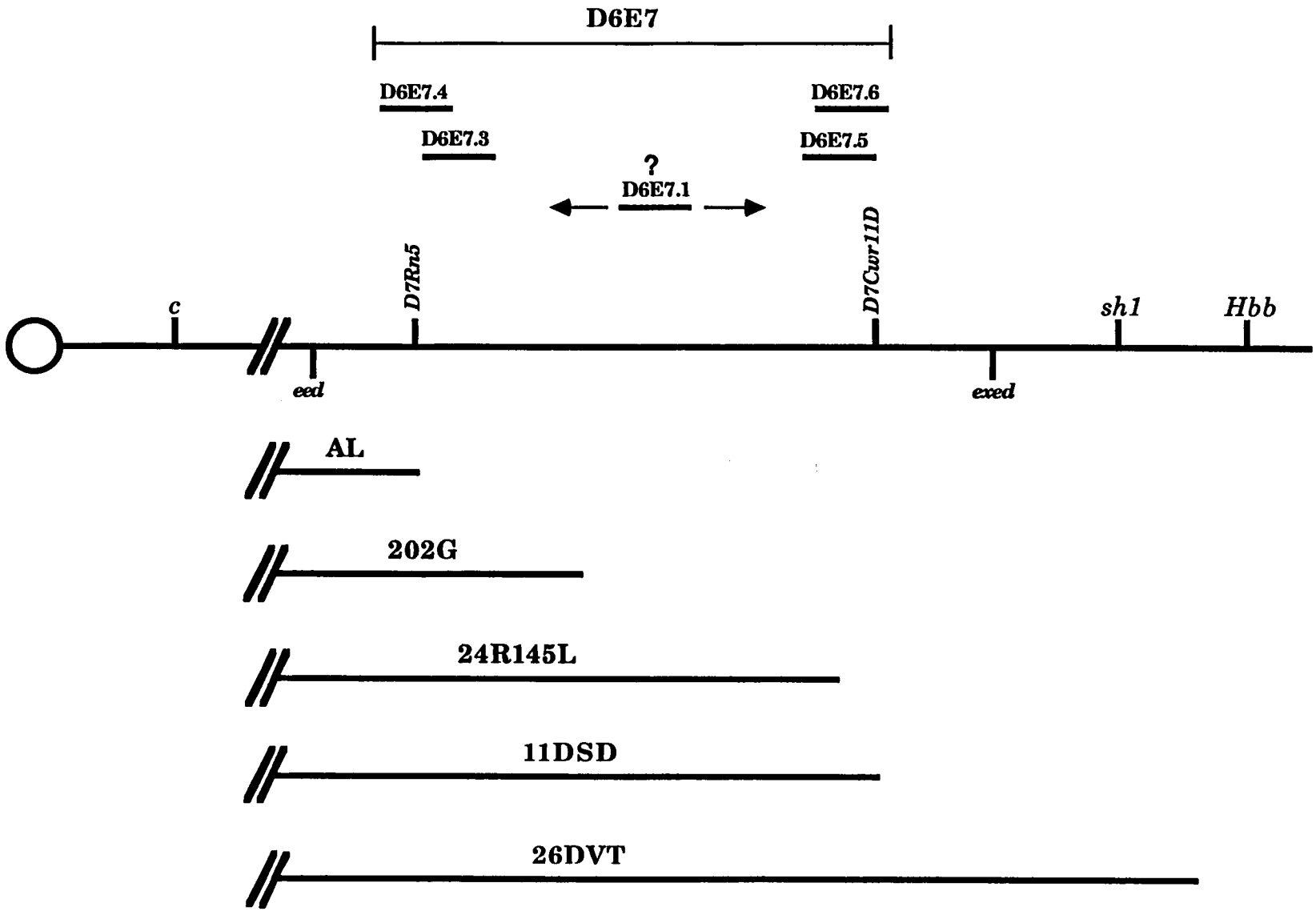
D6E7
D6E7.4
D6E7.6
D6E7.3
D6E7.5
?
D6E7.1
D7Rn5
D7Cwr11D
c
sh1
Hbb
eed
exed
AL
202G
24R145L
11DSD
26DVT

FIGURE 23. Mapping FEID4$_{dist}$ To The Interval Between The Distal Breakpoints of The c^{202G}-$c^{24R145L}$ Deletions.

Southern blots of *Bam*HI-digested DNAs of the indicated genotypes were hybridized with the FEID4$_{dist}$ probe. DNAs from *M. musculus*/*M. spretus* F_1 deletion heterozygotes [*Spt*/Df(*c*)], *M. musculus* deletion-heterozygote dams, and *M. spretus* sires (*Spt*) are shown. FEID4 detects a 22.8-kb *M. spretus*-specific fragment, and a 7.1-kb *M. musculus*-specific fragment. The absence of the *M. musculus* specific fragment in *Spt*/c^{26DVT}, *Spt*/c^{11DSD}, and *Spt*/$c^{24R145L}$ DNAs, and its presence in *Spt*/c^{202G} and *Spt*/c^{AL} DNAs show that FEID4 maps between the distal breakpoints of the c^{202G} and $c^{24R145L}$ deletions.

c^{ch}/26DVT
Spt /26DVT
c^{ch}/AL
Spt /AL
c^{ch}/24R145L
Spt /24R145L
c^{ch}/202G
Spt /202G
c^{ch}/11DSD
Spt /11DSD
Spt
FEID4dist.
22.8
7.1

FIGURE 24. A Summary of Physical Mapping Within The *fit1* Region.

The approximate positions of YAC clones D6E7, D18H2, and FEID4, presumed CpG-island sites identified in these YACs (designated by asterisks), cosmid clones derived from D6E7, the $FEID4_{dist}$ DNA probe, and a cosmid clone isolated with $FEID4_{dist}$ are shown. The *fit1* interval, as defined by complementation and physical mapping, is shown as the shaded box. At least part of the *fit1* gene must map between the distal breakpoints of the c^{202G} and $c^{24R145L}$ deletions, although part of the *fit1* gene could map distal to the $c^{24R145L}$ deletion distal breakpoint (as indicated by the shaded box containing the question mark). The physical distance from *D7Cwr11D* to the c^{202G} distal breakpoint is a minimum of 245 kb, but is less than 385 kb. The physical distance from *D7Cwr11D* to the $c^{24R145L}$ distal deletion breakpoint is $\leq$ 15.1 kb. Note that the lines beneath the chromosome represent deletion mutations, whereas the lines above the chromosome represent DNA clones. No physical distance is implied by the line representing the D18H2 YAC clone, with respect to the genetic loci shown.

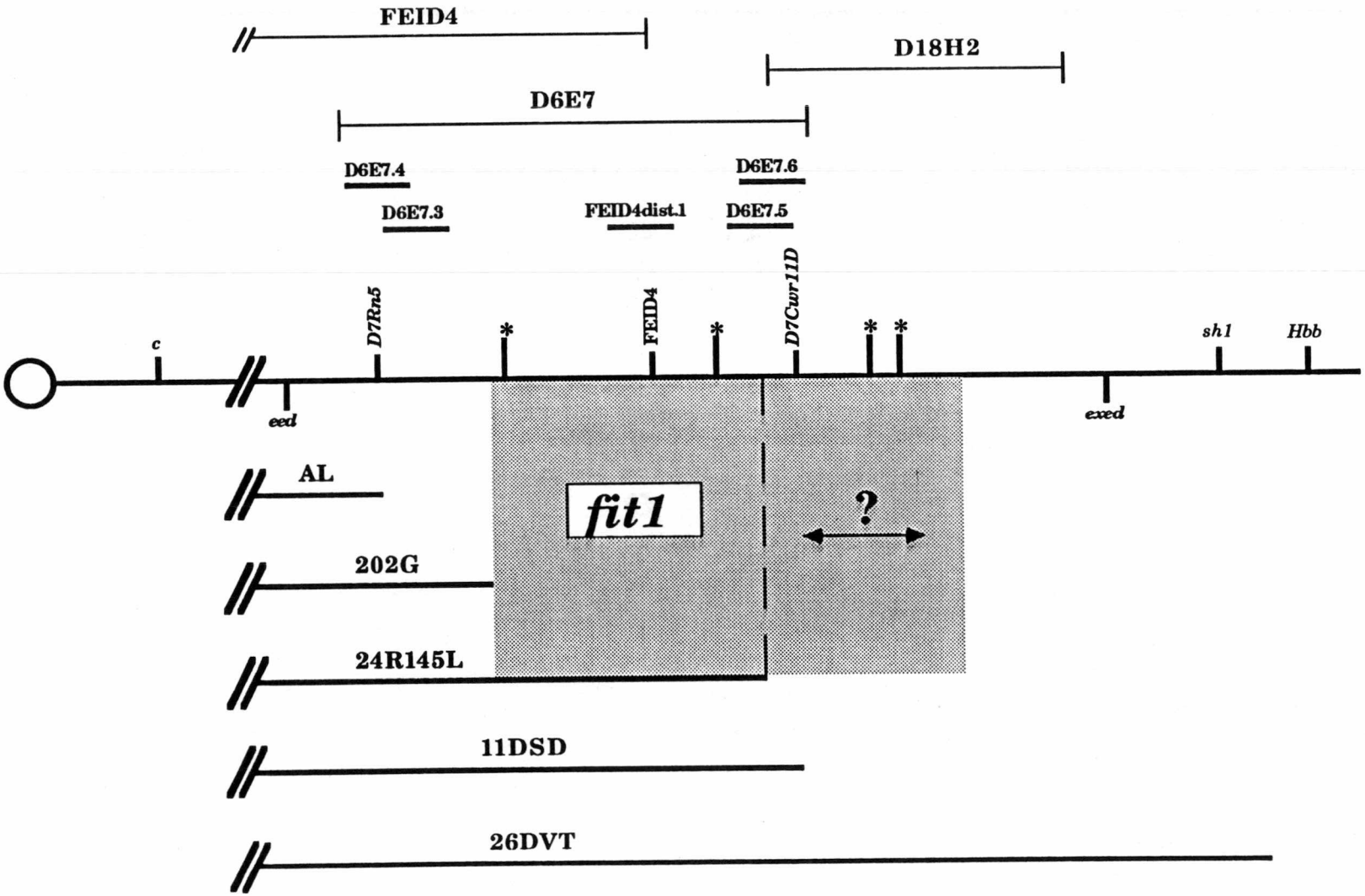
FEID4
D18H2
D6E7
D6E7.4
D6E7.6
D6E7.3
FEID4dist.1
D6E7.5
D7Rn5
FEID4
D7Cwr11D
c
sh1
Hbb
eed
exed
AL
fit1
?
202G
24R145L
11DSD
26DVT

FIGURE 25. Conservation of Synteny Map For the *Fes-Hbb* Region of Mouse Chr 7.

Regions of human chromosomes showing conserved synteny with the *Fes-Hbb* region of mouse Chr 7 are shown as open boxes above the chromosome, and are labeled with the human chromosomal region assigned to that particular locus or loci. The homologous region associated with the *fit1* region has not yet been determined, as indicated by the open box containing a question mark. The conservation of synteny data indicated here were adapted from Mouse Genome, 92 (1), 1994.

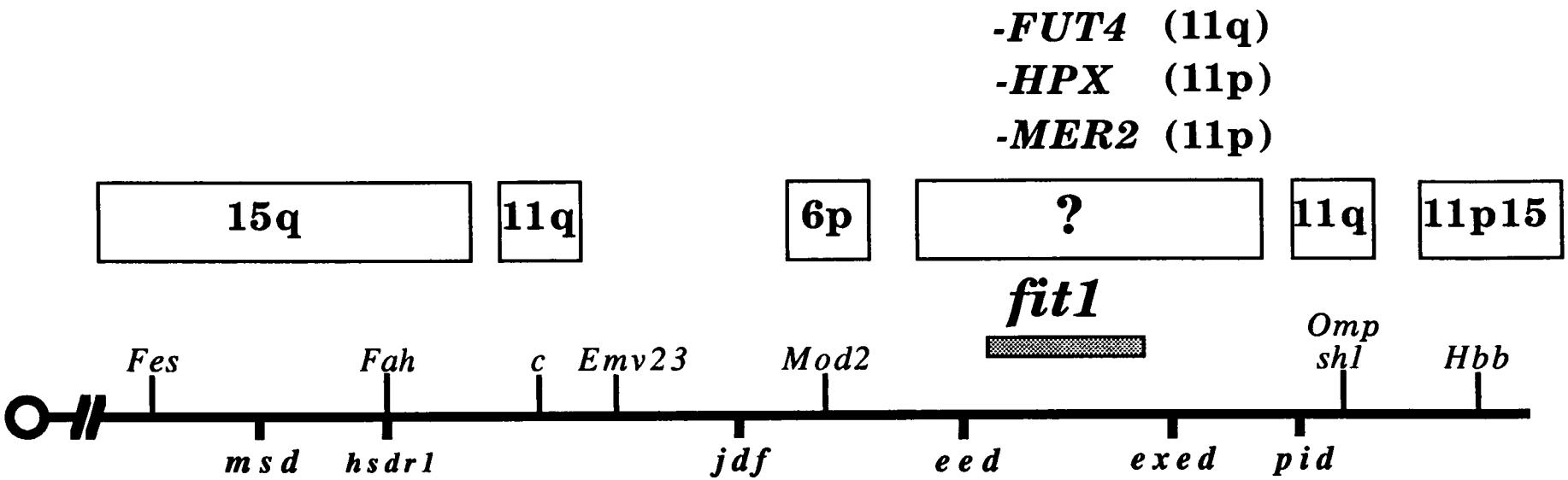
-FUT4 (11q)
-HPX (11p)
-MER2 (11p)
15q
11q
6p
?
11q
11p15
fit1
Fes
Fah
c
Emv23
Mod2
Omp
shl
Hbb
msd
hsdr1
jdf
eed
exed
pid

VITA

Mark Darnell Potter was born to Anna and Darnell Potter in Walnut Ridge, Arkansas on August 23, 1964. After graduating from Walnut Ridge High School in May of 1982, he obtained a Bachelor of Science degree in Biology from Arkansas Tech University in Russellville, AR in May of 1986. From August of 1986 to May of 1988, he was a graduate teaching assistant at Arkansas State University in Jonesboro, AR.

He entered the University of Tennessee Graduate School of Biomedical Sciences at Oak Ridge in the fall of 1988, and was awarded the Doctor of Philosophy degree in August of 1994. He will begin a postdoctoral fellowship at the Samuel Lunenfeld Research Institute at Mount Sinai Hospital in Toronto, Ontario, Canada.